Distribution
Category UC-28

SAND89-0298
Unlimited Release
Printed April 1989

Numerical Simulations of RADLAC, IBEX, Recirc, and PTØ in 1988

SAND--89-0298

DE89 000868

James W. Poukey

Plasma Theory Division 1241
Sandia National Laboratories
Albuquerque, New Mexico 87185

Abstract

The particle code MAGIC and the trajectory code TRAJ were used to model diodes, gaps, and conditioning cells for several of Sandia's linear electron accelerators. In this report we summarize the main results obtained and discuss their significance.

Outline

I. Introduction

In this report we follow the custom of previous years and document the main results of the numerical simulations of electron linacs performed in the past year.[1-6] Some of the results have been shown in part in various presentations, reports,[7,8] and articles;[9,10] and much of the work has been presented in more detailed, preliminary form in memos to the experimentalists requesting the calculations.[11-17] Instead of listing all relevant references, we simply state that the primary motivators of much of the work were M. G. Mazarakis (1242) and C. A. Frost (1242), who suggested many simulations, provided parameters from the laboratory, and helped interpret the results. Interesting discussions were also had with J. R. Freeman (1241), D. E. Hasti (1242), S. L. Shope (1242), J. M. Wilson (1245), and R. J. Adler (North Star).

The two codes used were the trajectory code TRAJ and the 2-D particle code MAGIC. TRAJ was used basically in its original form,[18] with modifications to allow warm beam input; the diagnostics (plotted output) have been improved somewhat. MAGIC was used in both its old form (written by B. Goplen (MRC)), and its new form (upgrade for slanted surfaces by T. Pointon (1265)).

We divide the discussion according to the machine being modeled. Section II presents results for PTØ (prototype Delphi). Section III discusses the Recirc injector work. Finally the lengthy Sec. IV summarizes the calculations for RADLAC/IBEX, including diodes, gaps, and conditioning cells.

II. Pierce Inserts in PTØ

In Sec. II of Ref. 5 we presented TRAJ runs resulting in an early design for PTØ (see Fig. 1 of Ref. 5). The trajectories are repeated in Fig. 1a, with the equipotentials in Fig. 2a and the applied B in Fig. 3. The main problem with this design (and others shown in Ref. 5) is that the beam expands radially for the first 10 cm nearest the cathode, making the beam (800 kV, 1 kA) difficult to focus and exacerbating the sensitivity problems (discussed in some detail in Ref. 5).

An improvement can be made using the "Pierce" technique, as discussed in Ref. 19. This may be defined as finding electrodes to produce a given flow, or more specifically a given E field at the beam edge; however, we shall only consider adding "inserts" or "shapers" to the cathode to produce a parallel or focused flow, and we shall proceed empirically using TRAJ. Figure 1b shows the result of adding a simple insert of rectangular cross section with 9-mm thickness in z just outside the beam edge. The result is to overfocus the beam. The thinner insert in Fig. 1c leads to a better result, but the best is shown in Fig. 1d, where the 9 mm-insert is used but moved farther out radially.

The problem here is that the Pierce insert has also reduced the current I from 1 kA to 0.66 kA. The reason is seen in Fig. 2, where the vacuum potentials $\phi(r,z)$ are shown. The old case of no insert (Fig. 2a), with $E = -\nabla\phi$ normal to the emitter, clearly has a larger $|E|$ near the beam edge than the case with insert (Fig. 2b), although the latter E points inward radially and so helps with the focusing. This is a general result: the Pierce method helps the focusing at the expense of reduced current. If we proceeded to build the system of Fig. 1d, the electric stress at the insert corners would be high and it would be difficult to prevent emission there, while allowing it over the desired emitting area (presumably felt-covered). Thus a more subtle design is needed.

A second problem with the design of Fig. 1d is that felt needs a stress larger than 100 kV/cm to turn on uniformly.[20] This, combined with the reduced current problem, leads to the reduced-gap d = 5.4 cm design in Fig. 4. Here, the emitter is recessed 4 mm, and the insert is tapered (at 24°) gradually to prevent large |E|, as seen in Fig. 4a. This is the best design obtained to date (Jan. 1989), and reflects other changes in dimensions made in the design process. Of course, the applied B must also be revised; the result in Figs. 4b and 4c employs three solenoids and a final focus coil. The trajectories for I = 931 A are shown in Fig. 4d; comparing Fig. 1a shows the progress made overall, especially in reducing the initial expansion, and in better laminarity.

By popular demand, phase space plots have been added to TRAJ; these show V_r or V_θ vs. radius r for the trajectories crossing a given z-plane. Figure 5 shows plots at z = 22.6 cm (entrance to small tube) and z = 66 cm (near rhs). At z = 22.6 cm, we see the beam is converging (5a) and rotating (5b) slightly. Near the rhs, the beam is diverging slightly (5c), and still rotating (5d). Note from Figs. 4b and 4c that there is a small flux (168 G) linking the cathode; it was verified that TRAJ conserves P_θ.

A few parameter studies were done with the new configuration. Varying the angle of the Pierce taper from 15° to 90° (no taper--insert sticks out normally as in Fig. 1) while holding the maximum insert thickness at 4 mm yields Fig. 6. Note the sensitivity to this angle, and note again that more stick-out near the beam edge implies greater focusing but smaller current. (The solenoids in Fig. 6 have not been adjusted for transport through the gaps.) An angle of 24° appears best, and so was used in the final design, Fig. 4.

If we wish to operate PTØ in a multiple-pulse mode, each pulse will have somewhat lower V than preceding pulses. For the design of Fig. 4, Fig. 7 shows the result for 700 kV (all beam out), and 600 kV (substantial loss). Note the general result that in the injector, lower voltage beams focus sooner; a B field guide system designed for 800 kV has some tolerance, but will not work at 600 kV.

A design for d = 7 cm was also completed, see Fig. 8. Besides the felt turn-on problem, the necessarily larger beam is harder to focus; note the larger V_r and V_θ in Fig. 9. However, this is a possibly viable option, especially if the wall radius of the small tube (1.5 cm here) can be increased.

III. Recirc (RLA) Studies

Earlier work on Recirc injectors was described in Ref. 5, Sec. III, where TRAJ studies of cold (foilless) diodes at 1.7 MV and 4 MV were described. In part A, we continue this work; perhaps the main element added is realism, in the sense of simulating actual hardware and designs now being considered; we have also added, in some cases, a calculation of the leakage, or throwaway, current. All these "cold" diodes involve magnetic transport of the beam to the foil separating the injector from the racetrack.

Another approach studied this year (part B) was the foil diode system, without applied B. The experiments have used this approach so far; instead of a coil system one uses IFR transport from the diode to the racetrack. Unfortunately, both approaches utilize at least one foil, with possibly serious consequences for emittance increase.

A. Foilless Diodes Plus B_z Transport

One of the best results to date for the diode and transport system at low voltage is shown in Fig. 10. The B field (a,b) is due to five coils and a solenoid; the value at the cathode (axis) is 89 G (could be reduced with a bucking coil). The applied potential V = 1.3 MV, based on what the (old) machine will deliver; the non-flatness of this pulse will probably be a problem. Part (c) of Fig. 10 shows the potential distribution with beam. The beam in part (d) expands, pinches, then expands again before hitting the foil at z = 140 cm; the beam here is of good quality, but past the foil pinches sharply and acquires a $\beta_\perp = 0.18$; this is not necessarily significant since the region past the foil is the transition to the racetrack curved channel and is not modeled correctly. We have included this short region past the foil in some TRAJ runs to illustrate that this region needs study; it is of little value to produce a good low-emittance beam if one then sends it through a foil/gas section where it acquires a large $\beta_\perp$. BUCKSHOT runs of this region are being done by J. S. Wagner (1241).

The run in Fig. 10 is the endpoint of a large number of parameter variation runs. Many of these runs involved moving the coils and varying their currents. The effect of increasing the solenoid current is that the beam focuses sooner. Variations in the current and position of coil 1 (nearest the A-K gap) show that 2 kA more or less causes overfocus or underfocus and beam loss; the z-position of coil 1 is also crucial. Of course, one gains more control if this coil can be near the A-K gap, but the price is a large $B_z(K)$, which leads to a large rotation. If this is not acceptable, bucking coils may be used in the cathode. The price seems to be increased beam sensitivity. The preliminary studies in Ref. 15 contain details of these variations about Fig. 10.

About 20 earlier runs with this same setup concentrated on trying to obtain a good beam at higher current (5.6 kA). Several examples are given in Ref. 15. The results are quite sensitive to parameter variations; in most cases the beam hit the corner or the wall. The problem is simply that 5.6 kA is too much current for this system; the beam is large radially and comes too close to the walls and coils to be easily controlled. Higher voltage is needed.

Other Recirc diode/transport systems were studied, for somewhat different geometries and voltage. At slightly larger voltage V = 1.7 MV we can control more current as shown in Fig. 11. The system is also slightly shorter; three coils and a solenoid were found to be sufficient. Comparing with Fig. 10, note that even a small increase in voltage helps (Pierce inserts have not been tried yet). As before, the region past the foil at z = 126 cm is treated as a vacuum, but this region needs separate study. A check of the forces near the pinch ($z \approx 1$ m) shows that all four (E_r, B_θ, B_z, centrifugal) are important. Spreading the coils axially, as would be necessary in reality, does not have much effect (see Fig. 11d, where the three coils were each divided into two coils carrying half the current and separated by one or two cm).

Another variation of the geometry is shown in Fig. 12. Here three coils and two solenoids were used in a slightly longer system. The maximum radial angle at the rhs foil is 1.7°, a nice beam (but the beam was only followed up to the foil). The current in the first solenoid needs to be controlled to about 50 A, and the voltage to better than 100 kV, as found by further TRAJ runs. Going to 1.3 MV causes a large beam loss. We have already studied a system which does reasonably well at 1.3 MV and 3.3 kA (Fig. 10); a simpler way around the sensitivity problem is to settle for less current. For I = 1.9 kA, for example, a good result was obtained on the first try, unlike the higher-I cases where the coil system always had to be tuned. The beam in this case is generally better, farther from the corner, and less sensitive to parameter variations.

Nevertheless, many runs were made in an attempt to generate a higher current beam at 1.3 MV. The best of these beams still skims the corner and fills the pipe near the exit foil. A slanted anode wall was tried, but the advantage of reducing the space-charge potential did not appear to be significant. The basic lesson seems to be that higher V and lower I are easier to work with; if one insists on the opposite combination then it pays to reduce the A-K gap d to as small a value as possible, consistent with non-emission except over $r < r(\text{emit})$, because this allows the desired I to be generated over smaller area; the beam stays farther from the walls and coils and is easier to control.

At 4 MV, the problem becomes easier, for reasonable currents, say $\lesssim$ 10 kA. Figure 13, for V = 4 MV, I = 7.2 kA, produces at the rhs foil a beam with rms $\beta_\perp = 0.042$, r = 1.9 cm. If the coil system is held constant and the voltage V is varied, Fig. 14 shows that as V increases, I increases and the first pinch point moves away from the cathode until the trajectories become nearly straight (5 MV, Fig. 14d). (Note there are really two pinch effects here; the first is due to the focusing B_z field, and focuses higher γ at larger z, according to Eq. (6) of Ref. 3; the second happens only at the higher V values, due to B_θ pinching at higher I as discussed on p. 8 of Ref. 3. Pierce inserts would not help in the latter cases.)

If we add 40 cm of vacuum past the foil (rhs), the beam of course pinches, then expands radially as in Fig. 15a. Reducing the current in the first solenoid, as in Fig. 15b, causes the beam to defocus somewhat and hit the foil at larger radius, but the basic result is the same: foil pinch and expansion. To improve this situation, two methods were tried.

In the first method, with a B field as in Fig. 16a, one might try to prevent the foil pinch.[21] With $B_z(\text{max}) = 5$ kG (Fig. 16b), some beam is lost and some pinch persists. Doubling the applied B (Fig. 16c) eliminates the pinch; but now the electrons expand after the foil because they follow the lines of the strong B.

The second method introduces an IFR channel in the region past the foil, and the result is shown in Fig. 17. Using the B field of Fig. 13, an IFR zone with neutralization fraction f = 1 does not change the trajectories up to the foil, but after the foil the beam pinches tightly and stays at small radius (2-cm rms output with $\beta_\perp = 0.1$). Of the two methods, this is clearly preferable; however, the final beam in the channel will be warm: $\beta_\perp \approx (\nu/\gamma)^{1/2}$.

Another cold diode design at 4 MV was studied in late 1988. Here we tried to include more realism, such as cathode shank effects on the emitter electric field, neglected previously in TRAJ runs. Figure 18 shows the best result, an 8.4-kA beam which reaches the foil (rhs) with rms r = 2.8 cm, $\beta_\perp$ = 0.083 (mostly in rotation). There are two solenoids and two focus coils, at z = 51 and 140 cm (Figs. 18a and b). Note the cathode corner has been "rounded off" (Fig. 18c); this increases $|\vec{E}|$ on the cathode face somewhat, increasing the current I by 0.6 kA (the opposite of a Pierce insert in this regard). The cathode is assumed to emit out to r(emit) = 7.2 cm, resulting in the beam of Fig. 18d.

However, JASON runs by M. G. Mazarakis (1242) showed rather high $|\vec{E}|$ on the "non-emitting" portions of the cathode, so MAGIC runs were made to check the effect of allowing the entire cathode to emit. First MAGIC was run for the same setup as in Fig. 18; the same answer was obtained, even in detail, after MAGIC reached a quasisteady state (Fig. 19a), except that the severe resolution problem with this large system led to a grid instability near the rhs. Next, emission was added from the rest of the cathode, but the resolution was inadequate, so a reduced system was studied, using the same applied B (Fig. 18a). To simulate the worst case, the cathode corner was not rounded. The result in Fig. 19b includes an aperture to bring the beam current down to near the desired value, but the main point is the leakage current of 70 kA, which originates on the shank and hits the anode corner. In short, this injector design will produce a reasonably good beam, but most of the current will be thrown away in leakage loss (~60%), or must be apertured out (~30%). Note from the phase spaces in Figs. 19c and d that the aperture removes the "hot" part of the beam in both r and θ.

B. Foil Diodes Plus IFR Transport

Figure 20 shows a simulation of a recent experimental setup. The latest version of MAGIC was used, including the slanted-surface algorithms of T. D. Pointon (1265). The voltage V is clamped at 1.5 MV via a radially inward TEM wave from the top at R = 20 cm; this leads to a small TM_{010} cavity mode oscillation (± about 10%, period 1.7 ns) in V at the A-K gap, but a good macroscopic steady state is reached anyway for $t \gtrsim 5$ ns, with a 2-ns rise assumed on V(t). In fact, the same result is found for "outgoing-wave" boundary conditions at R = 20 cm, with less ringing; but, one must guess the input wave amplitude. The results in Fig. 20 are I = 11.9 kA (total), of which 9.1 kA originates on the shank including the big slant, and 2.4 kA comes from the small slant near the tip. To be more precise, the electron sheath currents at the z locations of the four cathode corners in Fig. 20 are, left-to-right: 2.7, 4.4, 9.1, and 11.4 kA. The distribution on the anode foil has most of this current near the outer radius; in fact, the distribution agrees with the measurements.[22]

It is interesting that this relatively nice beam can be generated without applied B_z, but unfortunately it will be seriously perturbed in passing through the rhs foil into the IFR cell, as found by separate TRAJ runs. Here the input beam pinches tightly and expands to fill the tube; the output $\beta_\perp$ is much larger than the input. This result is not very sensitive to the details of the input beam; cases with cold input, warm input, and charge neutralization fraction f changed from 1.0 to 0.5 all yield about the same answer.

Another Recirc foil diode is shown in Fig. 21. This is the MAGIC run of a recent experimental setup, with a small gap d = 1.25 cm, so that at 1.5 MV we get I = 22.5 kA passing through the thin foil at z = 25 cm. Beyond the foil we have included a section of the gas cell, modeled as a region of charge neutralization (f = 1). Again we note the tight foil-induced pinch and the beam heating. Note from Fig. 21a (and the blow-up version in 21b) that this setup apertures out the shank current; of the 22.5-kA diode current, only 6.5 kA reaches z = 40 cm, and this part is hot: $\beta_\perp \approx 0.3$, in agreement with $(\upsilon/\gamma)^{1/2}$. Although the diode itself works well, this is not the way to generate a high-quality beam.

Some parameter studies were made; more detail is given in Ref. 15. Some of these runs are listed in Table I. Run 4 used a diode with tapered stalk and outer system radius R = 10 cm. The current is about the same as for the straight stalk, Run 5, suggesting that a tapered region does not actually contribute much current to the beam. For the small-gap straight-stalk case of Run 6, of course, more I results and a smaller beam.

The Runs 7-9 show the effect of increasing voltage V. As expected, I increases and the beam becomes smaller. An even smaller beam obtains for smaller gap (Run 10). Note these cases have a slanted-tip cathode; the angle is 45° to try to represent a rounding-off. Run 15 is like Run 12 except for the tip shape. The currents (7.8 kA) and flows are so similar that we conclude there is no substantial effect of "rounding-off" the tip.

The purpose of Run 17 was to compare new and old MAGIC (with and without slant emission)(see Run 5). We checked V, I, beam angle, and a number of computer parameters (number of particles, energy conservation, etc.). The typical differences were 1 or 2%; the largest difference was in the output beam edge radius: 7% smaller in new MAGIC.

Runs 18-22 used an outer R = 20 cm (see Figs. 20, 21). This is found to be important; comparing Runs 12, 4, 18 for R = 5, 10, 20 cm, respectively, we obtain I = 7.7, 10.0, and 11.9 kA. Thus for purposes of comparing with experiment the "realistic" R = 20 cm cases should be used. The reason for this increasing I with R is suggested by Jason code runs done by M. G. Mazarakis; as R increases, the equipotentials move closer to the shank, i.e., the E field increases. The implication for MAGIC runs is that $E_z(z,R)$ cannot be taken as constant (as in the clamped-V option) unless $R \gtrsim 20$ cm. This seems reasonable since the injector length is L = 25 cm.

Another possible experimental setup (IBEX foil diode on Recirc) was considered in Dec. 1988. These runs 4I, 5I, and 7I of Table I are nominally 4 MV, and as in Fig. 21 we wish to aperture out the hot shank electrons. A large gap (d = 10 cm) and no aperture lead to a large-radius, hot beam (see Fig. 22a, Run 4I); a small gap (d = 2 cm) and an aperture to r = 8.7 mm yield a small warm beam at about the desired current, 11 kA (see Fig. 22b, Run 7I). In this latter case we have produced a fairly good beam without B_z, with less wasted current than in the large-K system of Fig. 19b. Note that the current in Fig. 22b originates near the cathode tip, unlike the setup in Fig. 20; however, in all cases with small d and small cathode radius, we end up with a small beam with (after equilibration in the IFR) $\beta_\perp \sim (\nu/\gamma)^{1/2}$.

Table I. Recirc foil-diode runs with MAGIC. $B_z = 0$.
All runs with "new" MAGIC except 5 and 6.
Cathode notation: Sl = slant, Sq = square, Str = straight.

Run	Cathode		d(cm)	R(cm)	V(MV)	I(kA)	Comments
	Stalk	Tip					
4	Sl	Sq	3.2	10	1.45	10.0	Shank 8.2 kA
5	Str	Sq	3.2	10	1.4	10.4	Compare 17
6	Str	Sq	1.0	10	1.4	18.0	Small beam
7	Str	Sl	3.0	5	1.1	6.0	Vary V
8	Str	Sl	3.0	5	1.45	8.3	Vary V
9	Str	Sl	3.0	5	1.75	10.5	Vary V
10	Str	Sl	1.0	5	1.0	12.0	Vary d (see 7)
12	Sl	Sl	3.2	5	1.43	7.7	
15	Sl	Sq	3.2	5	1.40	7.8	Compare 12
17	Str	Sq	3.2	10	1.4	10.2	Compare 5
18	Sl	Sl	3.2	20	1.5	11.9	Compare 12
19	Sl	Sl	3.2	20	2.45	17.7	
20	Sl	Sl	3.2	20	1.45	11.2	Outgoing wave bc
22	Str	Sl	1.25	20	1.5	22.5	Exper. setup
4I	Str	Sl	10.0	15	3.2	26.0	Large d
5I	Str	Sl	2.0	15	4.0	48.0	
7I	Str	Sl	2.0	15	4.0	48.0	Aperture to 11 kA

In summary, both foilless diodes (with B_z) and foil diodes (no B_z, with IFR) have been studied using TRAJ and MAGIC. Each type has advantages. Overall, it seems better to go with the "cold" foilless non-immersed design (Fig. 18), and use IFR transport past the foil (Fig. 17), unless the entire cathode emits (Fig. 19b). If this emission cannot be avoided, then one may as well use the foil diode setup with small cathode and gap and no B_z (Fig. 22b). Given the Recirc constraints, there may be no way to avoid an IFR-induced $\beta_\perp$, in which case the need for a careful "cold" design becomes dubious.

IV. RADLAC and IBEX Studies

A great deal of simulation work with MAGIC and TRAJ was done for various elements of the RADLAC and IBEX experiments. Here we summarize the main results and refer to other documents for details. In parts A-E we discuss, respectively, RADLAC diodes, IBEX diodes, RADLAC accelerating gaps, the question of adiabatic beam expansion, and finally B_θ conditioning cells for both machines.

A. RADLAC Injectors

The purpose of this part is to document recent MAGIC runs of the RADLAC II feed-plus-diode system. The essential results are summarized in Table II and the accompanying figures. Various cathode shapes were tried, and generally the smallest ones had the least loss. The nominal voltage is 5 MV, but due to reflections and long L/R time, the full value was not reached in all cases. (Only final, quasisteady values are reported here.) I_{beam} (see Table II) refers to the current out the rhs in the figures; I_{loss} to the current striking any metal surface.

Numerically speaking, the diode gap is not well resolved in these simulations, in order to simulate the entire feed region. The beam currents seem reasonable, but an accurate diode simulation requires isolating the A-K gap region, as done in the past. The value of the runs lies in the calculation of I_{loss} for the whole feed. Figure 23 shows what may be the best result. (See Run 29 of Table II.) The applied B lines in Fig. 23a are based on the measured data; Fig. 23b shows $B_z(z)$ near the axis. This field was used in most of the runs. Figure 23c shows the electron flow. The 13 kA loss is in a thin radial beam originating on the cathode at the place where the B_z field becomes too weak to insulate the sheath. To the left of this place, the B_θ is large enough for insulation.

By using a small straight stalk (Runs 14, 16, and 26) we find even smaller loss, 11 kA, but the inductance is higher. The field is essentially the same, and the loss occurs at about the same position on the r_k = 9 mm stalk. The result for Run 14 is shown in Fig. 3 of Ref. 6.

Using a larger taper angle than 4° (Fig. 23) leads to more loss (Runs 20, 23), as does the old large-block cathode; see Fig. 2, Ref. 6. More details can be found in Ref. 12.

Table II. RADLAC Feed/Injector MAGIC Runs

Run	K shape	B(appl)	d(cm)	V(MV)	I_{beam}(kA)	I_{loss}(kA)	I_{total}(kA)
14	Skinny Stalk	Exp.	0.6	4.0	46	11	57
16	Skinny Stalk	"	0.6	5.0	56	12	58
26	Skinny Stalk	"	1.0	5.0	55	10	65
29	Taper 4°	"	1.2	4.75	45	13	58
20	Taper 8°	"	1.0	5.0	42	37	79
23	Taper 8°	"	2.0	5.0	33	42	75
24	Short Step	"	1.0	4.5	38	42	80
22	Long Step	"	1.0	5.0	46	74	120
31	Taper 4°	Large-r coils	1.2	5.0	36	14	50
35	Taper 4°	Exp.	1.2	3.3	30	11	41
42	Taper 4°	"	1.0	3.0	32	9	41
52	Taper 4°	"	1.0	4.8	62	13	75
50	Taper 4°	"	1.0	4.7*	63	5	68
44	Taper 4°	0	2.4	4.0	49**	0	49
43	Taper 4°	B_o***	2.4	4.2	33	14	47
45	Taper 4°	$2B_o$	2.4	4.4	25	23	48

* Split voltage run

** Beam hits wall of drift tube

*** The usual experimental field (Fig. 23a, b)

By adding coils at large radius as in Fig. 24a, we can eliminate the radial loss (compare Fig. 24b with 23c). However, the loss for this case now occurs near the drift-tube entrance, and the beam has a "halo." It does not seem worth the extra and very considerable field energy to pursue this approach. Of course, by varying the currents and locations of the large-radius coils one could in principle reduce the loss; the ultimate coil system would produce B lines exactly parallel to the cathode surface. However, the $B_z(z)$ must match to the 20 kG applied in the accelerator.

The experiments with a 4° taper cathode showed only a few kA loss, so a number of variations of Run 29 (Fig. 23) were made. These included changes in V, B(applied), A-K gap, tip shape, and mesh refinements. None of these, e.g. Runs 31, 35, 42, and 52 of Table II, reduced the loss much, including cases with lower V and I. All these cases applied the voltage via a TEM radial wave, as in Fig. 25a, b (Run 52). Examination of the details of the injector construction showed that a more accurate model would apply about half the voltage radially, and half axially (from the rhs) as in Fig. 25c, d. Comparing Figs. 25b and d, both give about the same total V on the cathode tip, so it is not surprising that the beam currents are the same. On the shank, however, Fig. 25b clearly shows more $|\vec{E}|$ near the leakage point than Fig. 25d. The result is that the split V model yields a smaller loss current, more in agreement with the experiment. The lesson is that when calculating the entire feed, care is needed in applying the voltage.

In Runs 43-45 (Table II) we look at the effect of the magnitude of B(applied) on losses (shape of B as in Fig. 23a). For no B(applied), the shank is well insulated everywhere as expected (see Fig. 26a), but the entire beam expands to the drift tube wall within about the first 20 cm of z-length. As the magnitude of B(applied) increases, the beam propagates but the shank loss increases and the loss point moves back along the shank (Fig. 26b). These effects are due to suppression of shank emission near the cathode tip, leading to less beam and thus less B_θ on the shank.

Since the diode gap region in these runs is not well resolved, if we wish to calculate beam emittance it is necessary to focus on the tip region, as generally done in previous studies.[1,2,4,6] Table III summarizes the main runs. For details, see Refs. 16 and 17.

Figure 27a shows a 40 kG, r_k = 6.4 mm diode in steady state. The parameters are given in Table III, Run 21. A rather nice 40-kA beam with $\beta_\perp = 0.094$ is produced. About 9000 particles were used for a system length L = 16 cm (chosen to get a few cyclotron wavelengths). For the same geometry but B_o = 20 kG (Run 20), the emittance is more than doubled and the radial oscillations nearly reach the wall; 20 kG is too weak for small r_k. Figure 27b shows the larger r_k case to 20 kG. Note the low $\beta_\perp = 0.066$.

The present RADLAC diode is characterized by an r_c = 9 mm cathode radius, producing an annular beam of nominally 5 MeV, 40 kA. The recent problems with the new coils lead to the need to examine the system when the old coils are in place. The applied $B_z(z)$ at r = 0 used in MAGIC is shown in Fig. 28a; the reasonably good match to experiment was obtained by simply trying different sets of coils. Figure 28b shows the resulting B lines and the problem set-up. Whether the B field agrees with the experiment at places other than the beam path is irrelevant.

Table III. RADLAC Diode Runs (MAGIC).

All cases used V = 5 MV.

r_k, R, r_{tu}, r_b are radii of cathode, outer wall, tube wall, beam (rms).

Run	B_z(kG)	r_k(cm)	Δr_k(cm)	R(cm)	r_{tu}(cm)	d(cm)	I(kA)	$\beta_\perp$	r_b(mm)
9	20	0.9	0.3	7	1.6	0.64	87	0.15	9
11	20	0.9	0.3	7	1.6	3.0	38	0.06	9
12	20	0.9	0.3	7	1.6	1.26	63	0.11	8
14	20	0.9	0.9	7	1.6	1.16	67	0.12	8.3
16	20	0.9	0.9	7	1.6	3.06	39	0.08	9
17	20	0.64	0.16	4	1.2	1.26	57	0.11	6.5
18	20	0.64	0.16	4	1.6	1.26	50	0.13	6.7
20	20	0.64	0.16	4	0.96	2.0	46	0.17	7.7
21	40	0.64	0.16	4	0.96	2.0	40	0.094	6.3
23	20	0.9	0.22	4	1.6	2.3	50	0.11	8.9
24	20	0.9	0.22	4	1.6	3.0	45	0.066	9.1
25	20	0.9	0.22	4	1.6	4.0	42	0.095	9.1
26	20	0.9	0.22	7	1.6	3.0	39	0.061	9.1
27	16	0.9	0.3	7	1.6	2.0	51	0.14	9.7
28	16	0.9	0.3	7	1.6	3.0	41	0.12	9.3
29	exp.*	0.9	0.3	7	1.6	3.0	41	0.20	10.0
30	exp.**	0.9	0.3	7	1.6	3.0	40	0.15	10.0
31	~~25~~ 17 exp.	0.9	0.3	7	1.6	3.0	38	0.09	8.3

*Rough approximation to experiment

**Good approximation to experiment

The resulting 5-MeV, 40-kA beam is seen in Fig. 28c. The loss (backward flowing electrons at z = 0) is not accurately modeled, but in fact agrees roughly with previous runs (Run 29, Table II) including the entire shank. The output beam (not phase mixed) has rms values $\beta_\perp = 0.15$, r = 1.0 cm (see Table III, Run 30). For comparison (see Ref. 16, Fig. 4 and Table III, Run 26) if the new coils produced uniform 20 kG, we would obtain $\beta_\perp = 0.06$ for the same d, V, and I. Thus, we are paying a substantial price by using the old coils; according to MAGIC the emittance is over twice as large. However, the beam of Fig. 28c is usable, if later sections of RADLAC do not add appreciable emittance.

In Fig. 28d we see the result of using the old coils, but with the coil currents increased by 25/17, to give B_z(max) = 25 kG. As expected, the higher field yields a better beam (Run 31 of Table III). The current is 2 kA less, due to suppression of some shank emission. Apparently the magnitude and uniformity of B_z are both important.

The conclusion is the same as stated many times previously: a strong uniform field produces the best beam inside the accelerator. The only price is an increase in canonical P_θ; for B_z = 25 kG and the geometry of Fig. 28 and γ(final) = 40, the final rotation after extraction will be 0.165 c (for final radius 9 mm) to 0.24 c (for final radius 6 mm, the cold beam matched value).

B. IBEX Diodes

These are MAGIC studies with the goals of producing a low-emittance, high-brightness beam, and comparing with the measurements. Regarding the latter, where checks have been made the code predicts current quite well, and $\beta_\perp$ seems reasonably close, considering the uncertainties. Table IV gives the main simulations; some details on the earlier ones can be found in Ref. 14.

Figure 29 (Run 17, Table IV) shows one of the best beams ever obtained, in both code and experiment.[23] The small r_k = 6 mm and B_0 = 24 kG produces 28 kA with $\beta_\perp = 0.07$ at 3.5 MeV. The emittance here (inside the uniform 24 kG) is smaller than any case with the older r_k = 9 mm; upon extraction the rotation (max) will be c/2, however, if r_b does not change. The question arises as to how far the small-r_k technique can be pushed.

By going to larger gaps and smaller r_k = 3.2 mm, we obtain Runs 22-25 of Table IV. The $\beta_\perp$ is larger, but this is more than compensated by the smaller r_b and final rotation after extraction. Note that a larger drift tube is used, so that these runs are near I_{SCL} = 17 kA. Figure 30 shows the d = 5 cm case for Runs 22, 23 at 22 and 16 kG; the higher field case (Fig. 30a) has about a factor two lower emittance (inside the field).

Figure 31 shows the beam for a tiny (solid-tip) cathode (Run 27). The beam current is reduced (12 kA), but $\beta_\perp$ is not greatly increased, and the final rotation will be about c/6 (max). Of course, such a small beam would have space-charge-limit problems in RADLAC, but if high brightness is the main concern, these small-cathode diodes may be the best approach.

Table IV. MAGIC Runs of IBEX foilless immersed diodes.

All cases used V = 3.5 MV except 12, 13 (4 MV).

run	r_k(cm)	d(cm)	r_{tube}(cm)	B_z(kG)	I_{tot}(kA)	I_{shank}(kA)	β_{e-}	Comments
1	1.0	0.6	2.0	10	59	44	0.32	large radial oscill.
2	0.91	1.6	2.0	10	37	28	0.11	good beam
3	0.91	1.6	2.0	10	38	27	0.12	DZ/2 test
5	0.95	2.0	1.9	7	39	30	0.20	B_z too small
6	0.95	2.0	1.9	10	34	26	0.10	
7	0.95	2.0	1.73	10	35	26	0.09	varied r(tube)
8	0.95	5.0	1.73	10	22	17	0.06	big gap, better beam
9	0.95	2.0	1.73	6	42	33	0.2	12 kA loss
12	0.63	1.0	1.73	24	32	22	0.13	small δR
13	0.63	1.0	1.73	24	33	21	0.15	DZ/2 test
14	0.63	1.5	1.73	24	31	22	0.10	
15	0.63	1.0	1.73	24	40	28	0.14	near I_{SCL}
17	0.63	2.0	1.73	24	28	21	0.07	great beam
19	0.63	2.0	1.73	12	33	27	0.17	scrape limiter
18	0.32	1.0	0.87	12	40	33	0.18	28 kA loss
20	0.32	1.0	0.87	24	33	27	0.17	
22	0.32	5.0	3.0	22	15	11	0.13	r_b = 3.2 mm
23	0.32	5.0	3.0	16	16	13	0.19	r_b = 4.0 mm; at I_{SCL}
24	0.32	10.0	3.0	16	15	12	0.13	r_b = 3.8 mm
25	0.32	10.0	3.0	22	14	11	0.09	r_b = 3.2 mm
27	0.16	7.0	3.0	22	12	11	0.17	r_b = 2.1 mm

C. RADLAC Gaps

There are two issues to be considered here, gap leakage currents and beam emittance growth. The former is a straightforward MAGIC calculation, assuming a uniform 20-kG field. A steady 2.5 MV was applied to the first accelerating gap, and the leakage calculated for beam currents I_b = 0, 20, and 40 kA. The result is seen in Fig. 32a (0-kA beam), and 32b (40-kA beam); with no beam we find 10-kA leakage from the stickout and 13 kA from the main area, with a 20-kA beam the stickout emission is partly suppressed to 4 kA, but the main area leakage is the same, and with a 40-kA beam the stickout emission is fully suppressed while the main area leaks about 10 kA. In short, for I_b = (0,20,40) kA the leakages are (23,17,10) kA. These calculations are pessimistic in assuming a low threshold for emission on all surfaces (10 kV/cm). Nevertheless, the results indicate the importance of suppressing gap emission. The leakage from the stickout at 20-kA beam current would be a problem if these electrons were accelerated through the system as a low-energy halo.

The goal of the emittance-gain simulations is to find the increase in $\varepsilon = r\gamma\beta_\perp$ for a beam traversing one or more accelerating gaps, as a function of input beam parameters, gap parameters, or applied magnetic field. Both MAGIC and TRAJ were used, and the comparisons showed, somewhat surprisingly, that TRAJ is more accurate than MAGIC for this type of problem, and, of course, much more efficient in terms of computer time.

Figure 33a (MAGIC) illustrates the type of grid instability one encounters if the grid is too coarse, and also shows the problem set-up. A 40-kA, 5-MeV (total energy) beam with $\beta_\perp$(rms) = 0.11 is injected from the lhs and passes through two gaps with 2.5 MV on each. The applied Bz is uniform at 20 kG. The $\beta_\perp$(out) is 0.15, but from this run alone we cannot tell what part of this is due to real emittance growth caused by the gaps, and what part is numerical. The problem is not due to the "diagonal" model in MAGIC, because a rerun with a stair-step gap wall yields about the same result.

One possible cure is to use standard smoothing techniques to reduce the short-wavelength noise. Such a method has been used in Fig. 33b, which is otherwise the same system as Fig. 33a. Note the great improvement; the instability is almost gone (but not quite). Here $\beta_\perp$(out) is only 0.065 (compared with 0.11 input); the product $\gamma\beta_\perp$ (proportional to emittance) is nearly conserved, i.e. no emittance gain in two gaps. But now the question is, in damping the grid noise have we also damped the real physical emittance gain?

Returning to Fig. 33a, this case was rerun with the grid spacing in z halved, and stair-step boundaries (due to limitations on the diagonal model). The grid instability was still present, but somewhat mitigated. Here the resulting $\beta_\perp$(out) = 0.084 (compared with 0.12 input); see Table V. The obvious next step is to reduce the grid spacing further until the answer doesn't change; however, reducing the z-spacing another factor two puts us over the storage limit. The next best thing is to study only one gap at a time. These results are shown in Table V (all cases except first).

Figure 34a shows a one-gap case for the same beam, gap, and applied field parameters as before. We have chosen to study the first gap on the assumption that it will cause the largest emittance increase. The phase-space plots show that the grid effects are now small (not gone, however). In Fig. 34, we have also included gap emission, leading to an 11-kA loss, a substantial parasitic current,

which agrees well with the above leakage runs (Fig. 32) where the main area always leaked 10-13 kA. However, this will only occur if the gap surface is allowed to emit. An idea of the numerical noise present is shown in the Ez(z) plot, Fig. 34b.

The effect of changing the gap shape was studied by running a square gap. The beam behavior is quite similar, even though the shape of the accelerating field Ez(z) differs considerably. From Table V, there is little difference in the emittance increase; however, it is difficult to tell what part of the gain in $\gamma\beta_\perp$ is numerical, because lack of serious instability does not guarantee accuracy.

The last two cases in Table V show the results with warm and hot input beams. Of course a hotter beam spreads radially and the phase space patterns are thicker. Note from Table V that warmer beams have a smaller relative emittance gain.

Another approach to the problem is to use the trajectory code, TRAJ. Modifications were made to allow random $\beta_\perp$ input. Figure 35a shows every fifth trajectory for cold input beam in the converged solution for the first two RADLAC gaps, with the corresponding equipotential lines in Fig. 35b. Cray running time here is 4 min., as opposed to about an hour for the MAGIC runs. The mesh is 225(z) by 66(r). There is no particle/grid interaction in a trajectory code, so there is no grid instability; there are still questions of accuracy, of course, since finite difference methods are still employed. But, the results were found to be independent of mesh size and number of trajectories (within reasonable limits). From Table VI, which summarizes the TRAJ two-gap RADLAC runs, the output $\beta_\perp = 0.017$. Note that in this table we show the change in $\gamma\beta_\perp$, not $\gamma\beta_\perp r$, because with the uniform 20 kG applied, the change in r is negligible.

Figure 36 shows a warm-beam case; this is the TRAJ version of the "two-gaps" case of Table V, where the output $\beta_\perp$ is 0.084, somewhat larger than the 0.069 result in Fig. 36. The tentative conclusion is that the noise and grid effects in MAGIC cause an artificial emittance increase of about the same magnitude as the "real" one (see Table VI). With MAGIC, $\gamma\beta_\perp$ increases by 30%, with TRAJ by 13%. However, recall that TRAJ is strictly an equilibrium code; the actual system will have some physical cavity modes, voltage variations, etc., so that "reality" may lie between the two calculations.

Note from Table V or VI the general result that hotter beams have relatively smaller emittance increase. This is not to say that hotter beams are better; of course the goal here is still to minimize $\beta_\perp$, so cold beams are always better in this sense. It is of interest to note from the last column of Table VI that hotter beams have relatively more of their temperature in θ-motion, and less in r-motion, than cooler beams.

The physical conclusion is that an input beam of good quality will not acquire a fatal amount of emittance in passing through the first two RADLAC gaps; later gaps should be even less of a problem because of the higher γ. Typically the $\beta_\perp$ values should decrease with gap number, although $\gamma\beta_\perp$ apparently always increases. The numerical conclusion is that for equilibrium studies of the type reported here, TRAJ is better than MAGIC, although electromagnetic and time-dependent effects must still be studied with the latter.

Table V. RADLAC MAGIC Runs:

emittance growth in one or two gaps.

Beam: 5 MeV, 40 kA, $r_b = 1$ cm.

$B_0 = 20$ kG. V = 2 1/2 MV/gap.

Case	$\beta_\perp$		$\gamma\beta_\perp$	
	In	Out	In	Out
2 gaps	0.12	0.084	1.0	1.3
1 diag. gap	0.083	0.077	0.71	1.0
1 sq. gap	0.082	0.080	0.71	1.0
warm beam	0.16	0.12	1.38	1.54
hot beam	0.25	0.18	2.1	2.3

Table VI. RADLAC TRAJ Runs:

emittance growth in two gaps.

Applied fields: $B_0 = 20$ kG; 2 1/2 MV/gap

Beam: 5 MeV, 40 kA, $r_b = 1$ cm.

In the last column, the fraction of $\beta_\perp$ in rms radial motion is shown.

$\beta_\perp$		$\gamma\beta_\perp$		$\beta_r/(\beta_r+\beta_\theta)$
In	Out	In	Out	Out
0	0.017	0	0.28	85%
0.024	0.026	0.21	0.42	63%
0.059	0.041	0.51	0.66	58%
0.118	0.069	1.01	1.14	50%
0.198	0.107	1.70	1.81	42%

Next we use TRAJ to study the first accelerating gap with the actual non-uniform applied B field. As input we inject a 40-kA, 5-MeV beam (3.9-MeV kinetic, 1.1-MeV potential) with rms radius 8.3 mm, and apply 2.5 MV to the gap. Since beam radius can now change, emittance will be measured by $r\gamma\beta_\perp$.

As a basis for comparison, Fig. 37a shows a case with cold input beam and uniform 17 kG. The gap geometry is as before based on the actual design; the tube radius increases from 1.6 to 1.9 cm to help reduce the amplitude δR of radial oscillations induced by the gap. In Fig. 37a this amplitude δR is very small and $\beta_\perp(\text{out}) = 0.028$. The case of no applied B at all is given in Fig. 37b; the beam blows apart and hits the wall.

In Fig. 38a we plot the "actual" $B_z(z)$ on axis as obtained by trial-and-error placement of coils. The values agree within a few percent with the recent measurements. For a cold beam input the equilibrium is shown in Fig. 38b; comparing Fig. 37, the actual B_z leads to larger δR and $\beta_\perp(\text{out}) = 0.079$. For reference, Figs. 38c and d give the vacuum and final potentials (normal derivative boundary conditions, i.e., $E_z = 0$, were applied at both ends). Note that the applied E field is concentrated in the gap region.

A number of cases were run with warm input beams. For each case, both the actual B and a uniform B were used. Table VII shows the results. The equilibrium beams for the case of input $\beta_\perp = 0.15$ are given in Fig. 39. For the warm beams in Table VII the uniform field ($\beta_\perp$ decreases) gives a much better result than the actual field ($\beta_\perp$ increases). (But even for the uniform field, the emittance $r\beta_\perp\gamma$ increases, as it must.) For the hot beams the uniform-field result (Fig. 39) is only slightly better, and $\beta_\perp$ decreases in both cases. If the field magnitude is scaled up to 25 kG, it does not matter much whether the field is uniform or not. Note that for a warm beam, scaling up the field can compensate for non-uniformity.

The conclusion of the first-gap studies is that for the warm beams ($\beta_\perp \approx 0.08$) we hope to achieve, we pay a price in emittance growth by having a substantial dip in B_z at the gap (Fig. 38a). For hotter beams, it becomes less important to shape the B at the gap carefully, and for such beams there is little value in increasing the magnitude of B. For cold beams, the higher the field, the better. If low emittance is the main concern, there seems to be no substitute for high or uniform fields, preferably both, both on the gap and in the diode.

D. RADLAC Beam Expansion

The purpose of this study is to answer the question: Is it better to make a small-r_k high-brightness diode at $B_0 = 40$ kG and then adiabatically expand the beam to larger radius, or should we simply design a larger-r_k diode at $B_0 = 20$ kG in the first place? The relevant diodes are shown in Fig. 27.

For the beam expansion problem we use TRAJ, and begin with the output beam of Fig. 27a. This beam is in a $B_z = 40$ kG, and we wish to expand it into 20 kG. If this change is made over a short scale length, of order one cyclotron wavelength as in Fig. 40, the beam oscillates. On average the electrons follow the B lines, so $r \propto B^{-1/2}$, but there is overshoot and the finite cyclotron radius is clearly seen for this cold initial beam. Warm beam cases are shown in Fig. 41, and other runs are summarized in Table VIII.

Table VII. RADLAC First Gap Runs, TRAJ

Input beam: 40 kA, 5 MeV. U = uniform, V = gap voltage.

B_z	V_{MV}	$\beta_\perp$ in	$\beta_\perp$ out	r(mm) in	r(mm) out	$r\beta_\perp\gamma$ in	$r\beta_\perp\gamma$ out
U,17kG	2.5	0.0	0.028	8.3	8.0	0.0	2.8
actual		0.0	0.079	8.3	8.3	0.0	8.3
U,16.6kG		0.079	0.061	8.3	8.0	5.6	6.1
actual		0.079	0.089	8.3	8.6	5.6	9.9
U,16.6kG		0.15	0.106	8.3	8.4	10.7	11.4
actual		0.15	0.112	8.3	9.0	10.7	13.2
U,25kG		0.080	0.056	8.3	8.3	5.71	5.86
actual x $\frac{25}{17}$		0.080	0.057	8.3	8.2	5.71	5.88
U,16.6kG	0.0	0.082	0.122	8.3	7.8	5.9	7.2
actual	0.0	0.082	0.139	8.3	8.4	5.9	8.9

The last row in Table VIII shows the ideal adiabatic case, for which $r \propto B^{-1/2}$ (P_θ conservation) and $\beta_\perp \propto B^{1/2}/\gamma$ (magnetic moment conservation), so $\varepsilon = r\gamma\beta_\perp$ must stay constant.[24] We define a "medium" 40 → 20 kG transition as over a few wavelengths λ_c, and "fast" and "gradual" as over about one and many λ_c, respectively. For Table VIII and Fig. 41, note that the medium and gradual transitions lead (for warm input beams) to adiabatic behavior ($\gamma r\beta_\perp$ nearly conserved), while the fast transition (Fig. 40) does not. Cold input beams still follow B lines (P_θ is conserved), but the magnetic moment (still conserved in gradual transitions) is not simply $P_\perp^2/B$, and ε as defined here is not conserved.[25]

It was verified that just setting up an equilibrium in a uniform B_z leads to small $\beta_\perp$ (0.011 in the case run), and that moving the z-location of the 40 → 20 kG transition had a small (~2%) effect on the output beam r and $\beta_\perp$. Also, there is a few % spread caused by using a different set of random numbers for the transverse V_r and V_θ at injection (100 trajectories used for most runs), perhaps explaining why the medium transition gives about the same $\beta_\perp$(out) as the gradual cases. The $\beta_\perp$(out) = 0.074 (cases 4 and 12) is the lower bound of the cases run with $\beta_\perp$(in) = 0.094 (all but 7 and 3); this seems acceptably close to the adiabatic theory value of $\beta_\perp$(out) = 0.073. Perhaps Ref. 24 (particle code) did not see the cooling of $\beta_\perp$ (always seen for warm beams with TRAJ) for the same reason that gap emittance-gain calculations are difficult with MAGIC - particle codes are noisy.

Finally, we can answer the question about the value of starting with 40 kG in the diode and expanding into 20 kG vs. using a larger cathode at 20 kG in the first place (Fig. 27). Since the two methods yield about the same emittance (in fact the output $r\beta_\perp$ in Figs. 27b and 41 are the same, but there are uncertainties in each model), it is not worthwhile to complicate the system with an expansion region, and a high-field (40 kG) diode. It seems preferable to simply start with the larger cathode immersed in 20 kG.

Further, the total final emittance (squared) after phase-mixing in air is

$$P_\theta^2 + \varepsilon^2 = (eB_0 r_k^2/2)^2 + (m\gamma rc\beta_\perp(\text{random}))^2 \doteq 1.7\text{E} - 46 + 2.6\text{E} - 48 \ ,$$

so that the emittance will be dominated by the magnetic flux at the cathode. The random $\beta_\perp$ term is evaluated near the diode; as the beam traverses the accelerating gaps, γ will increase but $\beta_\perp$ will decrease such that $r\gamma\beta_\perp$ increases slightly (see Tables V, VI, VII). In fact, $r\gamma\beta_\perp$ would have to increase eightfold over all gaps to make the terms equal. Clearly, there is not much point in worrying about small improvements in $\beta_\perp$(random).

E. B_θ Conditioning Cells

Considerable effort using theory, TRAJ, and MAGIC was spent on this topic in 1988. The work complemented the IBEX experiments of C. A. Frost (1242) and the BUCKSHOT calculations of J. R. Freeman (1241).[26,27] For axisymmetric runs, MAGIC and BUCKSHOT (written by J. S. Wagner, 1241) gave nearly the same answers.[28] We divide the discussion into three parts:

Table VIII. Beam (5 MeV, 40 kA) expansion runs (TRAJ).

In all cases, B_z changes from 40 to 20 kG, and γ changes from 9.4 to 8.6 (because beam is farther from wall on rhs). The r and $\beta_\perp$ are rms values.

Case	Temp	Transition	r(mm)		$\beta_\perp$		$\gamma r\beta_\perp$	
			in	out	in	out	in	out
7	Cold	Fast	5.7	8.1	0.001	0.028	0.054	2.0
3	Cold	Medium	5.7	8.0	0.001	0.01	0.054	0.69
8	Warm	Fast	5.7	8.3	0.094	0.084	5.1	6.0
4	Warm	Medium	5.7	8.1	0.094	0.074	5.1	5.2
10	Warm	Gradual	5.7	8.2	0.094	0.077	5.1	5.4
9	Warm	Gradual*	5.7	8.3	0.094	0.076	5.1	5.4
11	Warm	Gradual**	5.7	8.2	0.099	0.077	5.3	5.4
12	Warm	Gradual**	5.7	8.2	0.094	0.074	5.1	5.2
adiab.***	Warm	> few λ_c	5.7	8.1	0.094	0.073	5.1	5.1

* Transition of B_z moved upstream 12 cm

** Different set of random numbers chosen at injection

*** The ideal adiabatic case for which emittance $\gamma r\beta_\perp$ should stay constant.

summary of the theory, results for IBEX, and results for RADLAC. Further details can be found in Refs. 14 and 17 for 1988; some preliminary work was described in Ref. 6, Figs. 13-16. Some work on classical IFR cells and preionized gas cells is given in Ref. 14.

1. Theory

The typical setup for the calculations is shown in Fig. 42. The beam is extracted from B_z, and passes through a foil into the cell itself. Here, the focusing force is provided by a small current-carrying wire. Besides the usual beam self-fields and the rotation (centrifugal), the forces on the beam are due to electrostatic attraction by the positive wire charge,

$$E_r(\text{wire}) = \frac{f_w I_b}{2\pi\varepsilon_0 r\beta_z c} \quad , \tag{1}$$

and the magnetic force of the combined applied and induced return wire currents,

$$B_\theta(\text{wire}) = \frac{-\mu_0(I_0 - I_R)}{2\pi r} \quad . \tag{2}$$

Here, I_0 = applied current, I_R = return current, I_b = beam current, and $f_w = \lambda_w\beta_z c/I_b$, the fractional charge neutralization by the wire, with λ_w = charge/length. As J. R. Freeman (1241) points out, for a 1-D system (far from endplates, no z-variation), with grounded wire and constant β_z so $\rho(r)$ and $j_z(r)$ have the same form,

$$f_w = I_R/I_b \ , \tag{3}$$

provided the B_θ fields do not soak into the metal walls or wire. The proof of Eq. (3) is that both electric and magnetic parts of the problem obey the same equations (R = wall radius, r_w = wire radius),

$$\nabla^2\phi = -\rho/\varepsilon_0 \qquad \phi(R) = \phi(r_w) = 0 \ , \tag{4}$$

with $\phi \rightarrow A_z$ and $\rho \rightarrow j_z$ for the magnetic part. The condition of $\int_{r_w}^{R} E_r dr = 0$ (grounded wire) or $\int_{r_w}^{R} B_\theta dr = 0$ (zero net flux) yields (magnetic part)

$$I_R \ln \frac{R}{r_w} = \int_{r_w}^{R} \frac{I_b(r)dr}{r} \quad , \tag{5}$$

with

$$I_b(r) = \int_{r_w}^{r} 2\pi r j_z dr \quad . \tag{6}$$

For the electric part, substitute $I_b \rightarrow \lambda_b$ (beam charge/length inside radius r), $j_z \rightarrow \rho$, and $I_R \rightarrow \lambda_w$. For a beam of radius r_b, these equations lead to[6]

$$f_w = \frac{I_R}{I_b} = \frac{\ln R/r_b + h}{\ln R/r_w} \quad , \qquad h = \begin{cases} 0 & \text{thin beam} \\ \frac{1}{2} & \text{uniform beam} \end{cases} \tag{7}$$

This same result, Eq. (7), has also been obtained by inductance arguments, and by energy minimization. The reason for deriving these results here is that TRAJ, being a steady-state code, needs to be given I_R/I_b, although the code calculates f_w as part of the Poisson solution. It is of interest that Eq. (7) was verified to at least one significant digit in Ref. 6, Figs. 13 and 14, by MAGIC runs (which calculate both f_w and I_R/I_b self-consistently); but the result was not appreciated then. More recent runs with RADLAC parameters have verified Eq. (3) to two digits in regions of the B_θ cell away from end foils. In fact, when equilibrium has been reached so that f_w and I_R/I_b are constant in time, we find that I_R is constant spatially (of necessity) along the wire, and f_w is also constant except for a few cm near each end.

The force due to the wire on a beam electron is, from Eqs. (1), (2), and (3),

$$-e(E_r(\text{wire}) - V_z B_\theta(\text{wire})) = -\frac{e}{2\pi\varepsilon_0 rc} \left(+ \frac{I_R}{\beta_z} + \beta_z I_0 - \beta_z I_R \right) , \tag{8}$$

where the three terms on the rhs are due to induced charge (inward), applied wire current (inward), and return current (outward). For $\beta_z \rightarrow 1$ the first and third terms cancel, leaving only the force of the applied I_0. This cancellation is to order $1/\gamma^2$ for small $\beta_\perp$, just as for the beam self-forces. As J. R. Freeman (1241) suggests, the result is useful in problems where the assumptions are valid, since no model for I_R is needed. However, we wish to include 2-D effects in our TRAJ model, so we have retained the freedom to specify I_R/I_b separately, and then checked the sensitivity of the results to various I_R/I_b values. If we set the force in Eq. (8) equal to the pressure, and use $P_\theta^2 + \varepsilon^2 = (m\gamma r\beta_\perp c)^2$, we obtain[6,26]

$$\beta_\perp = (2\nu_{wire}/\gamma)^{1/2}\,, \tag{9}$$

where ν_{wire} is $I_0/17$ kA.

2. IBEX Results

A TRAJ equilibrium is shown in Fig. 43. The applied B_z is indicated, and at the foil at z = 30 cm has fallen to 11.6 kG (down from the uniform value of 20 kG at z = 0). We apply a wire current I_0 = 15 kA, and inject an IBEX beam of 32 kA, 4 MeV, $\beta_\perp$ = 0.1, r(rms) = 5.7 mm. We have assumed $I_R = 0.41\ I_b$ (from Eq. (7)), and indeed the code finds f_w = 0.41. All three wire forces in Eq. (8) here are about the same size. Contours of ϕ(r,z) are shown in Fig. 43b; the max potential depth is 2.2 MV. Note the big E field near the foil. The primary result in Fig. 43 is that the beam gains considerable emittance in the wire cell; it emerges larger and hotter. The main advantage of the wire cell, in fact, may be its ability to center an off-axis beam;[26,27] but one also has the possibility of emittance tailoring, discussed below.

With Fig. 43 as a base case, we studied some parameter variations. One issue concerns the optimal position of the foil with respect to the B_z decay. Figure 44a shows the result of moving the foil out to where B_z = 2.7 kG. The beam expands before reaching the foil, pinches, then expands; 12 kA are lost. Figure 44b shows the result of moving the foil in to where B_z = 19.6 kG. Comparing Fig. 43a, we find nearly the same beam (slightly cooler but larger). Apparently the location of the foil in Fig. 43 is satisfactory. Moving it out of the B_z is definitely bad, and moving it farther in does not help substantially.

Next we examine the effect of varying I_0, the applied wire current. Decreasing I_0 leads to a larger cooler beam, with wall loss for $I_0 < 10$ kA. Doubling I_0 to 30 kA does not help; although the largest electron excursions are reduced, the beam becomes hotter than in Fig. 43. The optimum I_0 is apparently 15-20 kA; the I_0 = 20 kA case yields the same r(rms) as in Fig. 43 but slightly higher $\beta_\perp$ = 0.54. Pictures of the trajectories for these cases may be found in Ref. 14.

One might think of reducing the needed I_0 by lowering B_0 and thus the rotation. A run with B_0 = 10 kG and I_0 = 10 kA gives the smaller rotation, but this allows a tighter foil-pinch and violent expansion (10-kA loss to wall).

The sensitivity to several things must be tested. Results do not appear to change much with the numerical parameters (e.g., number of trajectories used), but there is some variation with the input random numbers assigned to the trajectories to simulate a warm beam. Rerunning the case of Fig. 43 with four different random number sets yields a spread in r(rms) of ±15%, in $\beta_\perp$ of about the same. Of course, the statistics could be improved by more trajectories, but about 100 as in most runs seems adequate for our present purposes.

In Fig. 43 (base case) we assumed $I_R/I_b = 0.41$, based on Eq. (7) for a thin beam, with the assumed $r_b = 7$ mm (input value). To test the sensitivity, we varied I_R/I_b from 0.35 to 0.51 (see Table IX), based on various r_b values and beam profiles; see Eqs. (5) and (6). The resulting $I_w = I_0 - I_R$ varied from +3.8 to -1.4 kA (recall that $I_b = 32$ kA). As seen in the Table, the output r(rms) varied over 10 to 13 mm, $\beta_\perp$ over 0.35 to 0.51. For the type of calculation needed thus far, these spreads are not serious, but if one wanted accurate final emittance values, a more self-consistent I_R/I_b would be necessary. The case in column 3 of Table IX is, in fact, the most self-consistent; the profile is closer to uniform than δ-function, and the assumed r_b is close to the actual r_b. In future work I_R/I_b could be adjusted during the run, by, say, setting it equal to a space-averaged f_w.

It is also tempting to set the force on the electrons in the wire cell to $-e\beta_z I_0/2\pi\varepsilon_0 rc$ (i.e. neglect all self- and induced-field forces). This might be acceptable except near the foil for a RADLAC conditioning cell run ($\gamma = 40$), but is not accurate here (IBEX) because of some of the large $\beta_\perp$ values; recall $\beta_z^2 = 1 - 1/\gamma^2 - \beta_\perp^2$ and see Eq. (8).

For completeness, we mention here one of the most promising IBEX wire cell runs, a combination of wire and gas focusing. In Fig. 45 the usual IBEX beam (32 kA, 4 MeV) is injected into a wire cell with $I_0 = 30$ kA, and $f_e = f_m = 1$ (no electric force, only the $I_0 - I_R = 16$ kA magnetic force). Or, if no I_R would be driven in a preionized plasma medium, then the only force is due to $I_0 = 16$ kA. The $\beta_\perp$(out) = 0.42, and r(rms) = 0.63 cm; comparing Fig. 43, the beam is slightly cooler and considerably smaller. This run demonstrates, incidentally, why one cannot just drop all forces in the wire cell except that due to I_0; if we could, this case would look nearly like Fig. 43 (with $I_0 = 15$ kA). The final beam size seems to be determined in large part by the "kick" due to the foil and the "grabbing" by the wire forces near the foil, where z-variations are large. However, the good result in Fig. 45 may be based on an overly crude or unphysical model; further studies would call for some MAGIC runs where the plasma and I_R are treated self-consistently.

Another way to obtain a small beam is to start with one. A run with the usual IBEX parameters and a wire with $I_0 = 15$ kA, $r_w = 0.5$ mm, and an annular beam initially in $2 < r < 4$ mm, $\beta_\perp = 0.1$ yielded output $\beta_\perp = 0.41$, r = 6.1 mm. The problem is that the beam scrapes the wire: only 4-kA loss, but a tiny misalignment would cause much more loss. Very small beams may not be suitable for conditioning with B_θ cells.

Table IX. TRAJ B_θ Cell runs to check sensitivity to assumed return current in wire.

Note that less net I_w implies cooler but larger beams.

I_R/I_b	0.35	0.40	0.41	0.51
r_{assume}	1.4	0.7	1.1	0.7
beam profile	unif	δ	unif	unif
I_w(kA)	3.8	2.3	1.9	-1.4
r_{out}(cm)	1.0	1.1	1.2	1.3
$\beta_\perp^{out}$	0.51	0.41	0.40	0.35

Another issue studied is the effect of an output(rhs) foil; all B_θ cells have foils or at least some type of holder at both ends. Figure 46 shows equipotentials and trajectories for cold IBEX beams, with and without a rhs foil, and we see that the results differ only near this foil. Table X shows the beam output for input cold and warm beams, with and without the endfoil. With the foil, the beams are cooler and smaller than without; but note that the overall emittance including γ is higher with the foil. The difference is small, however, and we conclude that the rhs endfoil has little effect, at least for these parameters. What matters much more is the medium beyond the foil, and the applied field in the vicinity.

In particular, one may ask about the effect of adding field coils near the input lhs foil, to try to minimize the foil-pinch and wire-grabbing effects on the beam, seen in Figs. 42-46.[29] Figure 47 shows two TRAJ runs, without (a,b) and with (c,d) a "bump" in B_z, arbitrarily chosen as 20 kG (added to a uniform 20 kG). The output beam with the bump has slightly smaller emittance, but not enough is gained to warrant the extra coils. The same type of calculations were made for RADLAC (40 kA, 20 MeV) for a variety of conditions (large and small radius beams, cold and warm input, and several I_0 values) with the same result; the extra B_z near the foil helps (usually, but not always), but probably not enough to make the extra trouble worthwhile. To be definitive, further studies of this question should probably involve a 3-D code and small realistic beam offsets.

3. RADLAC Results

Assuming the beam behaves as expected, emerging from the accelerator with $\gamma = 40$, 40 kA, annular, and centered, we wish to condition it with a wire zone. Figure 48 shows a MAGIC run of this process, assuming the input beam annulus is $7 < r < 10$ mm, with an ideal cold beam extracted from 20 kG through a foil, into a B_θ cell where the wire applied current is 20 kA. Figure 48a shows the applied B lines and the setup (only the first 80 cm of cell are simulated). The $B_z(z)$ near the axis is shown in parts b and c, without and with the beam; note the beam contribution to B_z after spin-up is about 15%. The beam itself (part d) at $t = 24$ ns (steady state) pinches near the foil, spins up and heats, but no beam is lost. The time dependence of r(rms) and $\beta_\perp$(rms), i.e., the tailoring, is given in parts e and f. After the risetime (15 ns), the beam quickly equilibrates at $r = 6.5$ mm, $\beta_\perp = 0.24$. Part g shows the final transverse momentum space, the displacement in $P_3 = \gamma V_\theta$ indicating the net rotation (final $V_\theta = 0.22$ c from P_θ conservation, corresponding to 2.7×10^9 in the figure).

A question of interest is the prediction of the charge and current neutralization induced in the wire by the beam. Figure 48h shows $E_r(z)$ near the wire; using the average value (ignoring the variation near the foil due to the beam pinch) yields $f_w = 0.57$. Figure 48i shows a small time dependence of this quantity. Figure 48j shows $B_\theta(z)$ near the wire; the variation is less here because return I tends to be conserved along the wire; the time variation is given in part k. From these plots we obtain $f_m \equiv I_R/I_b = 0.56$, in good agreement with theory Eq. (7) (0.52 thin beam, 0.65 solid beam), and we check the expected result $f_w = f_m$ (see Eq. (3)). Note that $I_R = 22$ kA, exceeding $I_0 = 20$ kA, so the wire is magnetically slightly defocusing. The overall focusing, however, is simply linear in I_0 (see Eq. (8)).

Table X. TRAJ study of rhs endfoil effects in IBEX B_θ cells.

All cases 4 MeV, 32 kA, extract from 20 kG, r_b(input) = 5.7 mm, I_0 = 15 kA, I_R = 13 kA. Output beam results are shown.

Cold Beam ($\beta_\perp^{in} = 0$)

w/endfoil				no endfoil			
$\beta_\perp$	r_{mm}	γ	$\beta_\perp r\gamma$	$\beta_\perp$	r_{mm}	γ	$\beta_\perp r\gamma$
0.35	9.2	9.4	30.3	0.43	11.1	6.2	29.6

Warm Beam ($\beta_\perp^{in} = 0.095$)

0.35	9.6	9.4	31.6	0.41	11.3	6.3	29.2

Repeating this run, but with a warm input beam ($\beta_\perp = 0.1$) and applied wire current of 15 kA, yields a situation where 6 kA of beam are lost to the wire (4 kA at the first pinch). The 34 kA which propagates has rms r = 7 mm, $\beta_\perp = 0.2$, so insofar as warm beams are concerned, loss to the wire may be the main problem. Of course, the loss could be reduced with a smaller-diameter wire.

Experiments on IBEX suggest the value (high brightness) of using smaller-diameter beams, so a case was run with the initial beam annulus in $4 < r < 7$ mm. Figure 49 gives the results. A smaller wire ($r_w = 0.5$ mm) was employed, carrying 15 kA. In Fig. 49a the steady beam pinches almost to the wire (no loss), and stays closer to it (compare Fig. 48d). The beam retains slightly more of the B_z after extraction, but the final rotation is slightly less, about 0.18 c (see Fig. 49b). In Figs. 49c and d we see the tailoring (15-ns beam risetime); the final rms values are r = 4.1 mm and $\beta_\perp = 0.20$. The E_r and B_θ plots in Figs. 49e-h imply $f_w = 0.65$, $f_m = 0.62$, again agreeing reasonably well with theory (0.65 for solid beam).

Comparing the larger (1-cm) and smaller (7-mm) beams of Figs. 48 and 49, respectively, the emittance tailoring has about the same shape, but the smaller beam has a final value of $r\beta_\perp$ which is about half that of the larger beam. (Of course, some of this is due to starting with a smaller beam.) However, the smaller beam would suffer some loss at the first pinch if it had some initial $\beta_\perp$. In view of the success of the IBEX experiments with small cathodes, it seems worth considering a smaller-beam option for RADLAC. How small the beam may be will be determined by space-charge limits and perhaps loss to the wire.

In discussing the IBEX results, we considered the effect of a rhs endfoil using TRAJ (Fig. 46 and Table X). The problem was also studied for RADLAC parameters using MAGIC; see Fig. 50. The smaller RADLAC beam (40 kA, 20 MeV) is extracted from $B_z = 20$ kG into a B_θ cell of length 80 cm with $I_0 = 15$ kA. The code yields $f_w = f_m = 0.62$, in good agreement with theory, and agreeing closely with the result in Fig. 49, which has no rhs endfoil. In fact, comparing Figs. 49 and 50 shows little difference, supporting the TRAJ conclusion that the rhs foil does not affect the beam much. Of course, the medium past the foil does matter; in Fig. 50b with vacuum for $z > 100$ cm the beam blows up, whereas in Fig. 50c with an IFR region (defined by electric f = 1, magnetic $f_m = 0$) for $z > 100$ cm the beam is nicely matched to the cell, in both r_b and $\beta_\perp$.

In summary, B_θ cells should work as beam conditioners, provided the parameters are chosen carefully: $I_0 \sim 15$ kA, $r_w < 1$ mm, R(wall) $\gtrsim 5$ cm. The price is a substantial increase in emittance, and possibly some wire and/or wall loss. The entrance foil should be placed well inside the applied B_z; variations in applied field near this foil may help some. A B_θ cell with preionized plasma gives one more control, and may provide the best beams, but is more complex to understand. Problems needing further work include 3-D and plasma effects, and optimization of wire size and cell length. We expect comparisons with experiments on IBEX (C. A. Frost, 1242) to be made soon.

V. Summary

The Sandia electron linacs were modelled extensively in 1988 using MAGIC and TRAJ. For the PTØ device, the Pierce insert technique was found useful in producing a cold focused beam, and several promising injector-plus-two-gaps systems were designed. For the RLA (Recirc) injector, a number of configurations were studied; it is unclear whether the non-immersed-cathode foilless diode with B_z transport or the no-B_z foil diode with IFR transport has the greater advantage, but foils and plasma channels may be unavoidable.

The simulations of immersed diodes for RADLAC and IBEX emphasized small cathodes and realistic effects such as feed loss and non-ideal applied fields (e.g., non-uniform B_z, details of voltage feeds). As usual, we find that good applied fields produce good beams. The optimum cathode size for RADLAC is probably in the range 6-9 mm (radius), but there does not seem to be much point in starting with small cathode and higher B_z, then expanding adiabatically into smaller B_z. One may as well use a medium-radius beam throughout, where the trade-off is between final rotation and space-charge limits.

The RADLAC gap studies clearly showed the advantage of TRAJ over MAGIC for emittance calculations. The physical result is that one can expect acceptably small emittance gains in the gaps, but it is very worthwhile to have a nearly uniform B_z.

Finally, the B_θ conditioning cell work yielded parameters which should work in principle, but the beam will be heated, and problems remain which need further study.

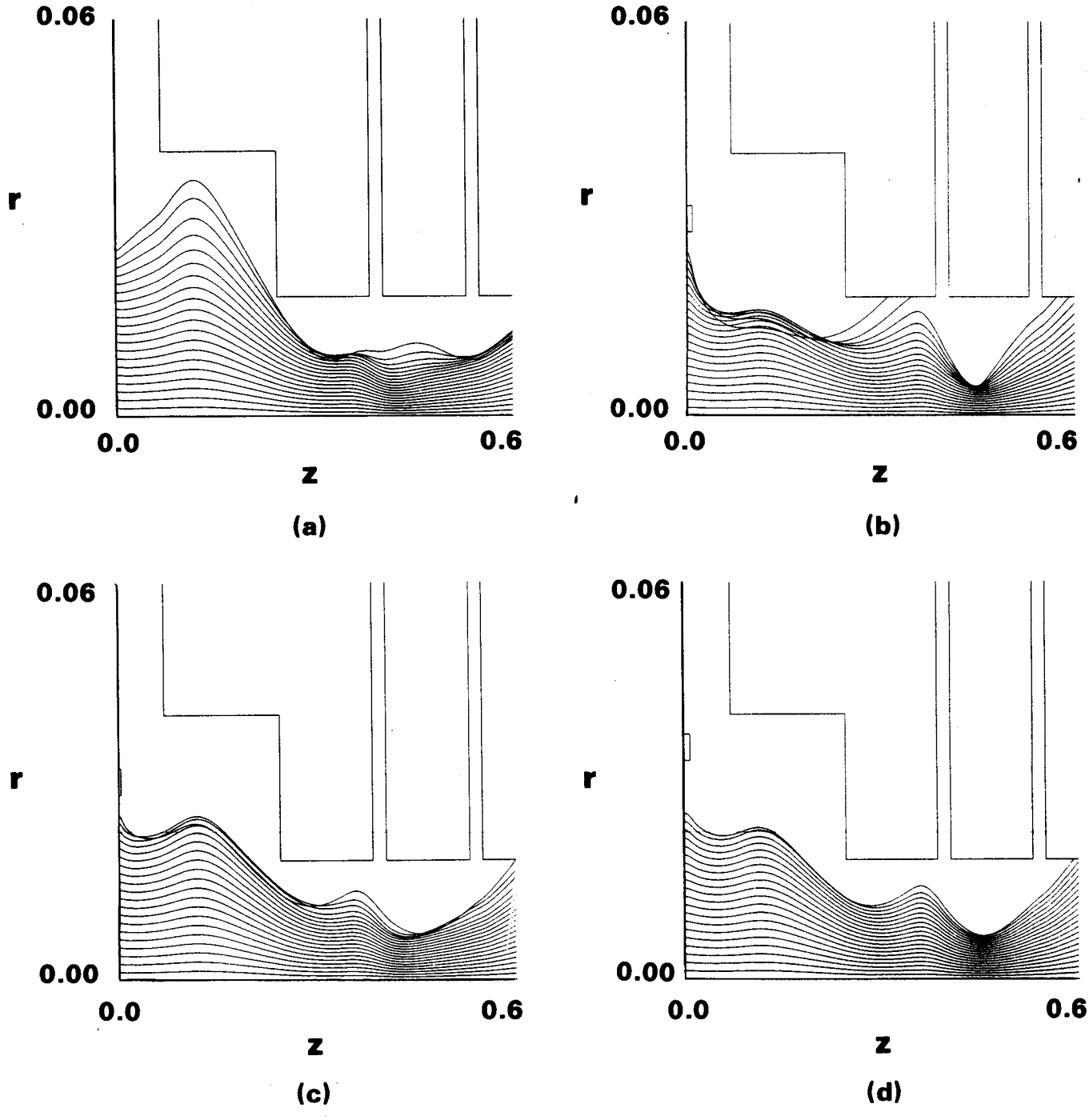

Figure 1. TRAJ electron flows for PT0 (diode 800 kV, 2 gaps 200 kV each, d = 7 cm, r[emit] = 2.5 cm, applied B in Fig. 3). All lengths in m.
(a) Old design, 1.0 kA.
(b) Add large, close Pierce insert, 0.5 kA.
(c) Small, close Pierce insert, 0.76 kA.
(d) Large insert farther from beam, 0.66 kA.

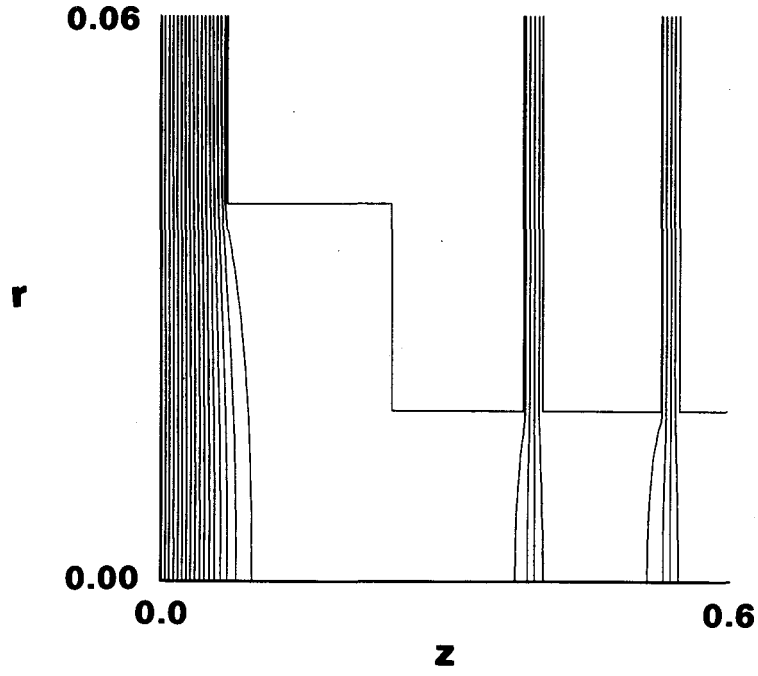

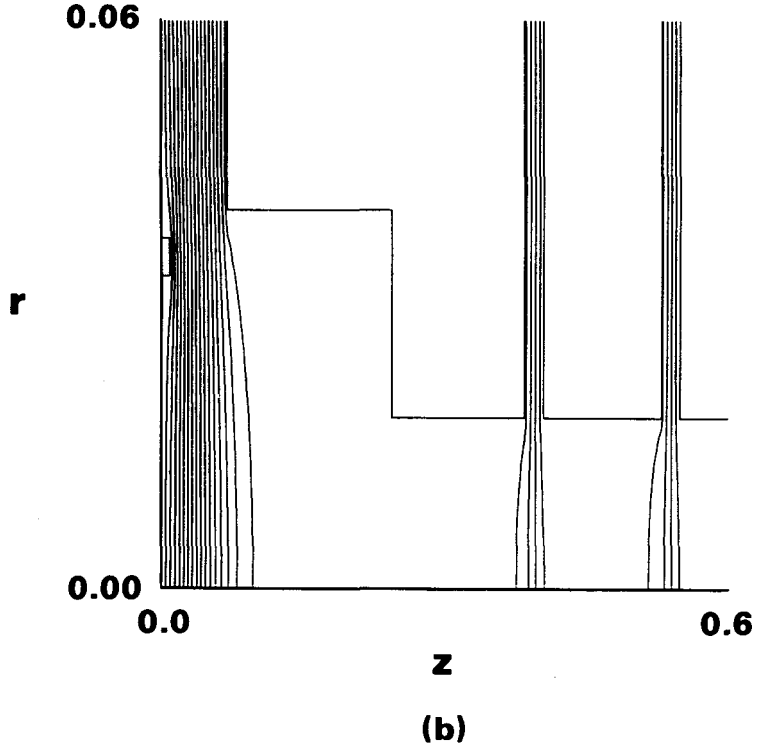

Figure 2. Equipotentials (vacuum) for Fig. 1.
(a) Fig. 1a.
(b) Fig. 1d.

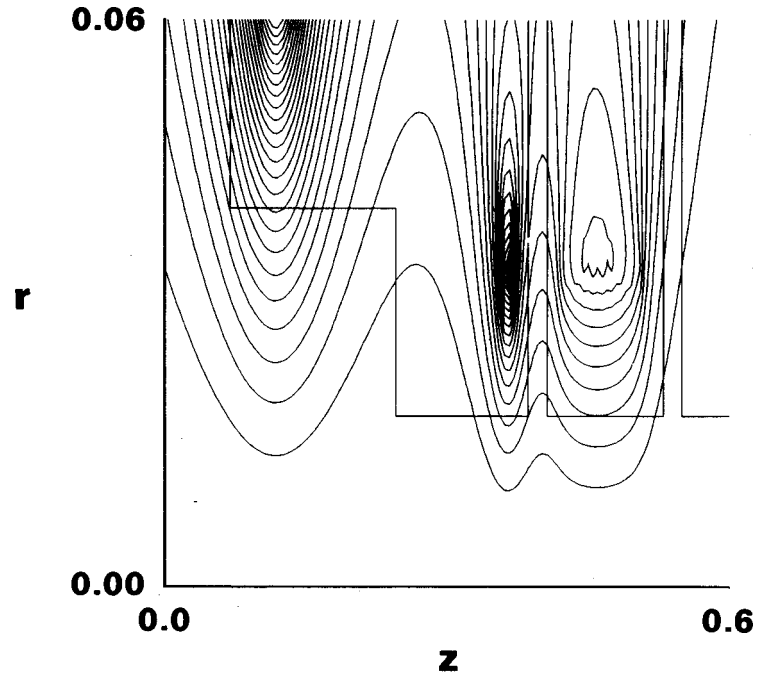

(a)

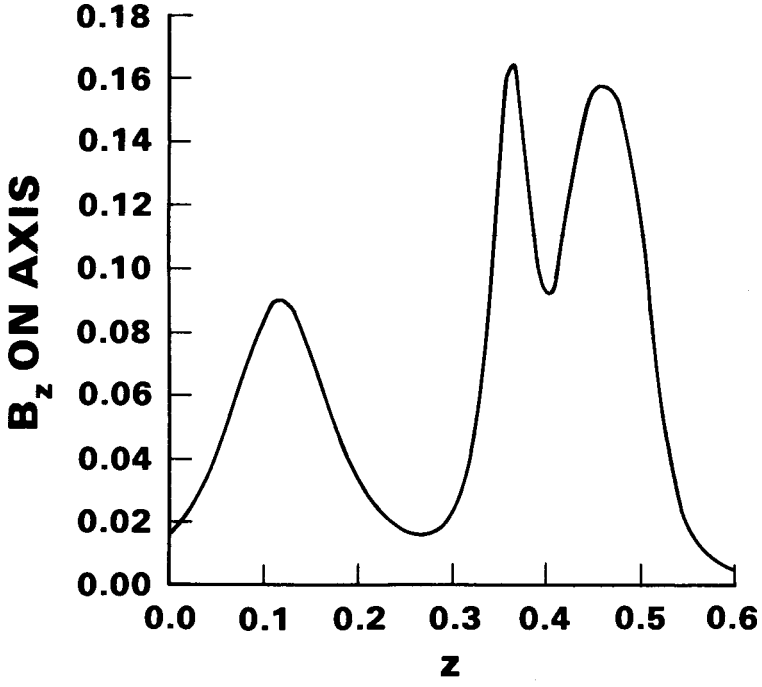

(b)

Figure 3. Applied B for Fig. 1.
(a) B lines.
(b) B_z (z, r = 0).

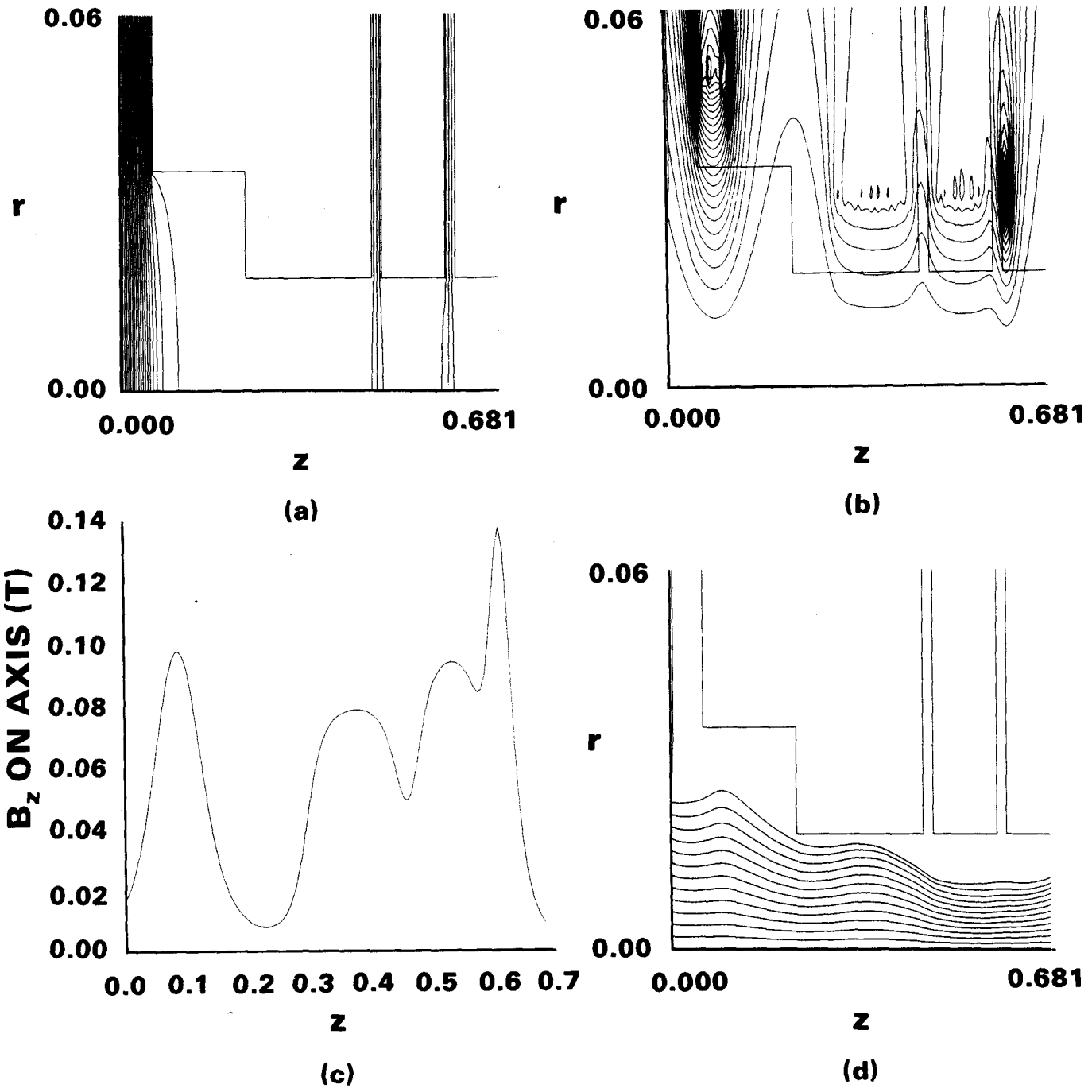

Figure 4. New PTØ design (diode 800 kV, gaps 150 kV, d = 5.4 cm, r[emit] = 2.3 cm, Pierce taper angle 24°, stickout 4 mm).
(a) Vacuum ϕ(r, z).
(b) Applied B lines.
(c) B_z(z, r = 0).
(d) Trajectories, I = 931 A, output beam r (rms) = 8 mm, $\beta_\perp$ (rms) = 0.046. Every fifth trajectory is plotted.

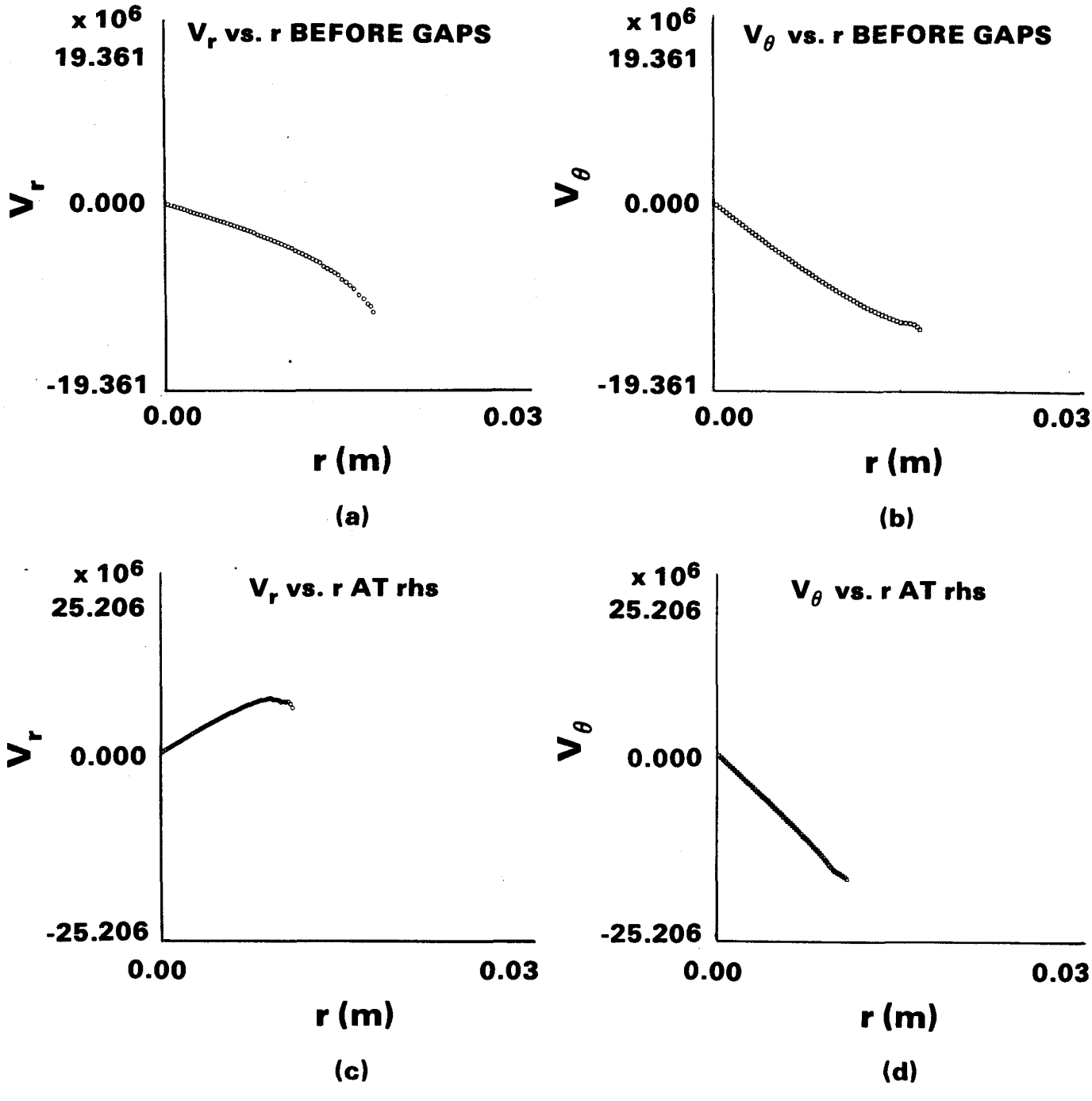

Figure 5. Phase space plots for Fig. 4.
(a) V_r vs. r, Z = 22.6 cm.
(b) V_θ vs. r, Z = 22.6 cm.
(c) V_r vs. r, output end.
(d) V_θ vs. r, output end. Each trajectory is shown as a circle or square.

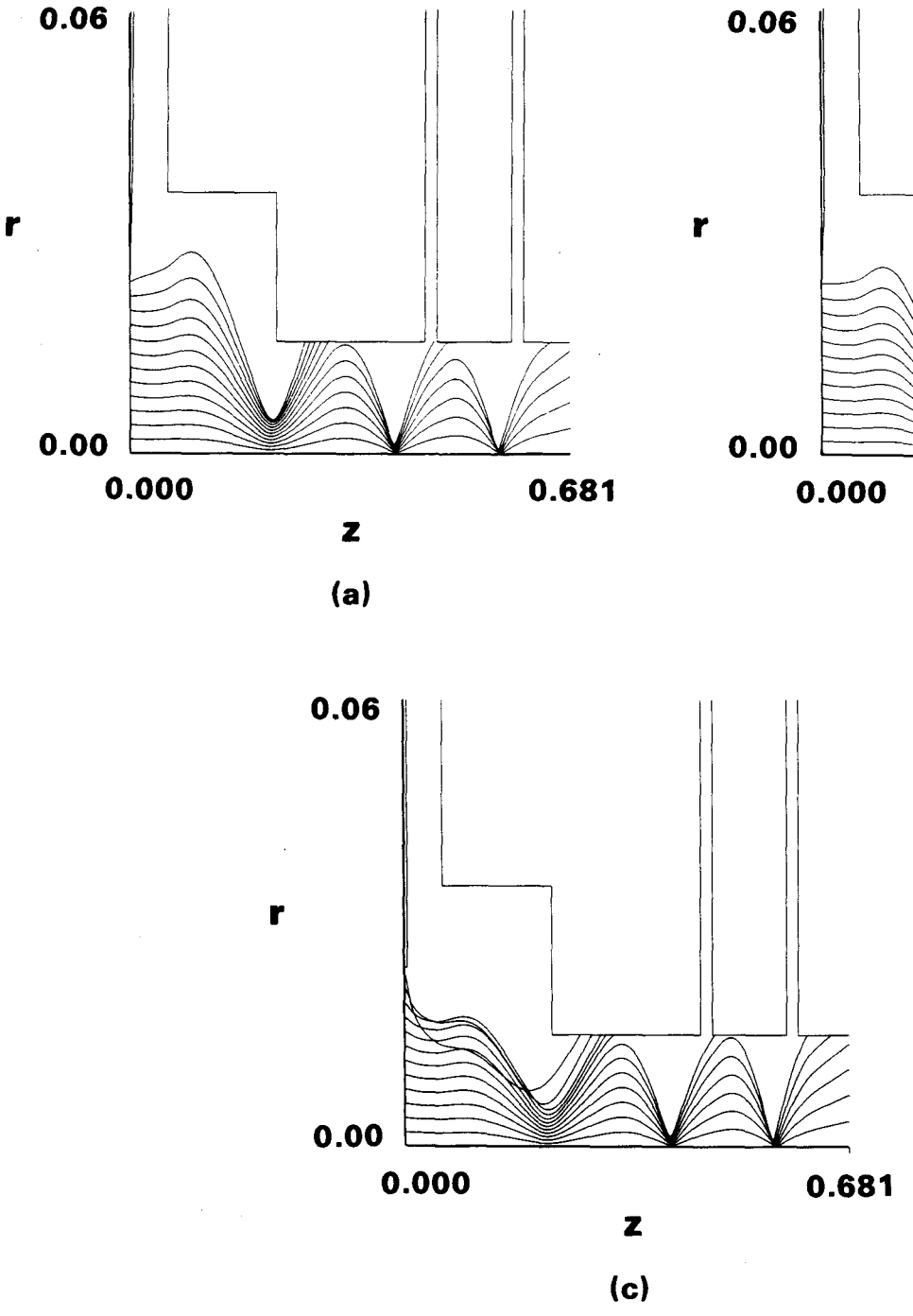

Figure 6. TRAJ plots of beams for various Pierce taper angles. In all cases d = 5.4 cm, r (emit) = 2.3 cm, V = 800 kV. Coils not optimized for transport.

(a) 15°, 990 A.
(b) 24°, 931 A, as in Fig. 4.
(c) 90°, 680 A.

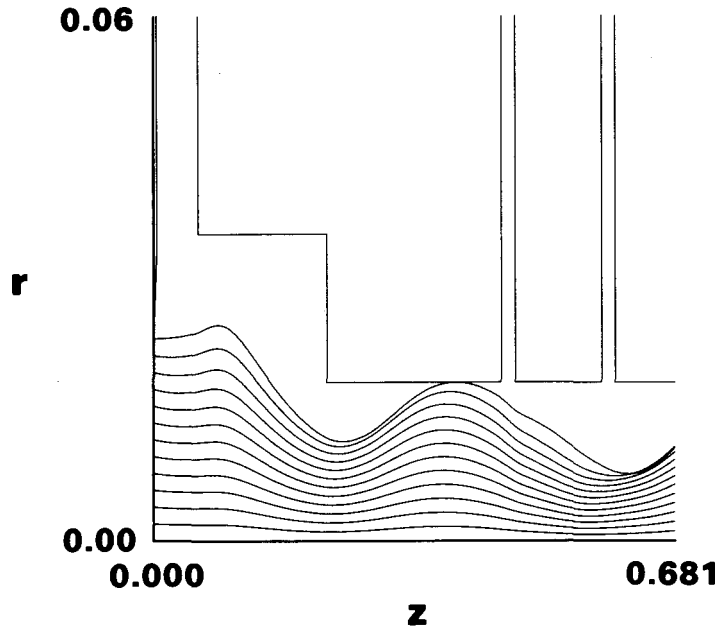

(a)

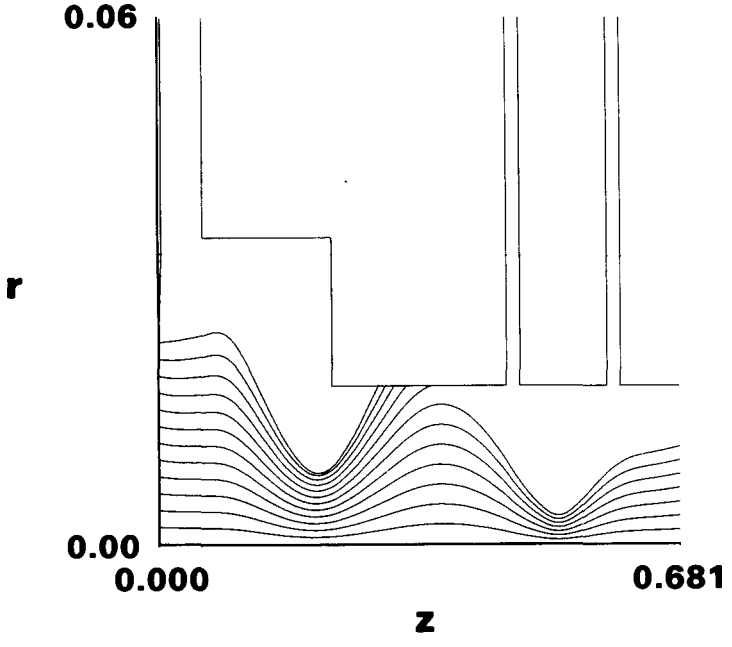

(b)

Figure 7. As in Fig. 4, but vary voltage on diode.
(a) 700 kV, 771 A all beam out.
(b) 600 kV, 620 A, 237 A out.

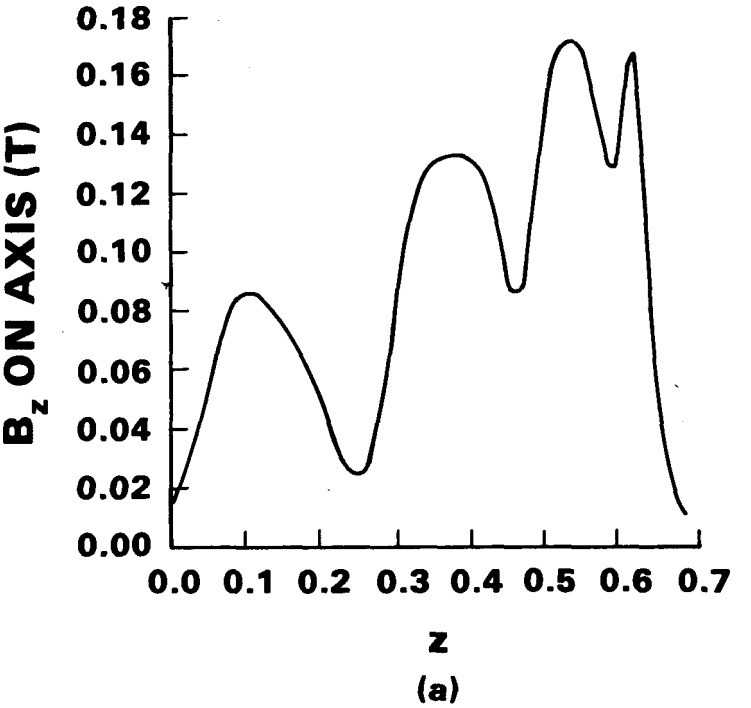

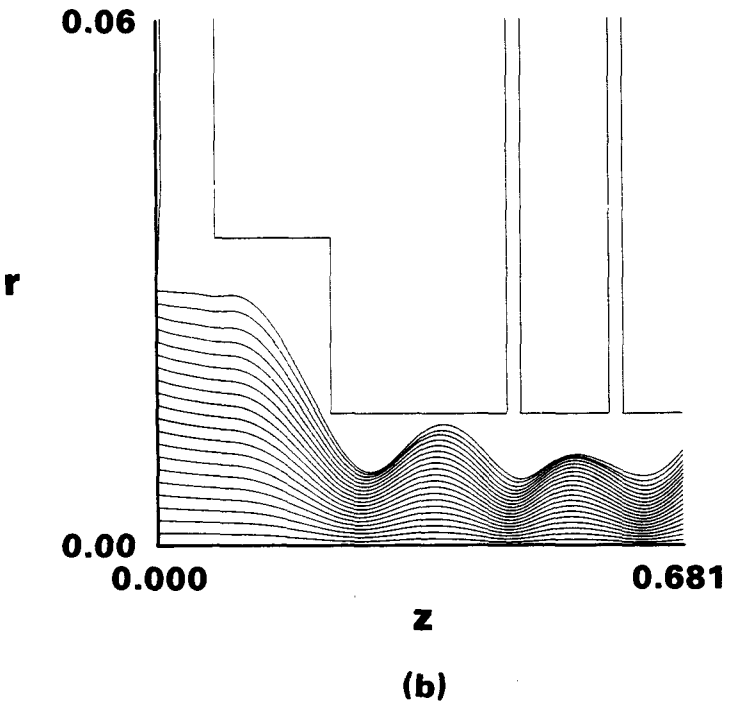

Figure 8. TRAJ design of PTØ for d = 7 cm (800 kV, gaps 150 kV, r [emit] = 2.9 cm, Pierce taper angle 25°, stickout 5 mm).
(a) B_z (z, r = o).
(b) Trajectories, I = 934 A.

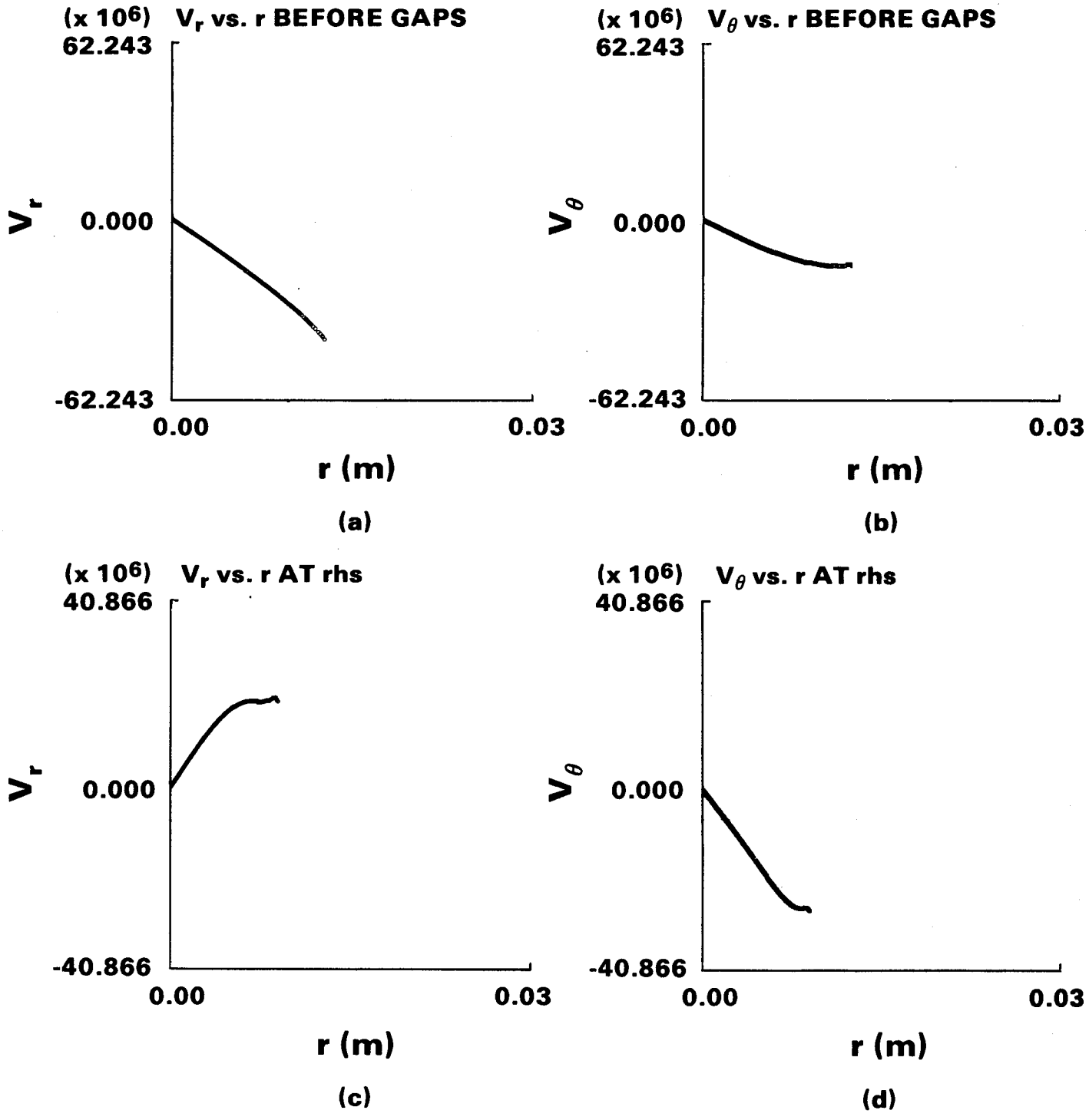

Figure 9. Phase space plots for Fig. 8.
(a) V_r vs. r, z = 22.6 cm.
(b) V_θ vs. r, z = 22.6 cm.
(c) V_r vs. r, output end.
(d) V_θ vs. r, output end. Compare Fig. 5.

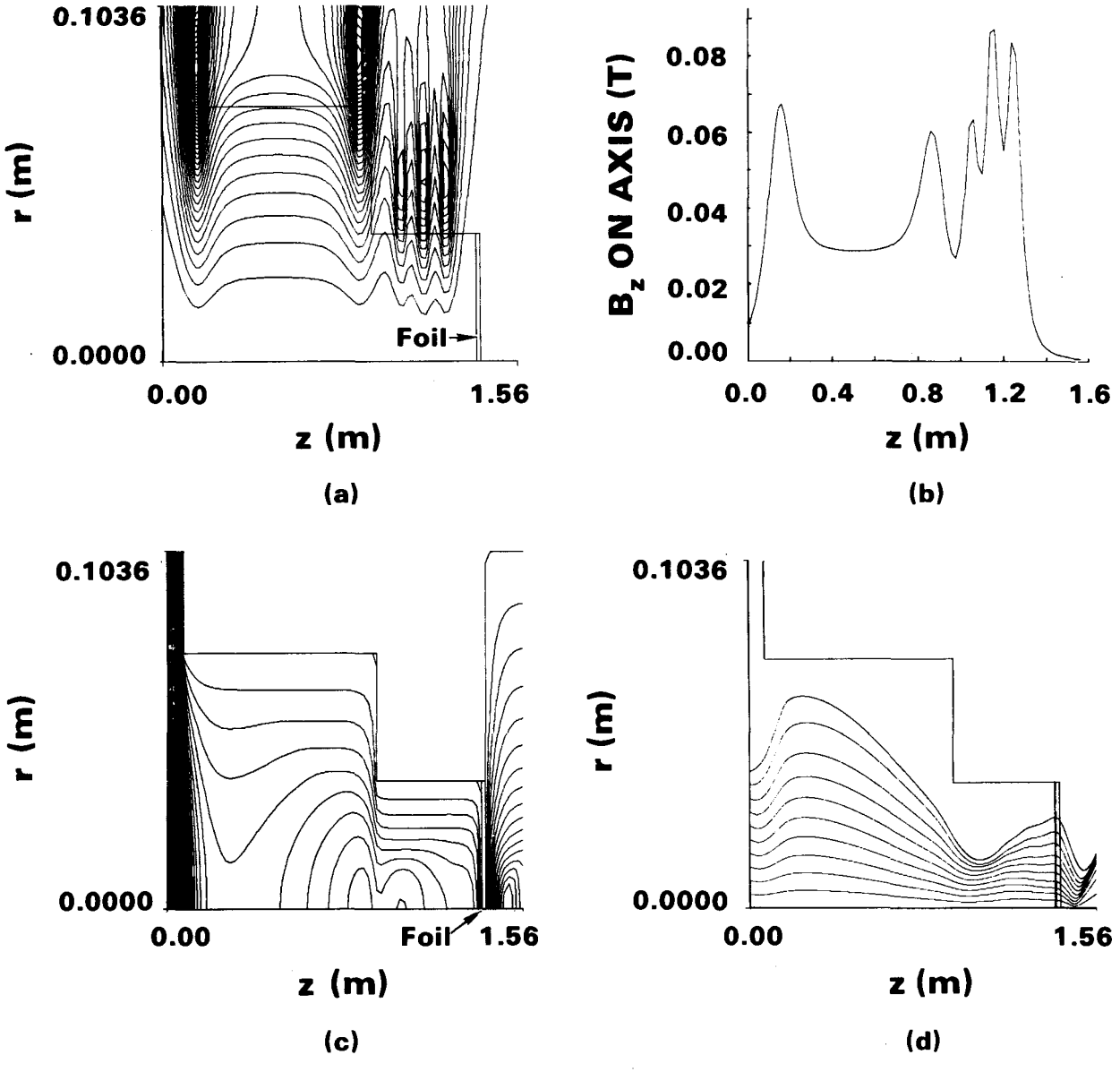

Figure 10. TRAJ run of Recirc diode plus coil transport system. V = 1.3 MV, I = 3.3 kA, B_z (k, axis) = 89 G. The foil on the rhs separates the diode from the racetrack IFR channel. A-K d = 7 cm; r (emit) = 4.07 cm on K.

(a) B Lines due to 5 coils and a solenoid (900 A, 1 turn/4 cm, r = 8.4 cm, $11 < z < 91$ cm). The five coils: I = 6, 5, 4, 6, 6, kA; r = 8.4, 8.6, 4.8, 4.8, 4.8 cm; z = 15, 87, 105, 115, 125 cm. Coils not allowed near rhs.

(b) B_z (z) on axis.

(c) ϕ (r, z) with beam. Region past foil treated as vacuum.

(d) Trajectories of every fifth electron. Output: r (rms) = 1.6 cm, $\beta_\perp = 0.18$, but note that the foil seriously perturbs the beam.

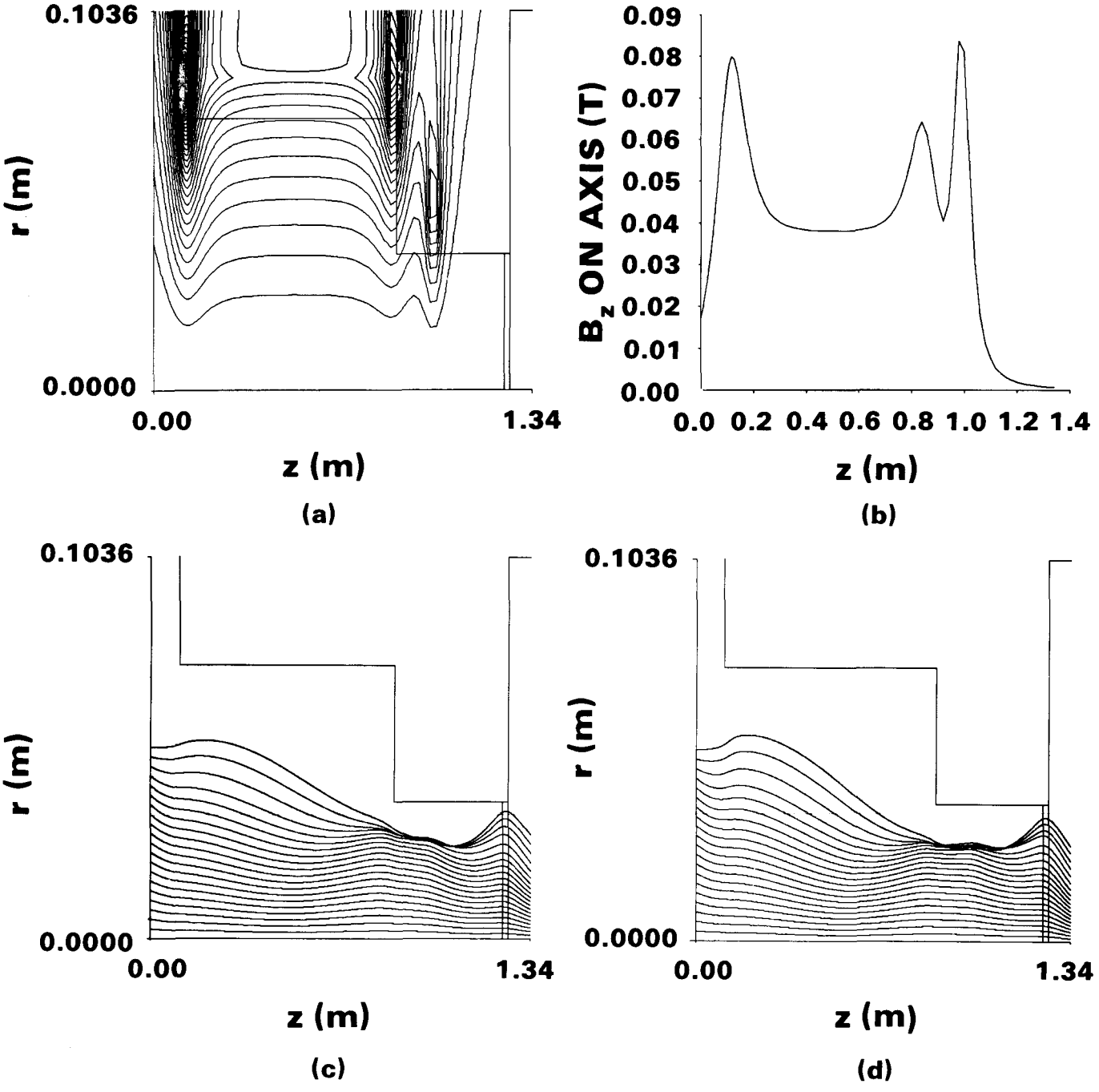

Figure 11. TRAJ run of Recirc diode/transport system at V = 1.7 MV, d = 10 cm, r (emit) = 5.2 cm. The result is 4.8 kA with B_z (k) = 170 G. Region past rhs foil is treated as vacuum.

(a) Applied B lines due to three coils and a solenoid. Coils not allowed near rhs.

(b) B_z (z) on axis.

(c) Trajectories (every fifth).

(d) Same as (c), but spread coils out by 1 or 2 cm axially.

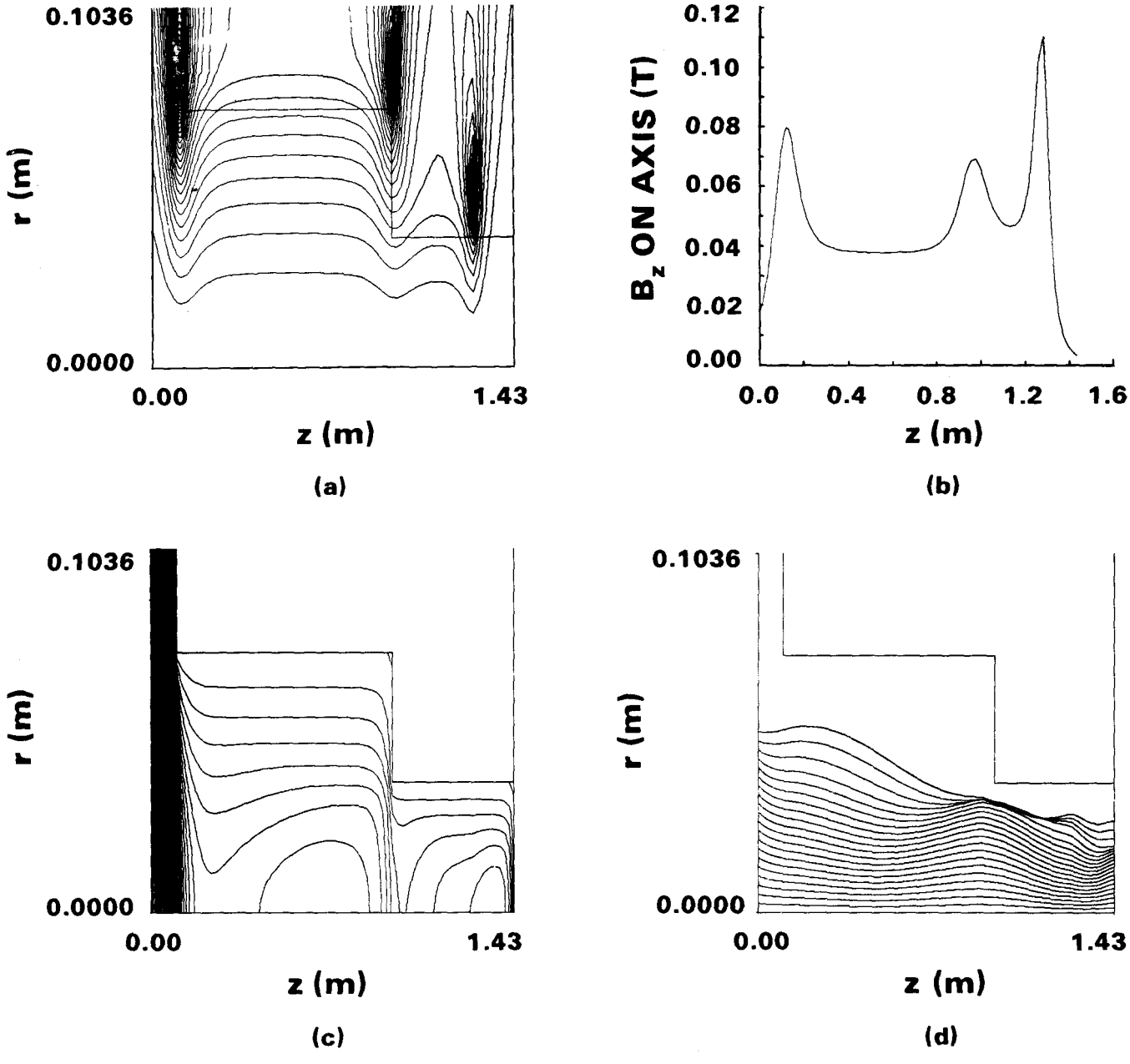

Figure 12. Another Recirc system. Calculation terminates at rhs foil, z = 143 cm. V = 1.7 MV, d = 10 cm, I = 4.8 kA.

(a) Applied B lines, due to 3 coils (8, 5, 7 kA) and 2 solenoids (600, 650 A; 1 turn/2 cm).

(b) B_z (z) on axis.

(c) ϕ (r, z) with beam.

(d) Trajectories.

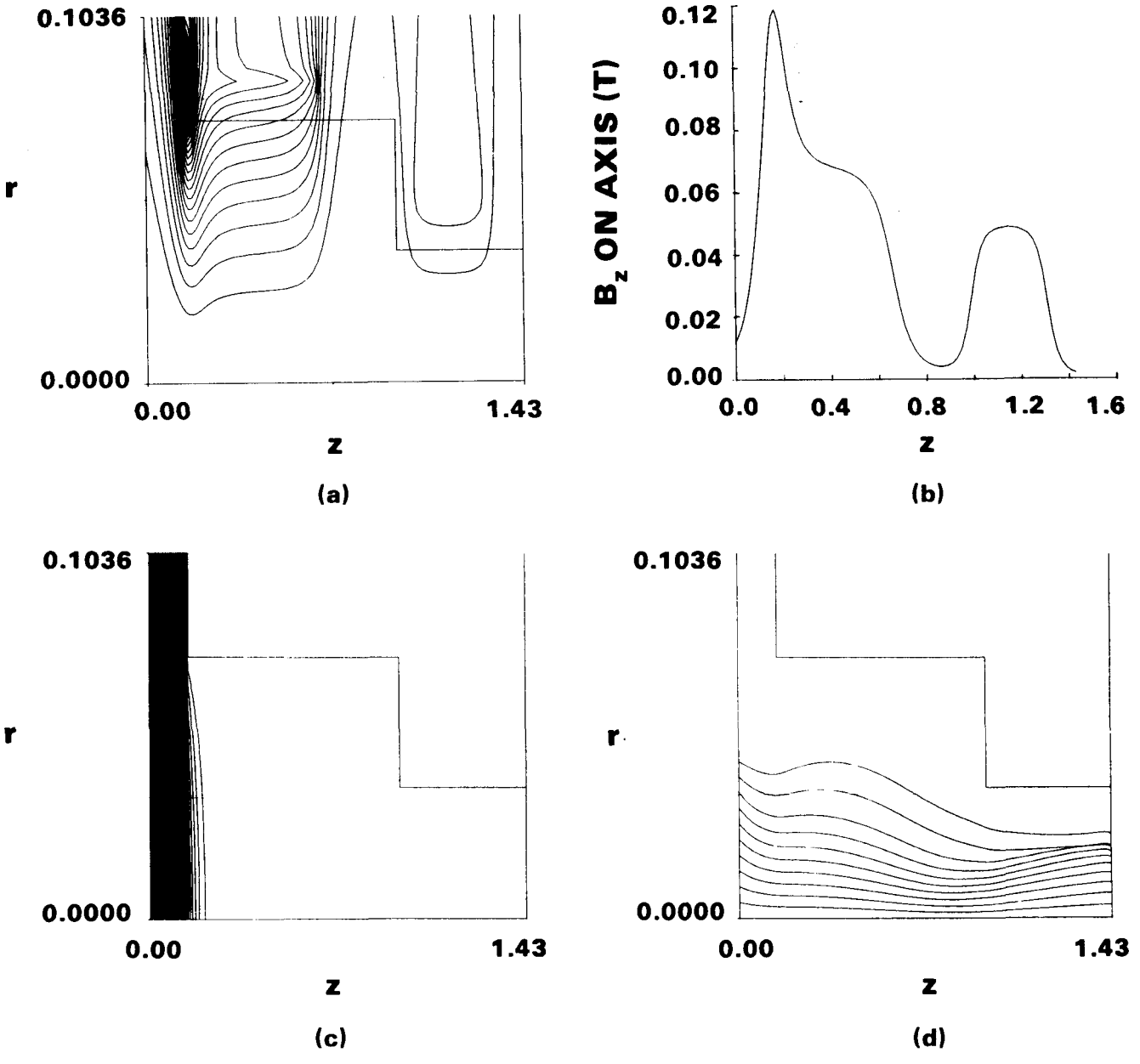

Figure 13. Recirc diode at 4 MV with TRAJ. Input: d = 15 cm, r (emit) = 4.4 cm.
(a) B lines due to focus coils and two solenoids.
(b) B_z (z, r = 0).
(c) Vacuum ϕ (r, z) contours.
(d) Trajectories, 7.2 kA.

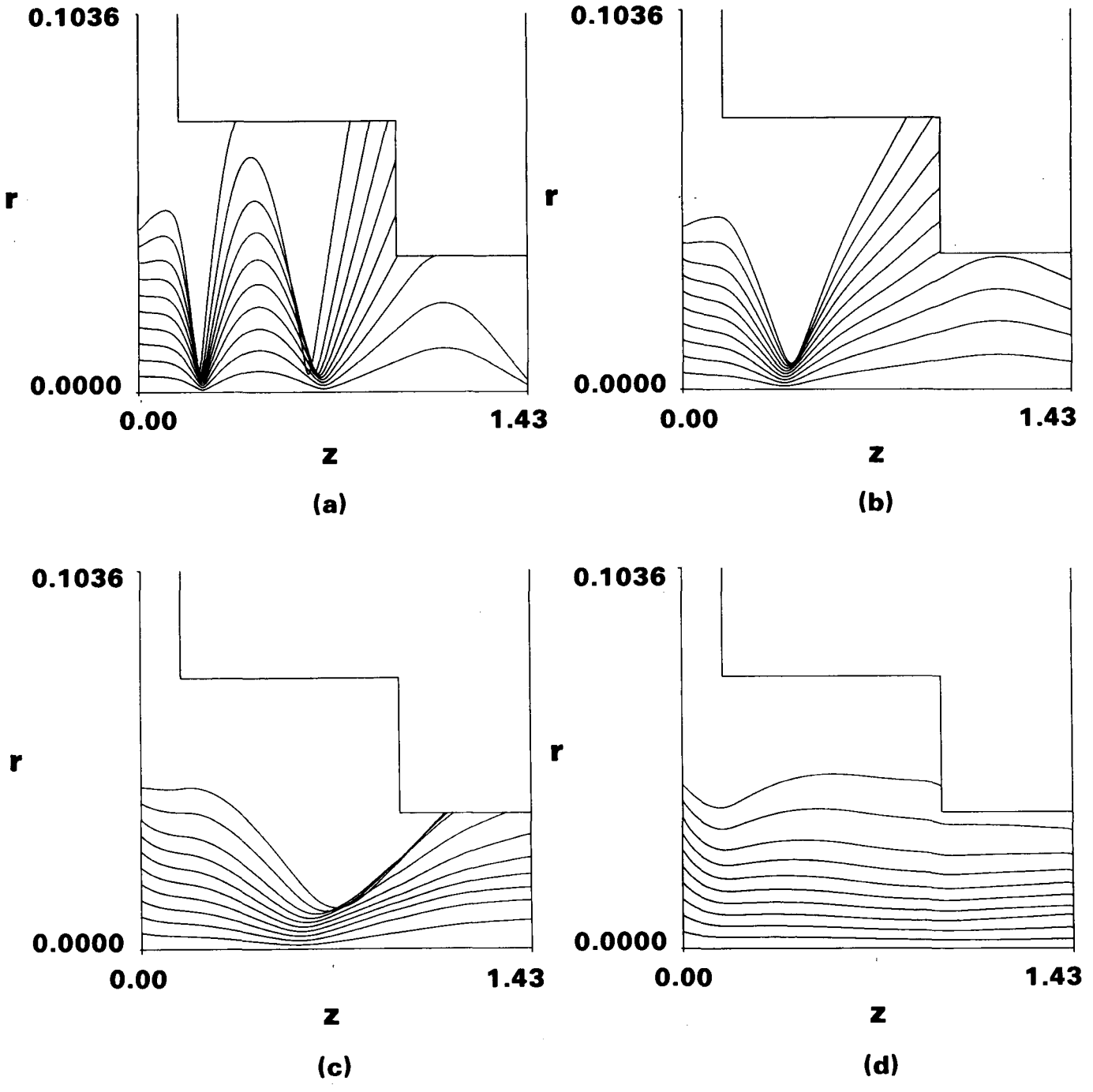

Figure 14. As in Fig. 13d, except
(a) 1 MV, 1.1 kA.
(b) 2 MV, 2.9 kA.
(c) 3 MV, 4.9 kA.
(d) 5 MV, 9.5 kA.

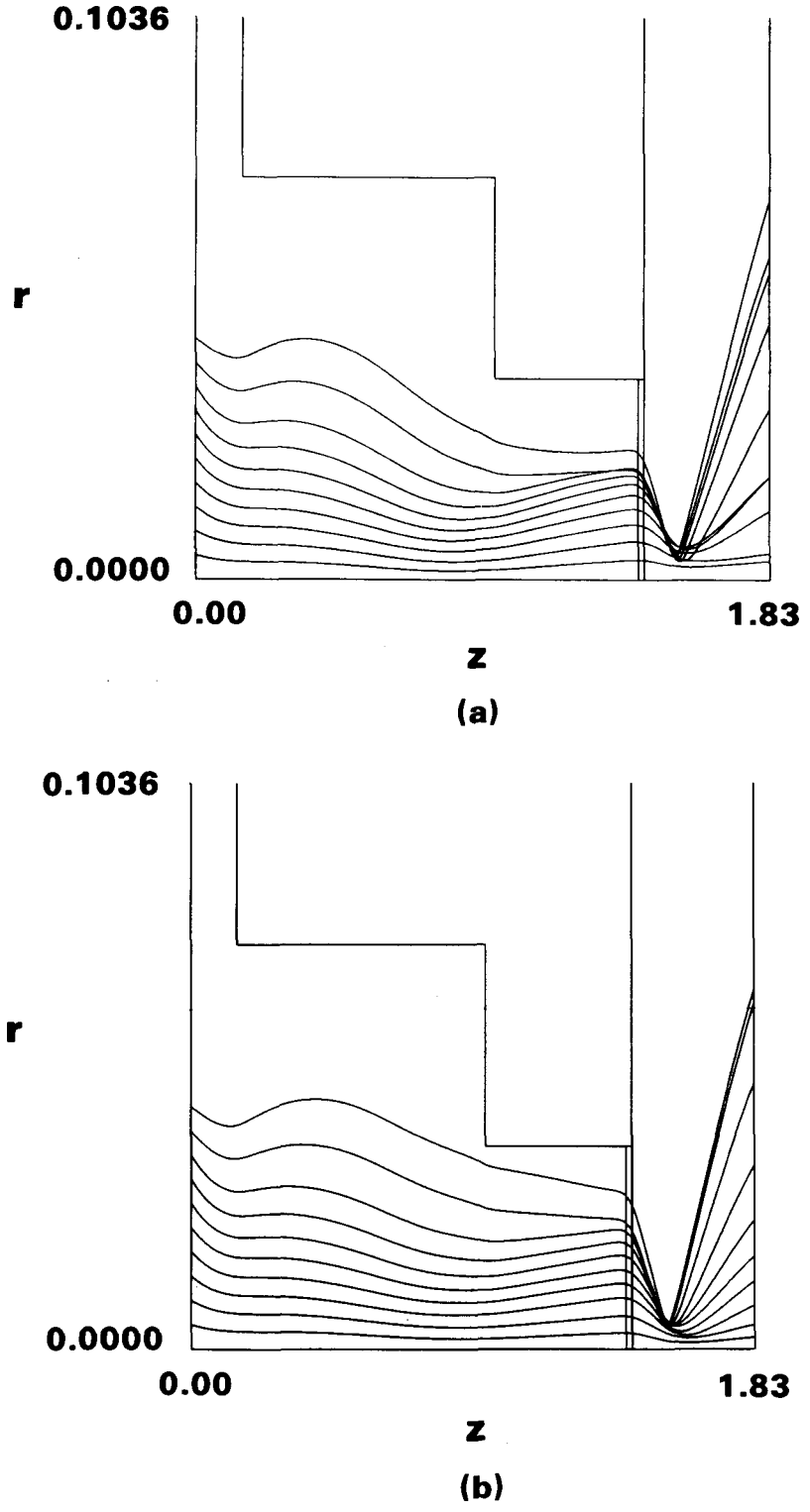

Figure 15. As in Fig. 13, except add 40 cm of vacuum past the exit foil. V = 4 MV, I = 7.2 kA.
(a) As in Fig. 13d.
(b) Same but reduce current in first solenoid by 100 A.

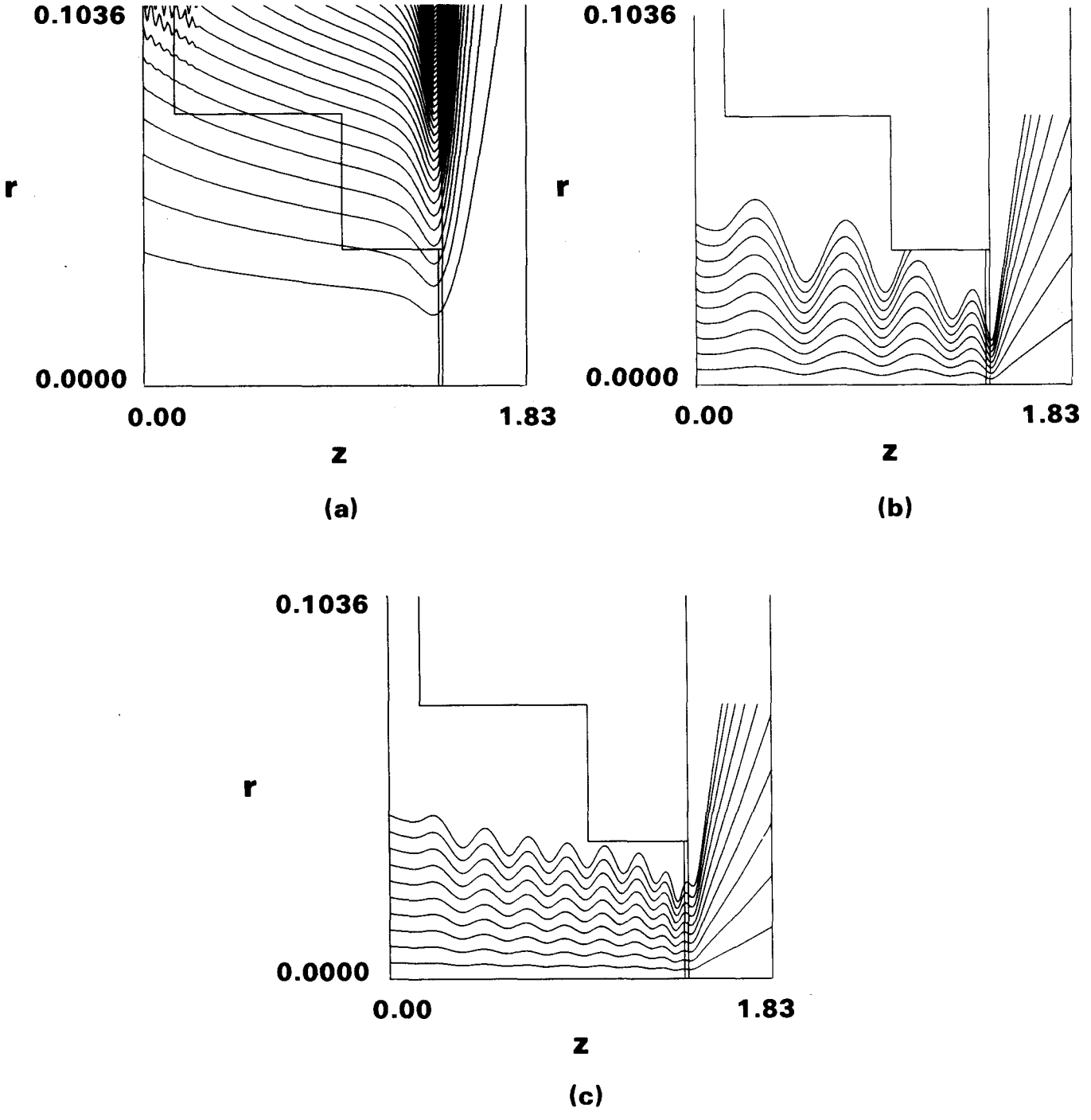

Figure 16. Recirc diode with converging B to suppress foil pinch. V = 4 MV, I = 7.3 kA.
(a) B lines.
(b) Trajectories for B_z (max) = 5 kG.
(c) Trajectories for B_z (max) = 10 kG. Max V_θ here is 0.75 c.

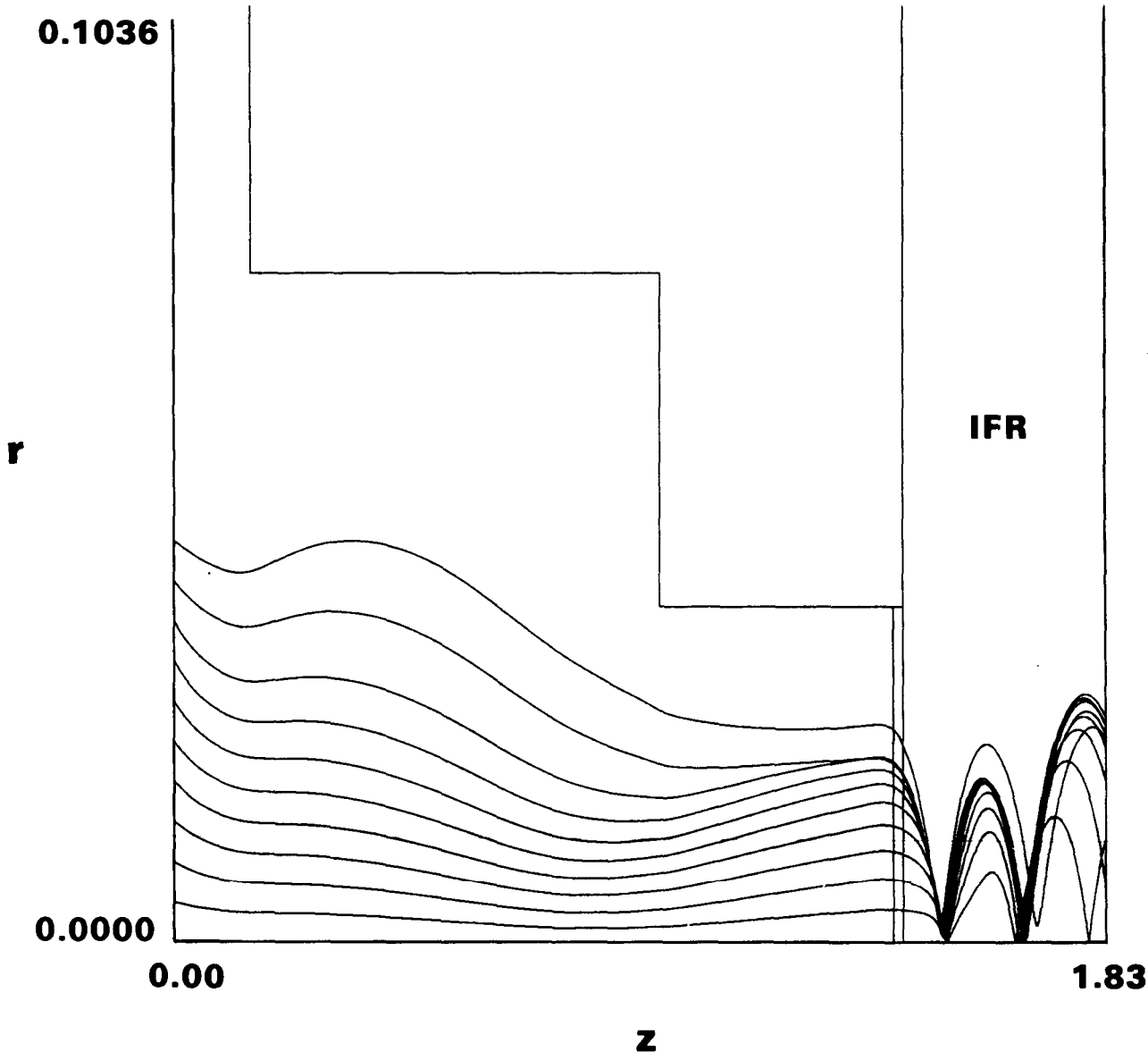

Figure 17. As in Fig. 15a, but add IFR channel (f = 1) for z >143 cm, i.e., past foil.

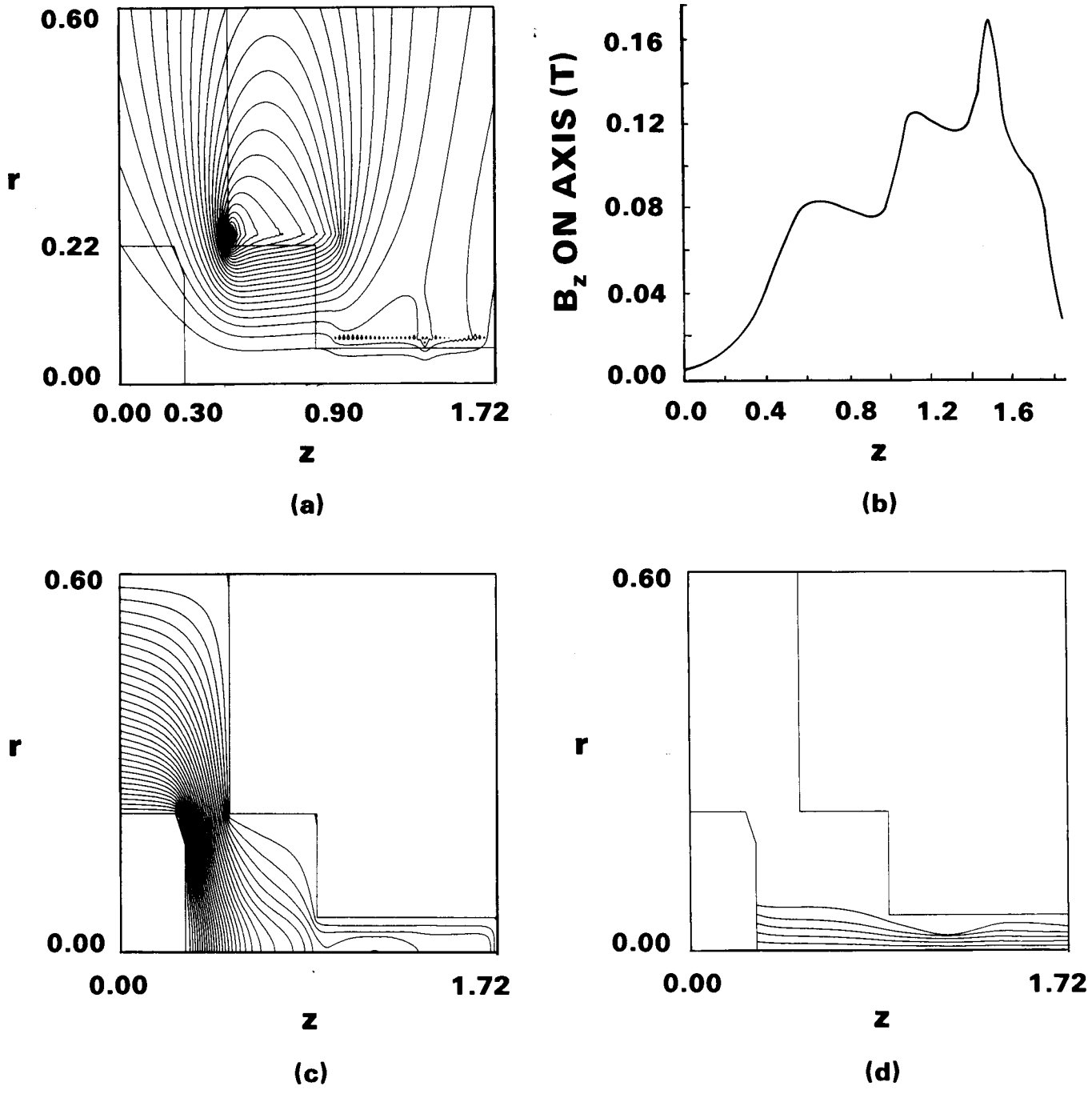

Figure 18. Recirc diode including cathode shank. V = 4 MV, I = 8.4 kA, d = 20 cm, r(k) = 22 cm, r(emit) = 7.2 cm.
(a) B Lines (2 solenoids and 2 focus coils).
(b) B_z (z, r = o).
(c) ϕ (r, z) with beam.
(d) Trajectories (every tenth).

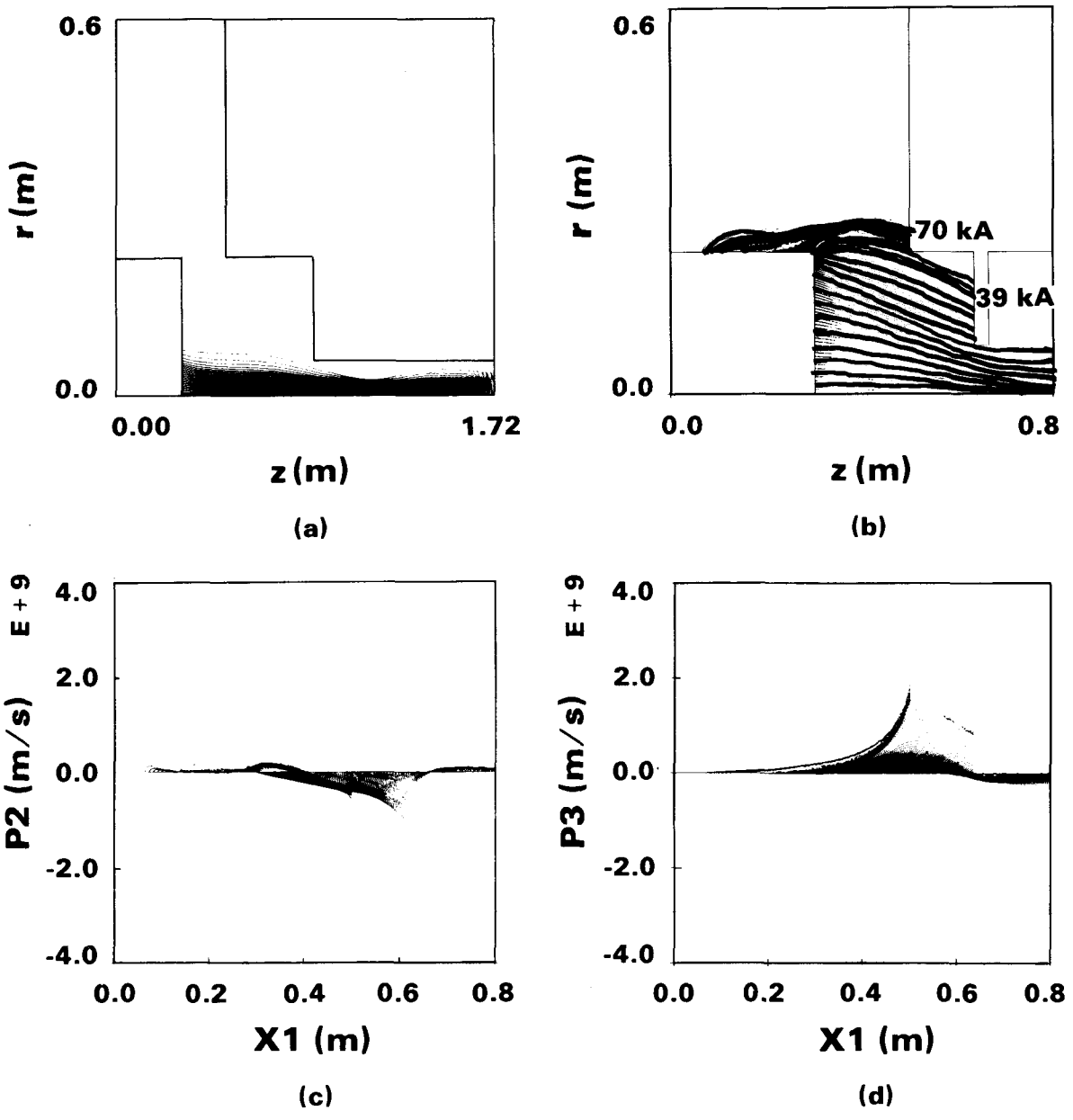

Figure 19. As in Fig. 18, but use MAGIC.

(a) Electron map in steady state, V = 4 MV, I = 8.4 kA (compare 18d).

(b) Same but include emission from entire cathode, corner not rounded, and aperture added to reduce beam current; here we simulate only the first 80 cm in part (a).
Output (rhs): 11 kA, rms $\beta_\perp$ = 0.05, r = 5.6 cm.
Total current 119 kA, 70 kA from shank.

(c) V_r vs. z phase space for part (b).

(d) V_θ vs. z phase space for part (b).

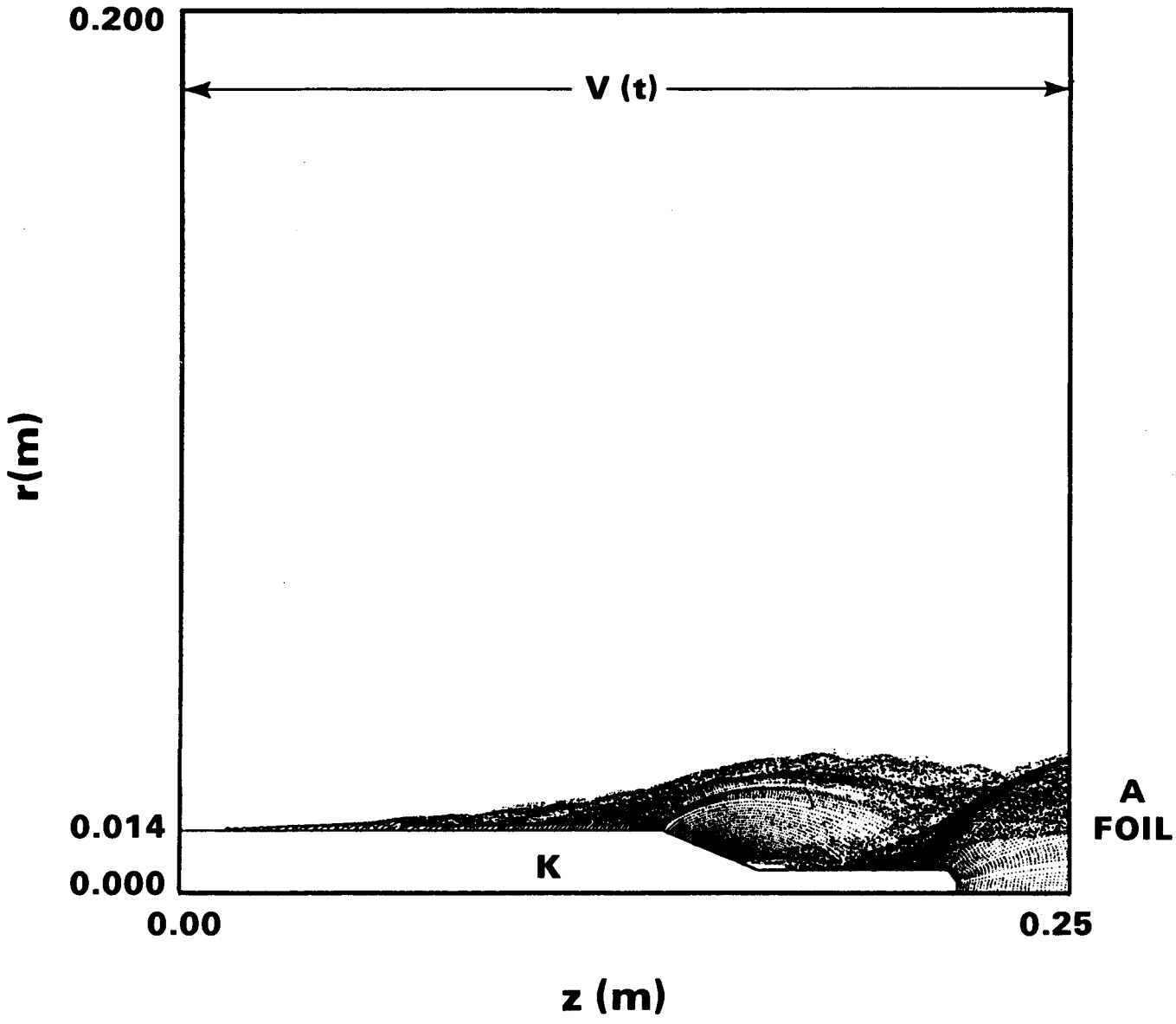

Figure 20. MAGIC run of Recirc foil diode including feed region. V = 1.5 MV, 2-ns rise, I = 12 kA for d = 3.2 cm. There is no applied B_z. Outer radius R = 20 cm. The steady state electron map is shown.

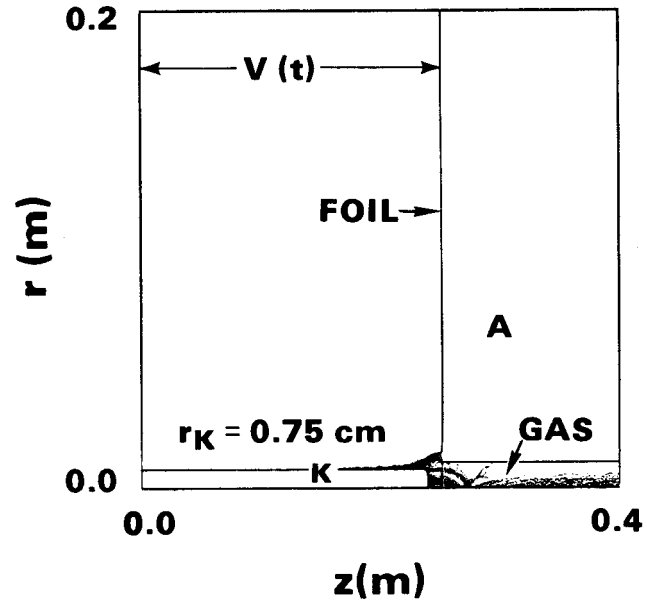

(a)

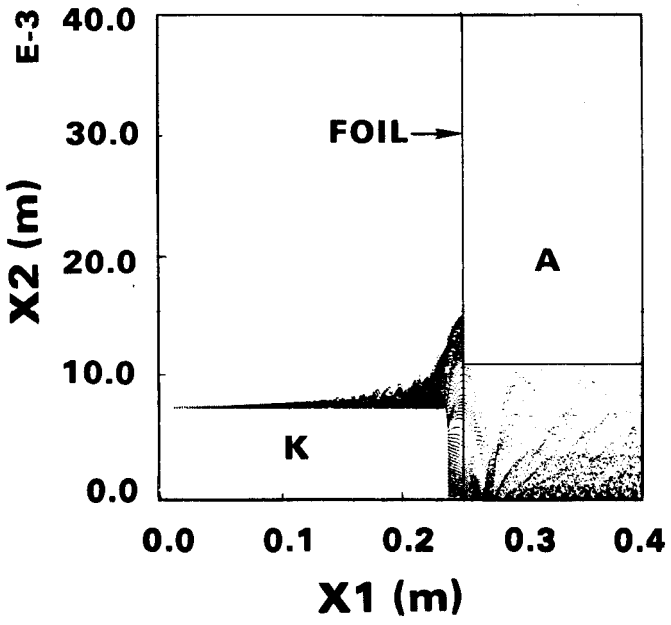

(b)

Figure 21. MAGIC run of recent Recirc diode, including L = 15 cm of IFR cell with f = 1 assumed (and no current neutralization). V = 1.5 MV (2-ns rise), I = 22.5 kA (diode), 6.5 kA (rhs). B_z = 0.
(a) Electron map.
(b) Blown-up electron map.

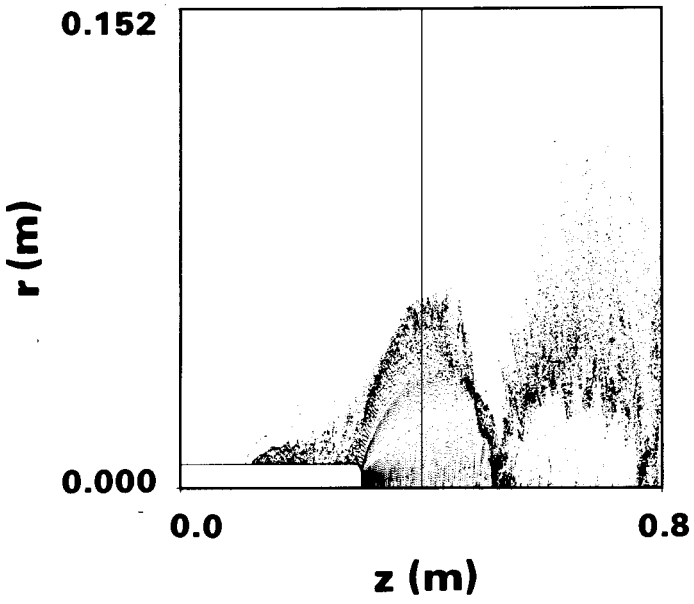

(a)

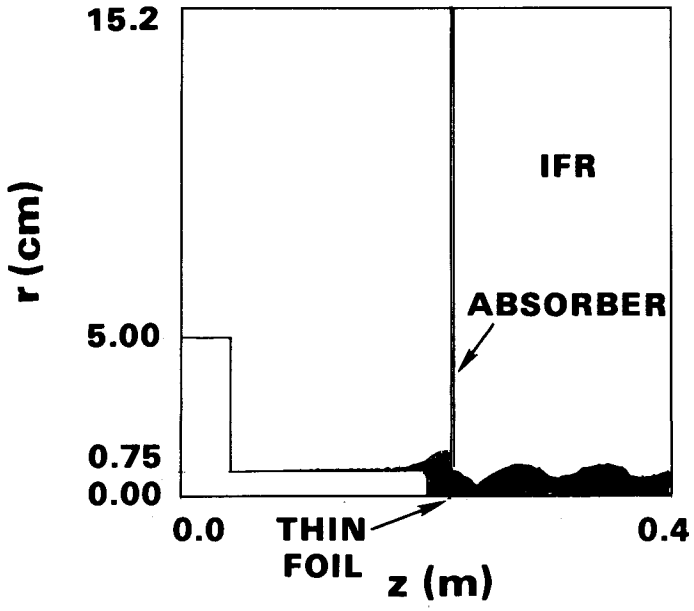

(b)

Figure 22. Recirc foil diode plus IFR (MAGIC) based on IBEX Parameters. $B_z = 0$.
(a) 3.2 MV, 26 kA, d = 10 cm, large hot beam. Run 4I, Table I.
(b) 4 MV, 48 kA total, d = 2 cm, aperture. Output beam: 11 kA, $\beta_\perp = 0.21$, r = 5.6 mm. Beam in IFR is not completely phase mixed. The larger-radius cathode (lhs) models the real system, but does not have much effect on the diode behavior for given diode voltage.

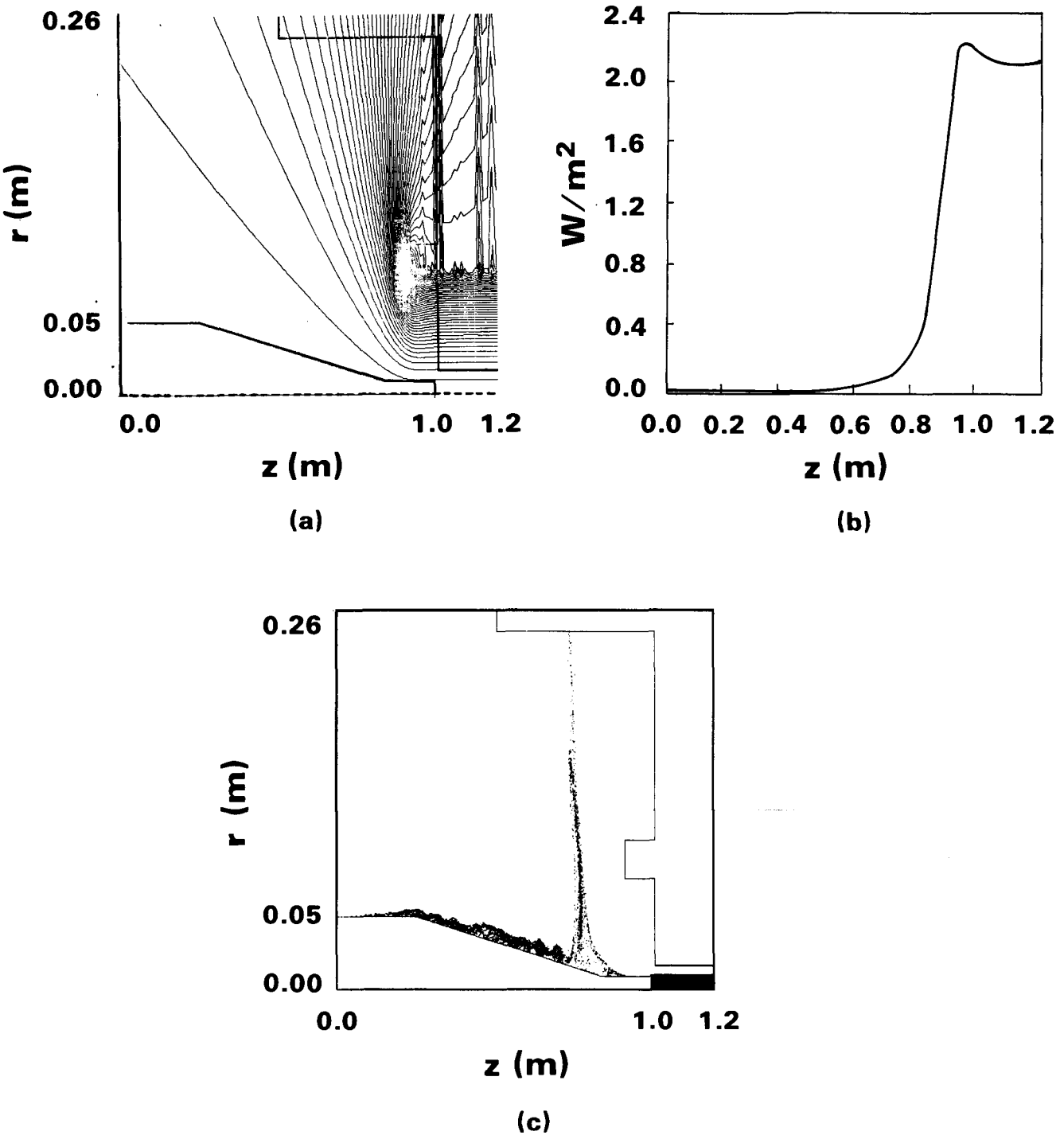

Figure 23. RADLAC feed/diode simulation for 4° taper, Run 29 of Table II. For a 1.2-cm A-K gap, V = 4.75 MV, the total I = 58 kA of which 13 kA is lost.
(a) B lines, based on measured values.
(b) $B_z(z)$ at r = 6 mm.
(c) Electron map.

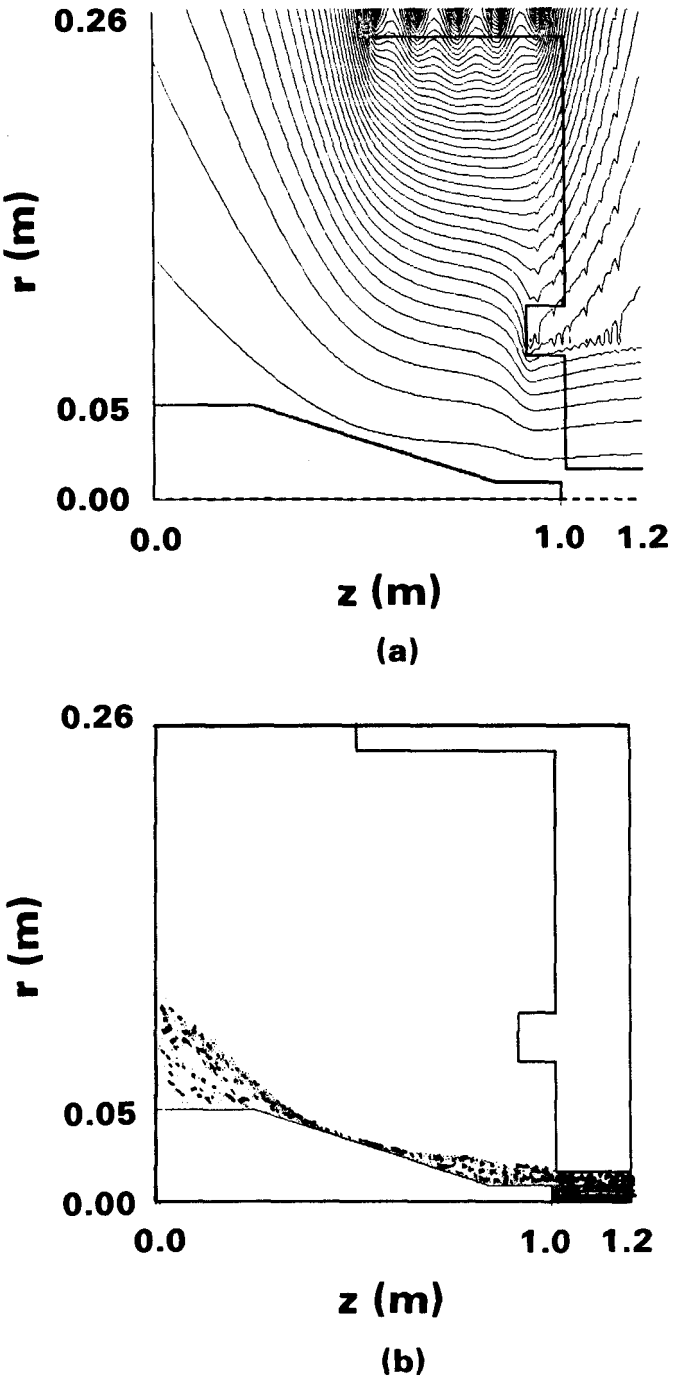

Figure 24. As in Fig. 23, but add five 160 kA coils at large $r \approx 25$ cm.
(a) B lines.
(b) Electron map. V = 5 MV, I = 50 kA (total), of which 14 kA is lost near the tube entrance.

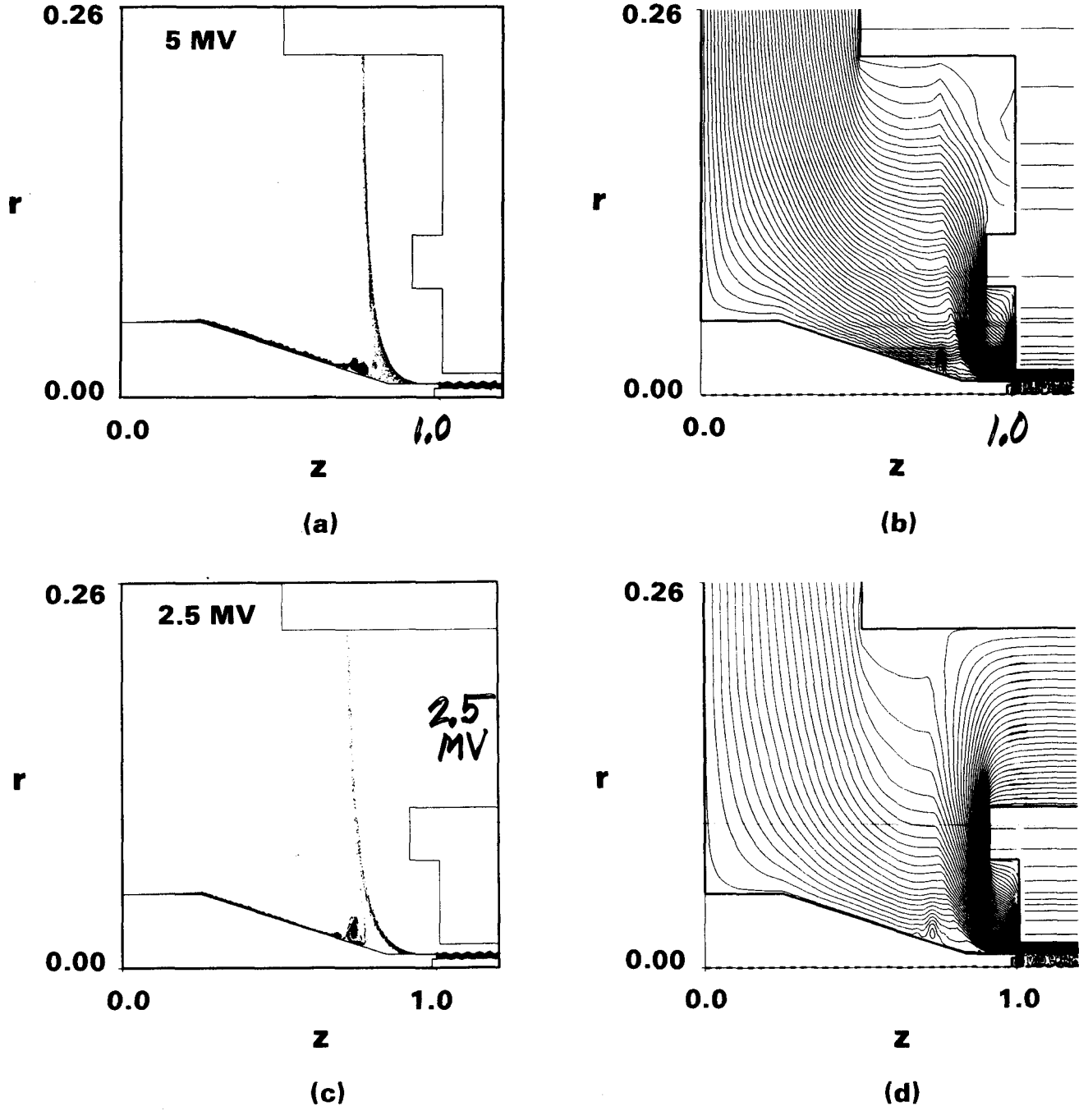

Figure 25. As in Fig. 23, but annular cathode, finer mesh, d = 1.0 cm. (Compare Fig. 23c.)
(a) 5 MV applied at r = 26 cm. Result: 62-kA beam, 13-kA loss (run 52).
(b) $\int E \bullet dl$ contours for (a).
(c) 2.5 MV applied at r = 26 cm, plus 2.5 MV applied rhs (closer to experiment). Result: 63-kA beam, 5-kA loss (run 50).
(d) $\int E \bullet dl$ contours for (c).

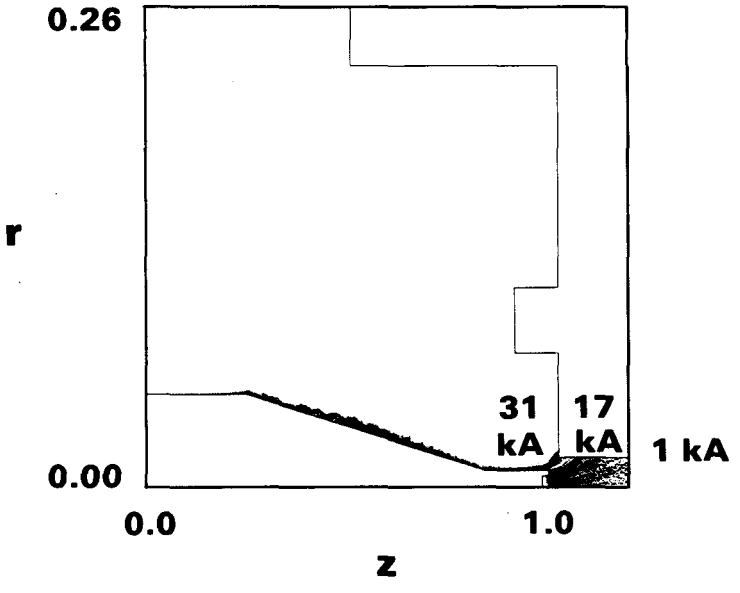

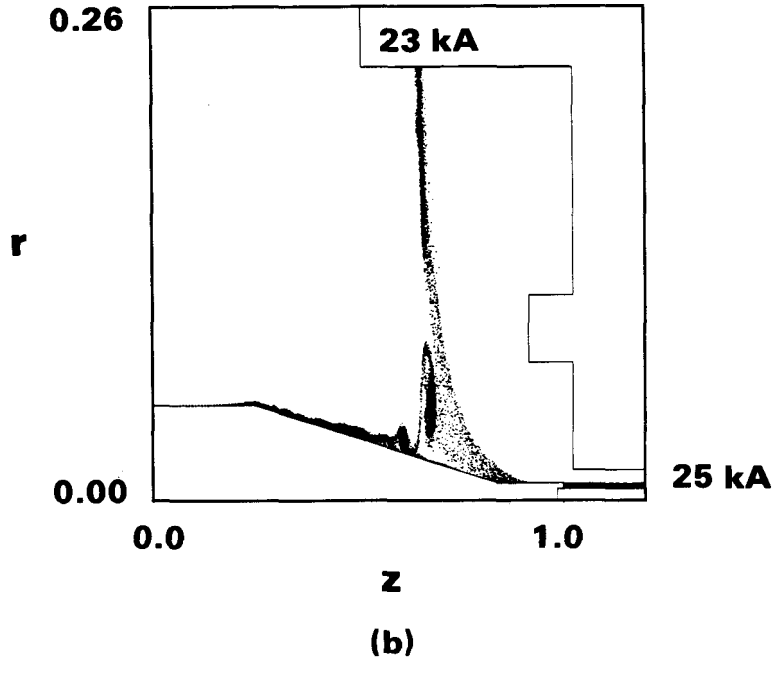

Figure 26. RADLAC feed/diode MAGIC run with
(a) no applied B (run 44, Table II).
(b) twice the experimental applied B (run 45).

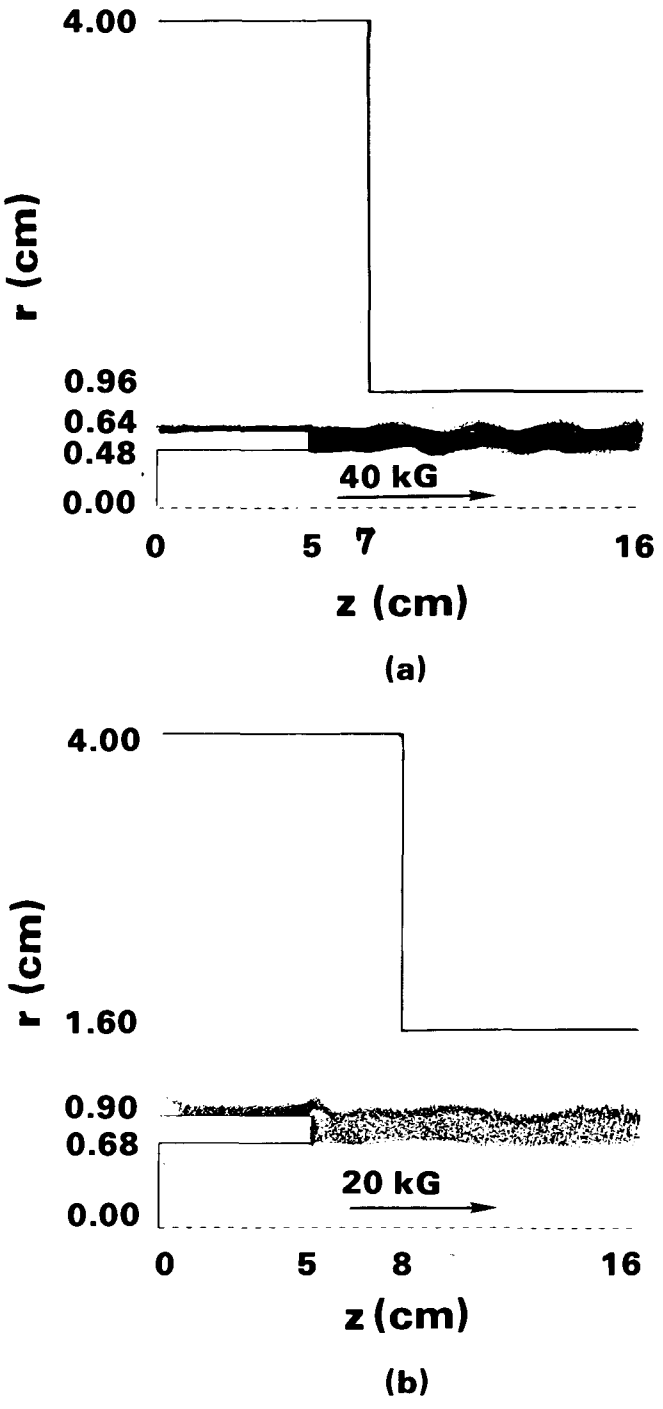

Figure 27.

(a) MAGIC run of small-cathode RADLAC diode at 40 kG (run 21, Table III). I = 40 kA (26 kA from shank).

(b) Larger-cathode RADLAC diode at 20 kG (run 24, Table III).

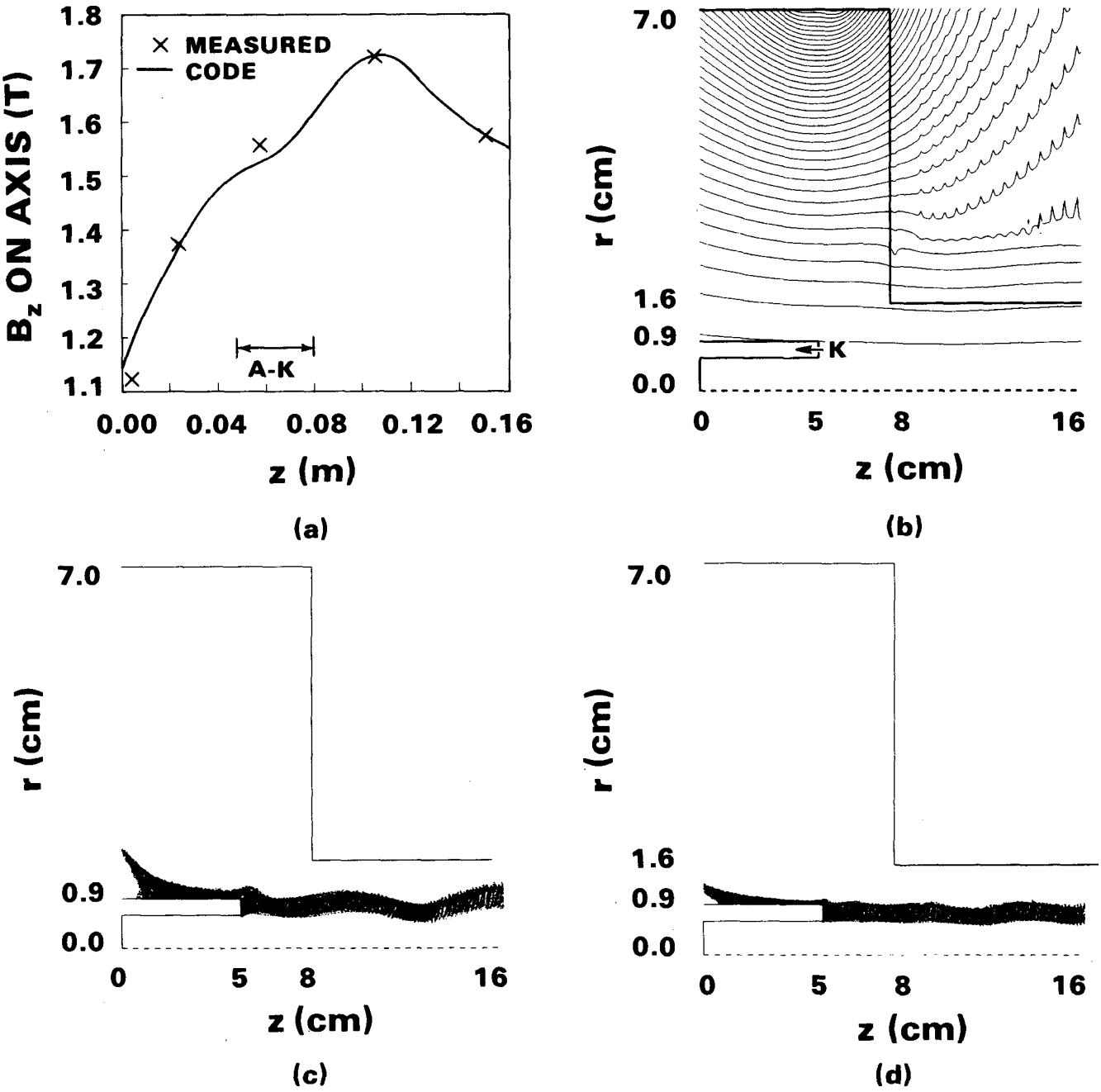

Figure 28. MAGIC run of RADLAC II diode, experimental case.

(a) $B_z(z)$ with X = measured values, solid line = values used in MAGIC.

(b) B lines and problem set-up.

(c) Electrons in steady state. Parameters: voltage 5 MV, current 40 kA, $\beta_\perp$ (out) = 0.15. Run 30, Table III.

(d) As in (c), but the magnitude of B (applied) is increased by 25/17; the output emittance is much improved: $\beta_\perp$ (out) = 0.09. Run 31, Table III.

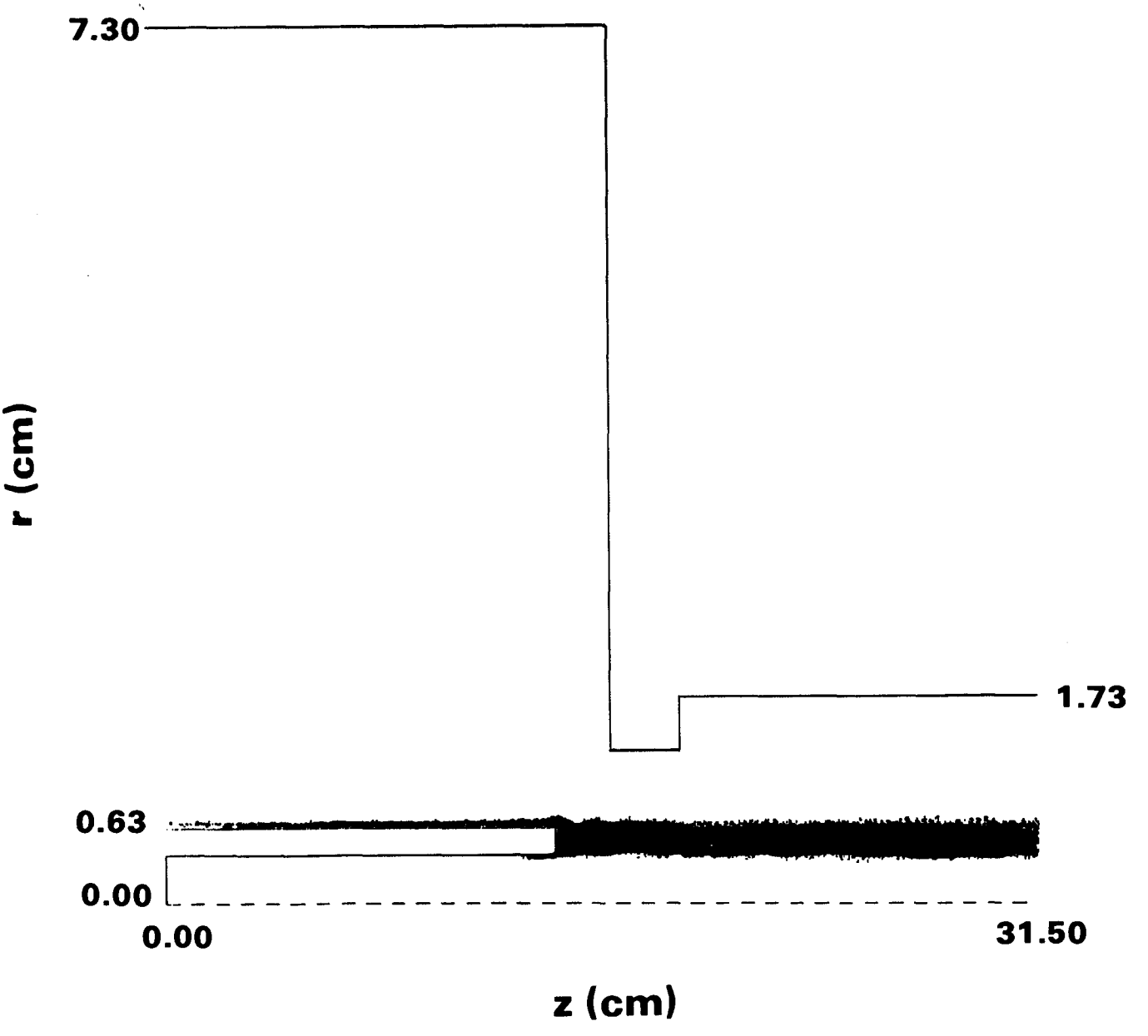

Figure 29. MAGIC run of IBEX foilless immersed diode (uniform 24 kG). V = 3.5 MV, I = 28 kA. See run 17, Table IV. A very good-quality beam.

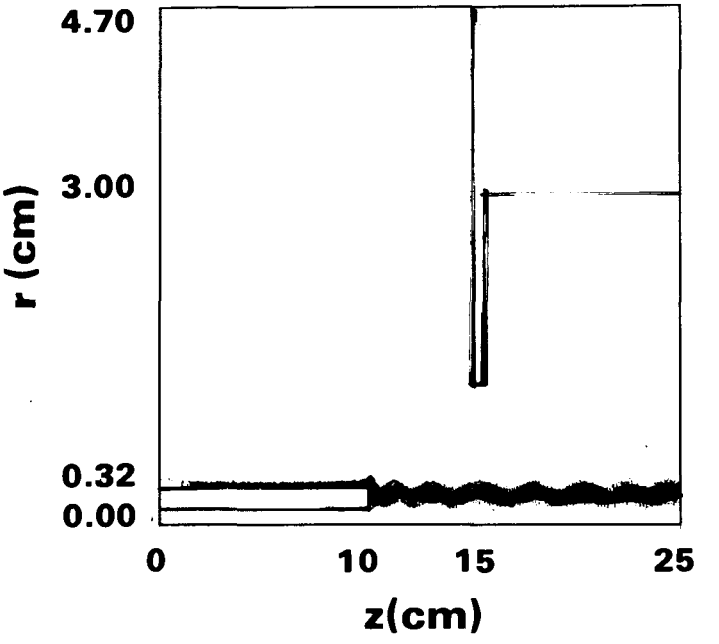

(a)

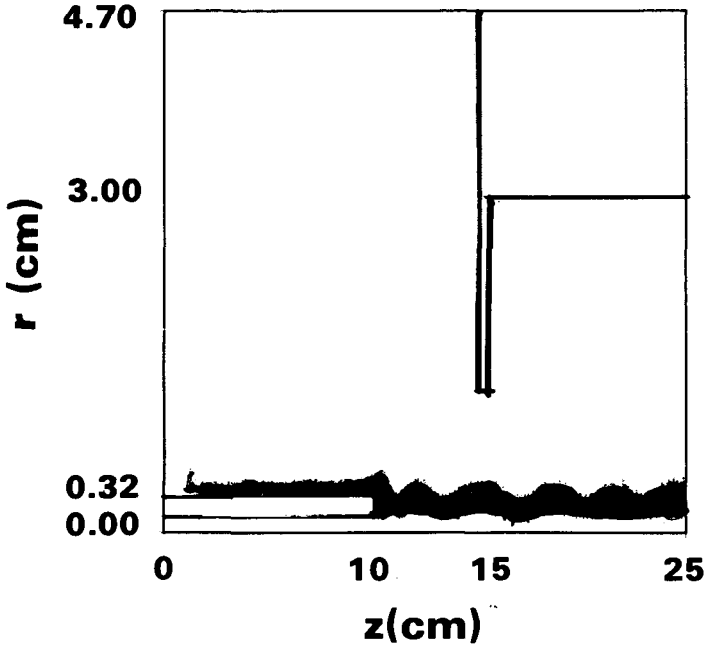

(b)

Figure 30. As in Fig. 29, but revised geometry.
(a) I = 14.5 kA, B_0 = 22 kG, run 22 of Table IV.
(b) I = 16 kA, B_0 = 16 kG, run 23 of Table IV.

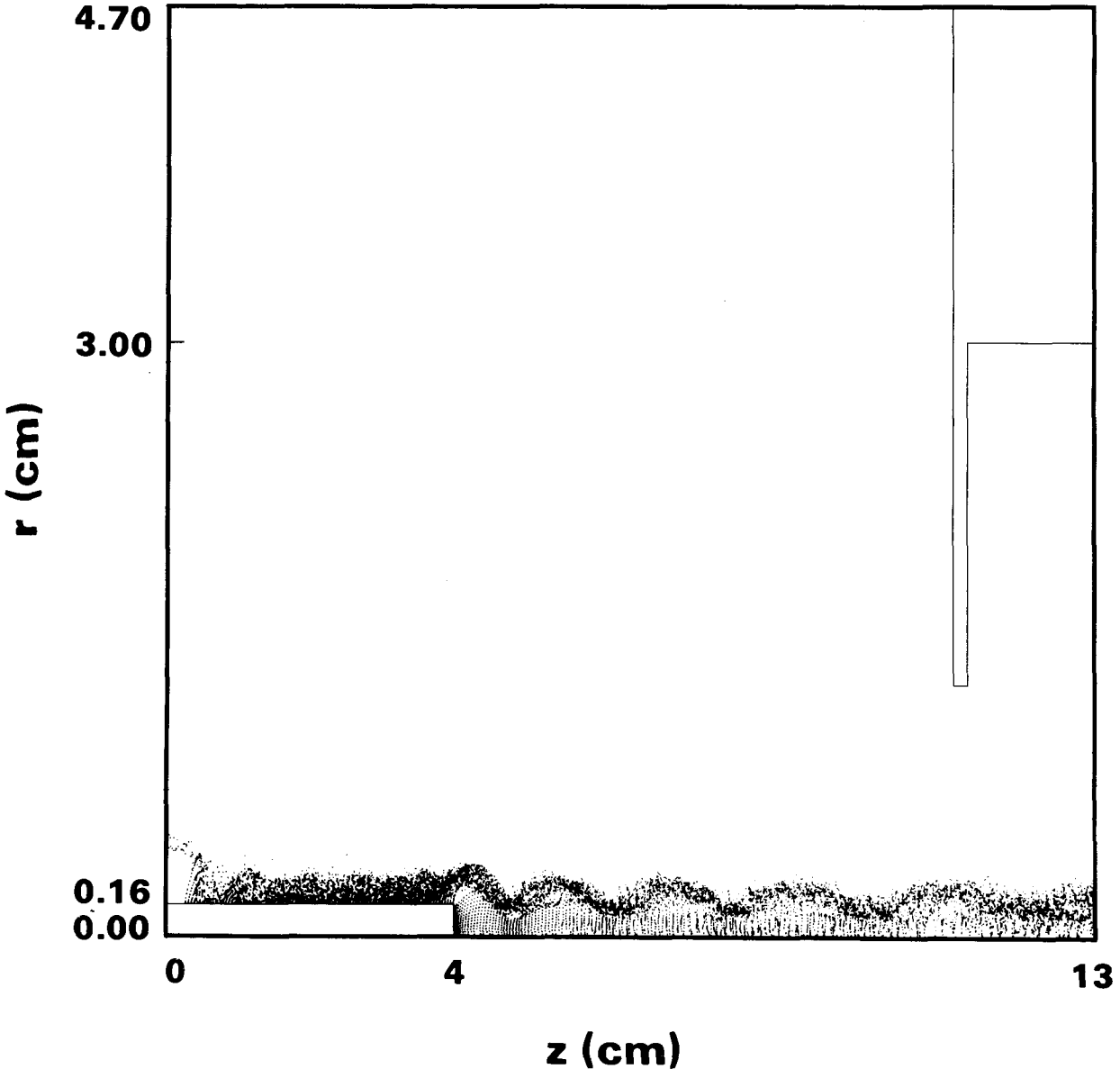

Figure 31. As in Fig. 30, but tiny cathode, r_k = 1.6 mm V = 3.5 MV, I = 12 kA, run 27 of Table IV.

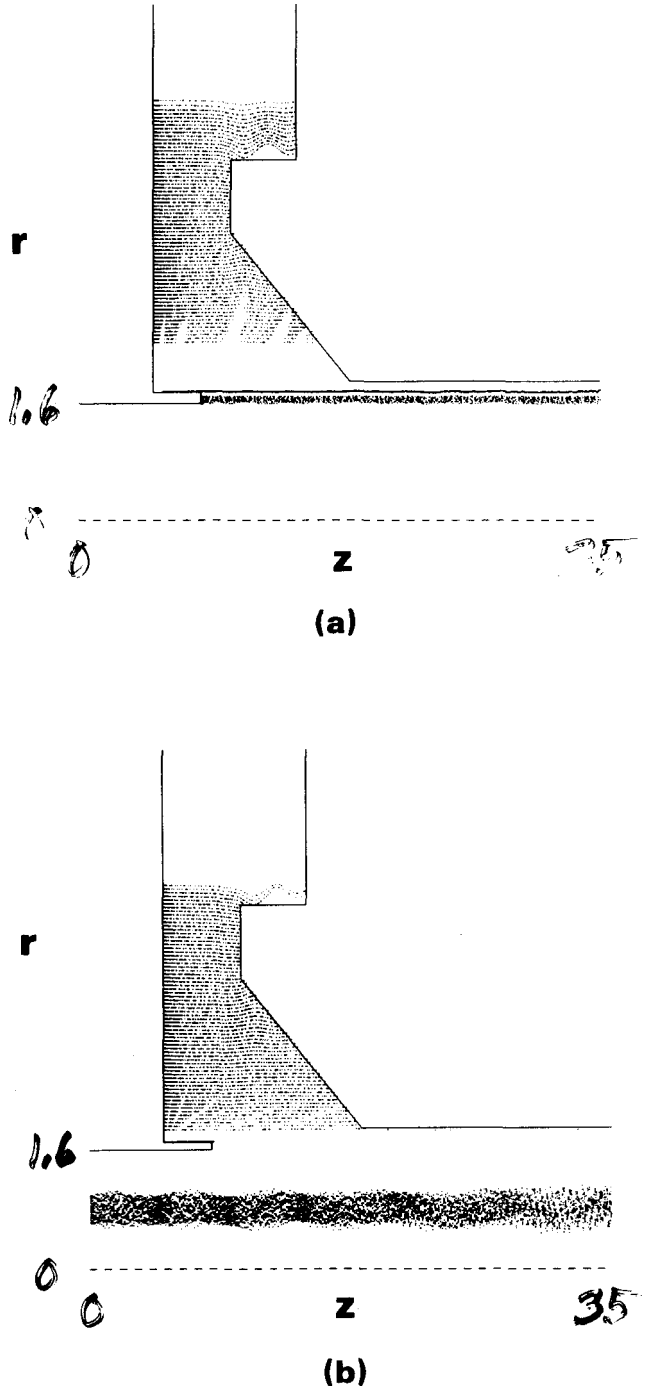

Figure 32. MAGIC calculation of leakage currents in gap one of RADLAC, assuming B_z = 20 kG (uniform) and V(gap) = 2.5 MV (steady).
(a) No beam, leakage 23 kA (10 kA from stickout).
(b) 40 kA beam, leakage 10 kA (none from stickout).

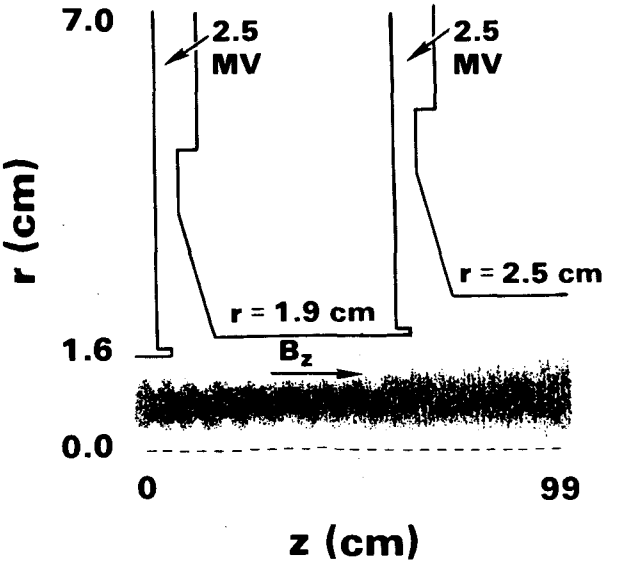

(a)

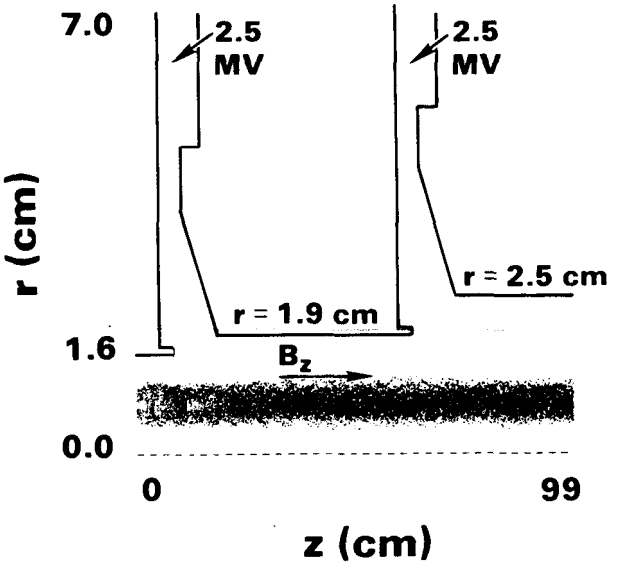

(b)

Figure 33. MAGIC simulation of 5 MeV, 40-kA beam passing through the first two RADLAC gaps. Gap voltage is 2.5 MV/gap. The drift-tube wall radius increases to reduce radial oscillation. Applied B_z = 20 kG. The $\beta_\perp$ increases from 0.11 to 0.15, mainly due to the grid instability.
(a) Electron map; I_{SCL} (lhs) = 95 kA; I_{SCL} (rhs) = 114 kA.
(b) As in (a), but using spatial smoothing on j_z and j_θ. The smoother-looking answer also may mask the real emittance increase.

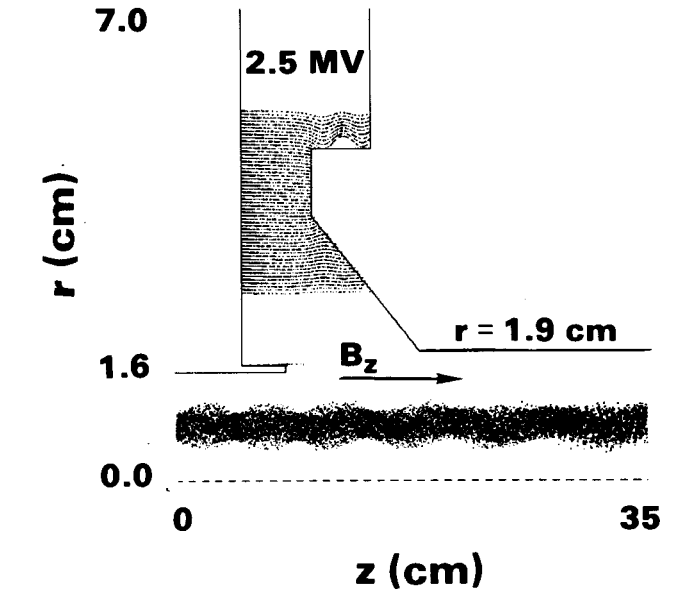

(a)

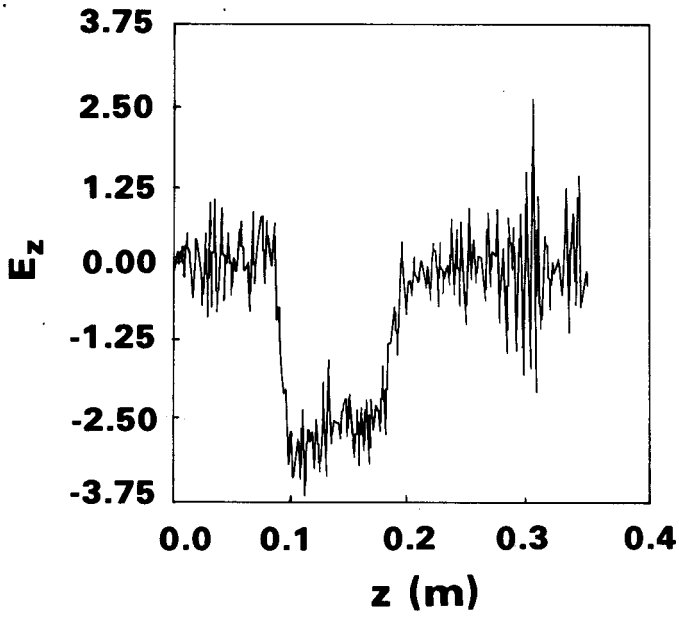

(b)

Figure 34. Single-gap simulation with parameters as before: 5 MeV, 40-kA beam, gap V = 2.5 MV, B_z = 20 kG. Electron leakage in gap is 11 kA. Output beam is 7.5 MeV (total energy; about 20% of this is potential) with $\gamma\beta_\perp$ about 30% larger.
(a) Electron map.
(b) $E_z(z)$ plotted at r = 1.05 cm.

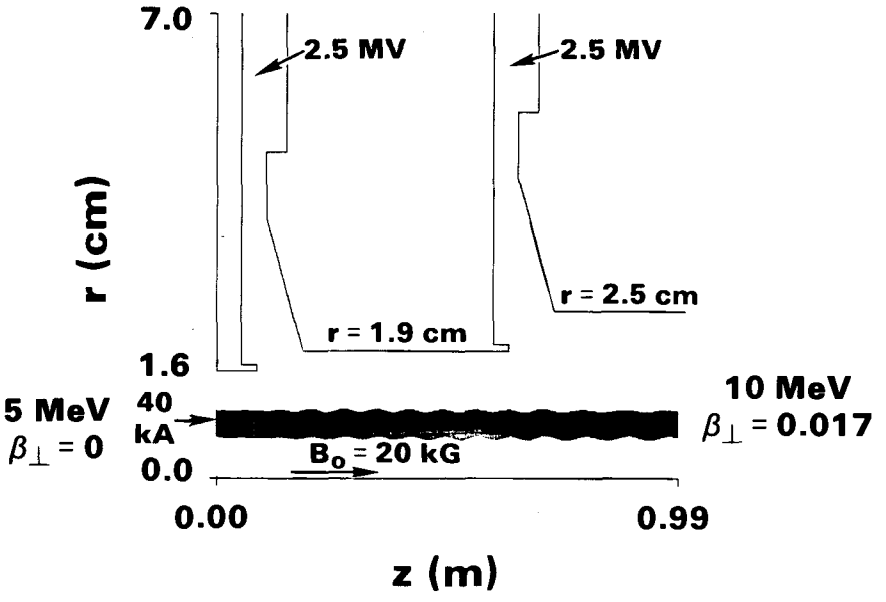

(a)

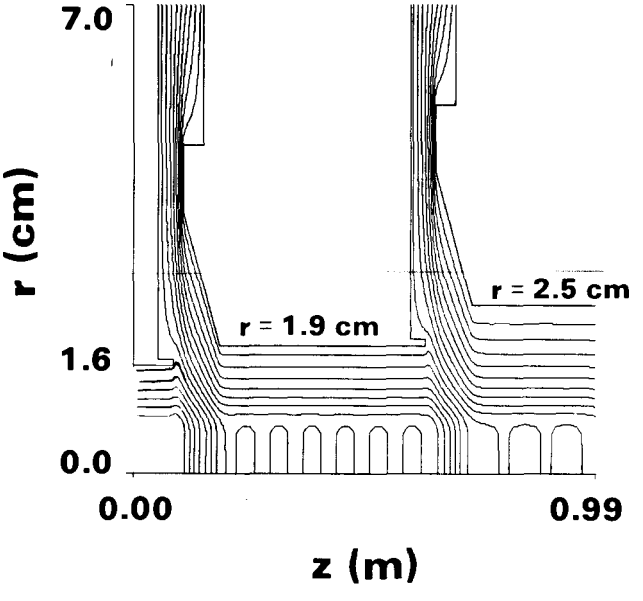

(b)

Figure 35. TRAJ solution to two-gap RADLAC problem for cold ($\beta_\perp$ = 0) input beam. Parameters as in Figs. 33-34 (beam 40 kA, 5 MeV; gaps 2.5 MV; B_z = 20 kG). Both ends, at z = 0 and 99 cm, are open (no foils) with E_z = 0 there. Output beam: 10 MeV (total energy), 40 kA, $\beta_\perp$ = 0.017, γ = 16.3, outer radius 1 cm.
(a) Trajectories.
(b) Equipotentials ϕ(r, z) = const, with beam.

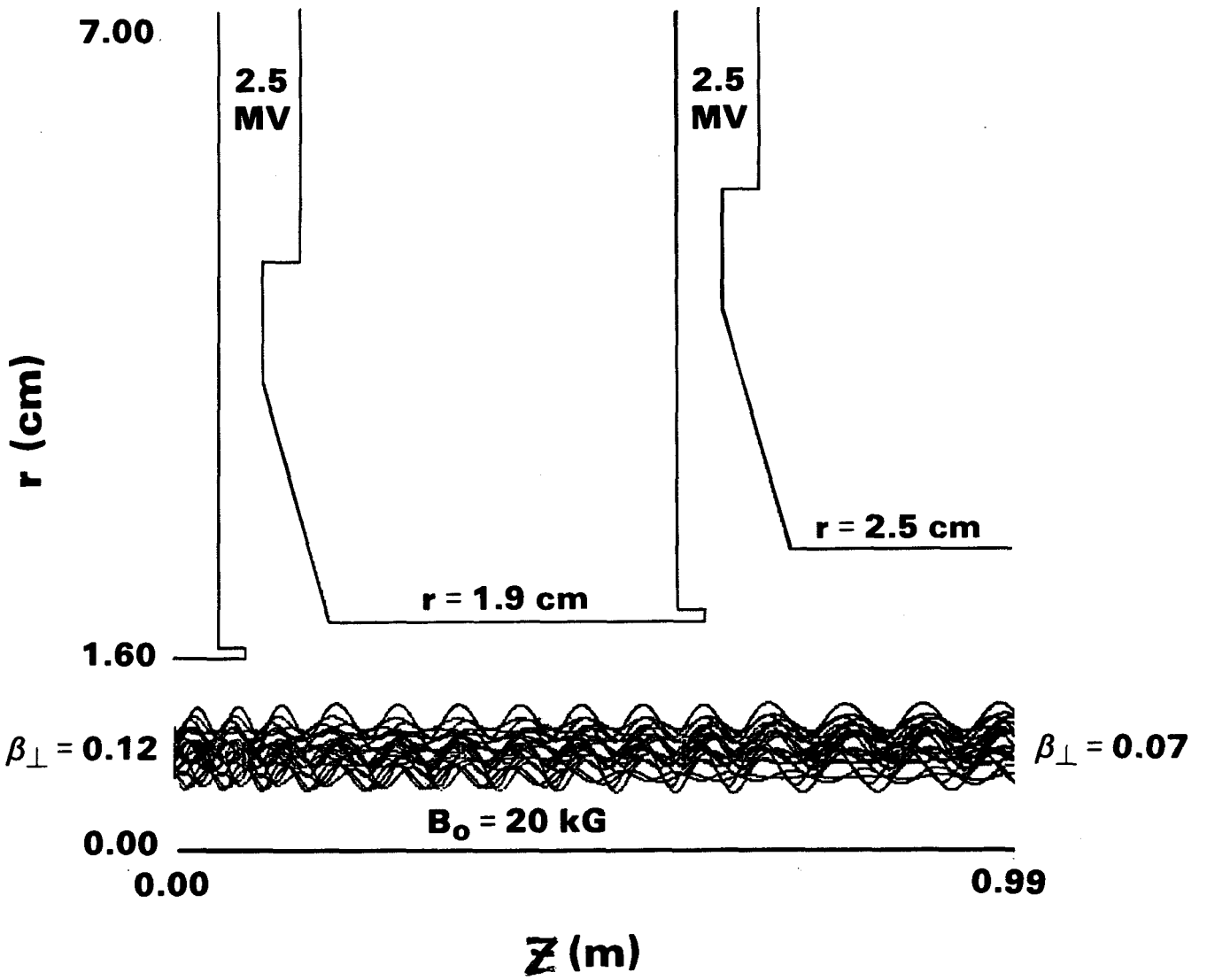

Figure 36. As in Fig. 35, but warm beam input, $\beta_\perp$ = 0.12.

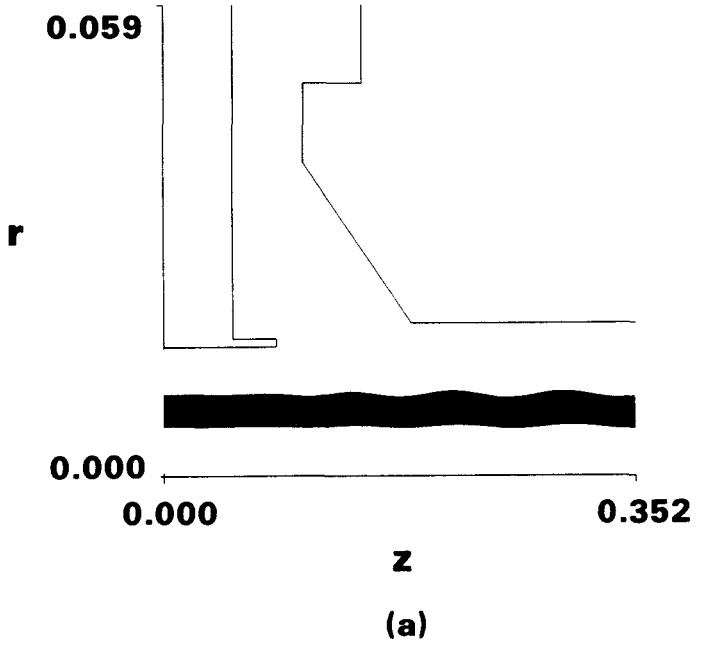

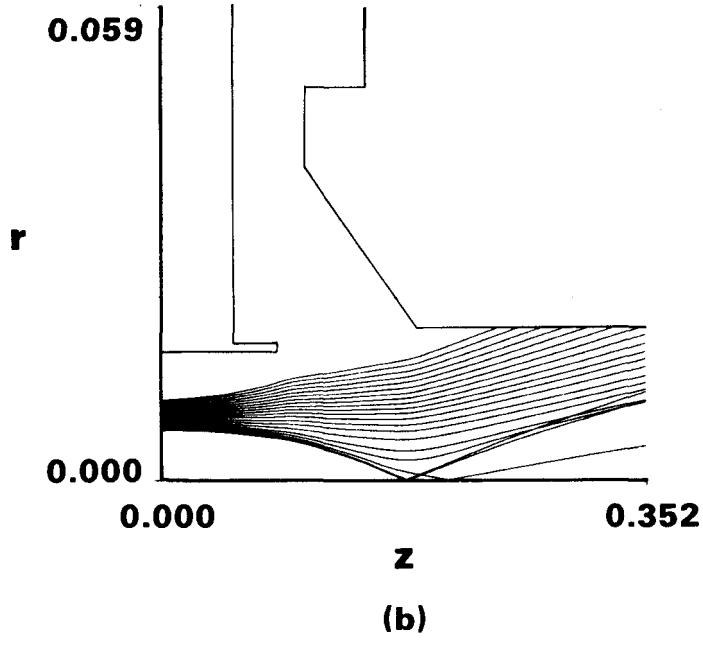

Figure 37. TRAJ equilibrium beam for first accelerating gap of RADLAC. Input beam: 40 kA, 5 MeV (total), r_{rms} = 8.3 mm, cold. Gap: 2.5 MV. Output beam: $\beta_\perp$ = 0.028, r_{rms} = 8.0 mm, 7.5 MeV (total). All lengths are in meters.
(a) With B_o = 17 kG, uniform.
(b) With no applied B.

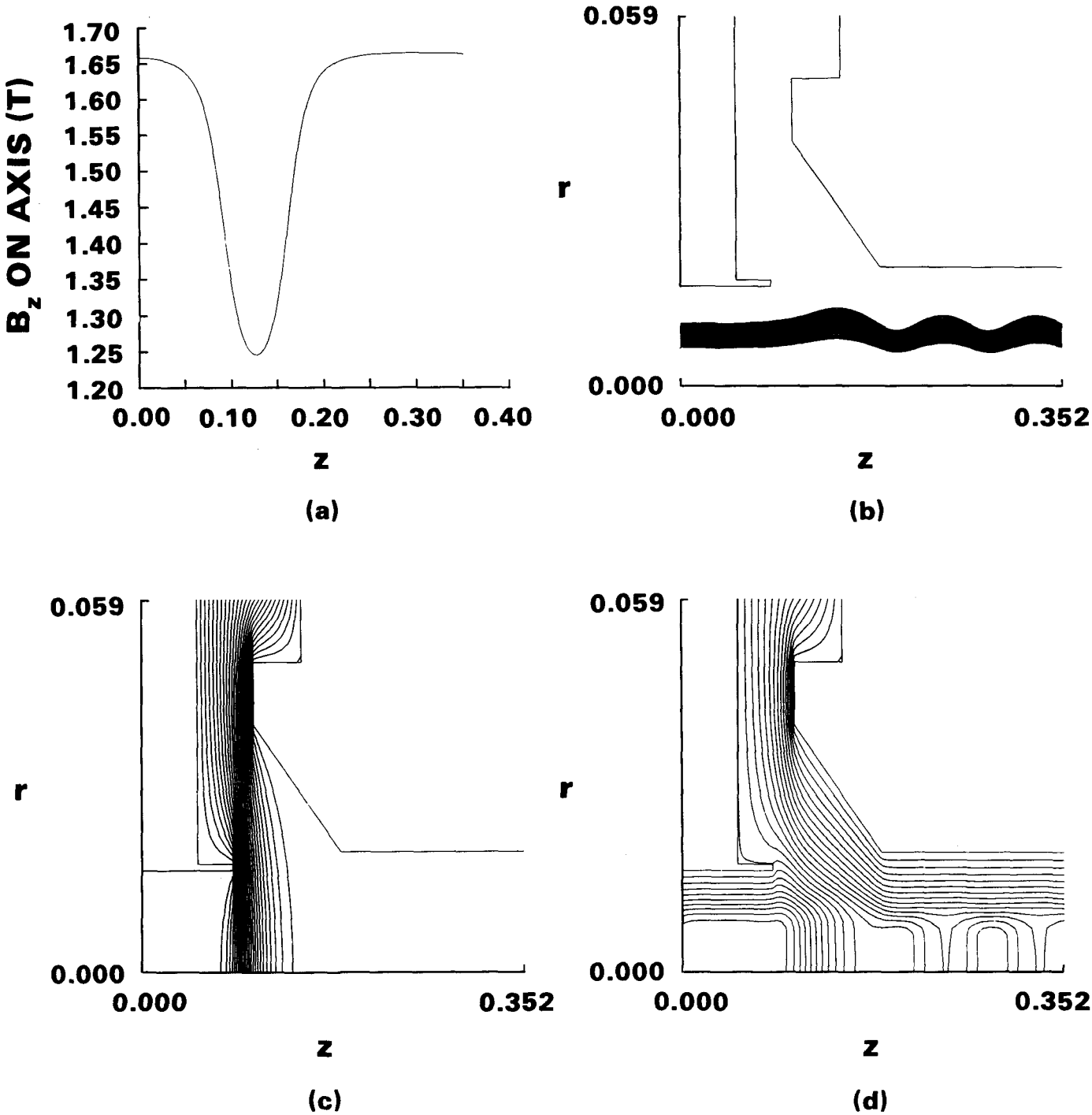

Figure 38. As in Fig. 37a, but apply nonuniform, realistic B_o.
(a) Code approximation to measured $B_z(z)$ on axis.
(b) Trajectories for cold input beam.
(c) Vacuum potentials.
(d) Potentials with beam (E_z = 0 at both ends).

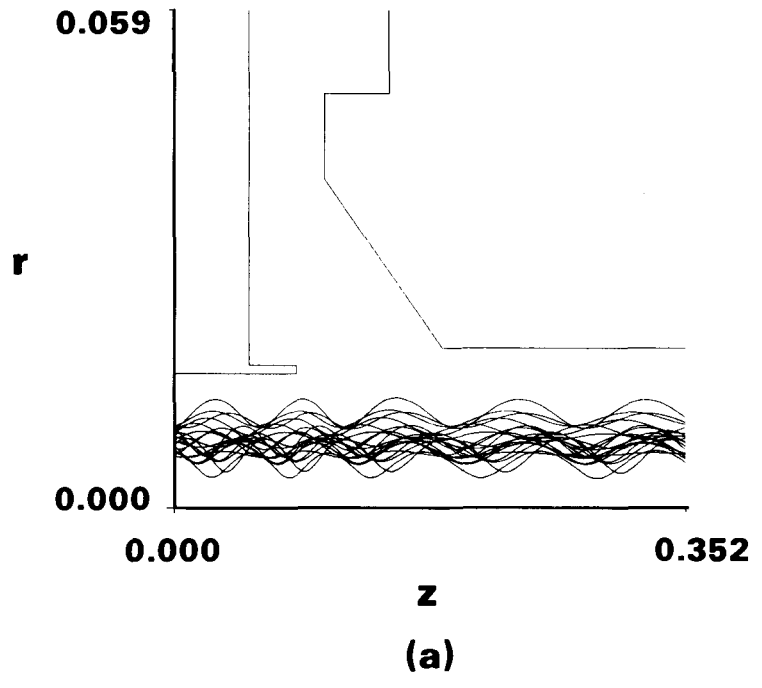

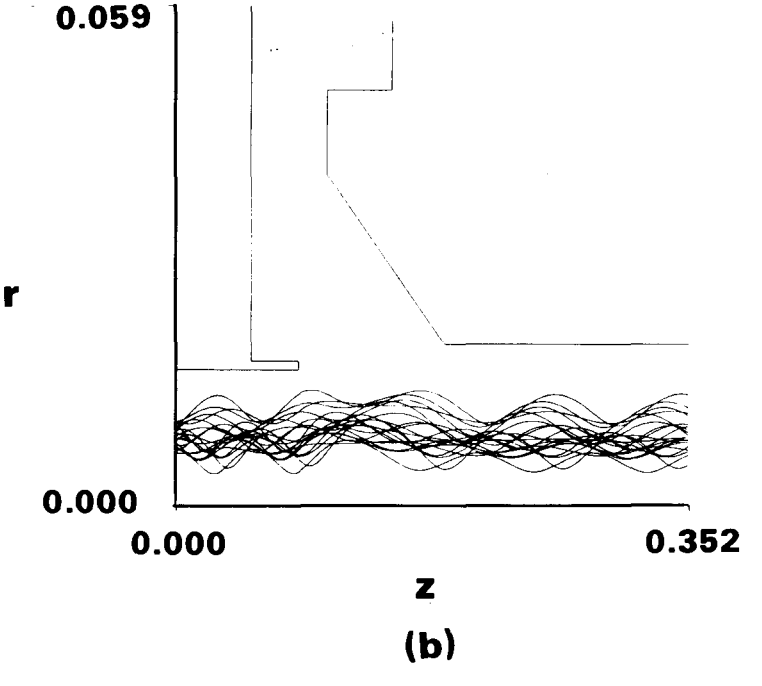

Figure 39. As in Fig. 37a, but warm input beams, $\beta_\perp$ = 0.15.
(a) Uniform B_o = 16.6 kG.
(b) Realistic B_o (Fig. 38a).

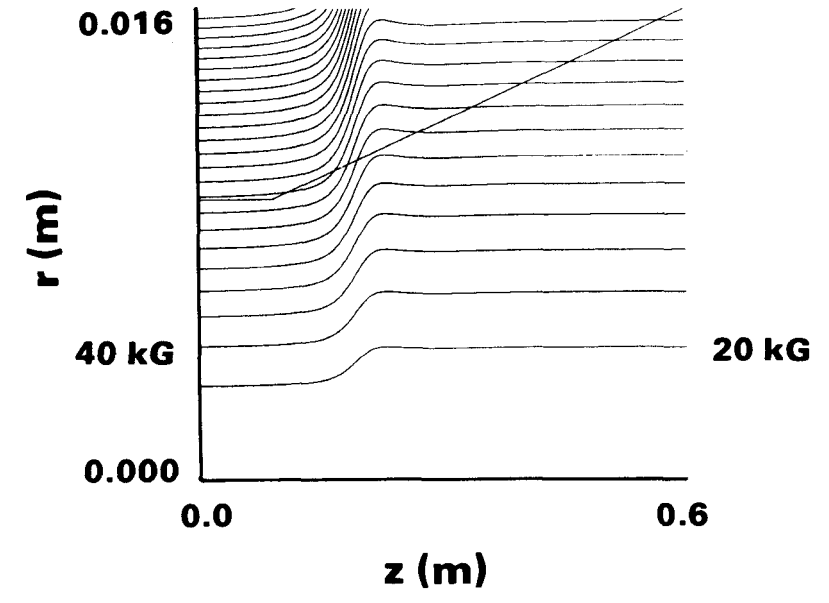

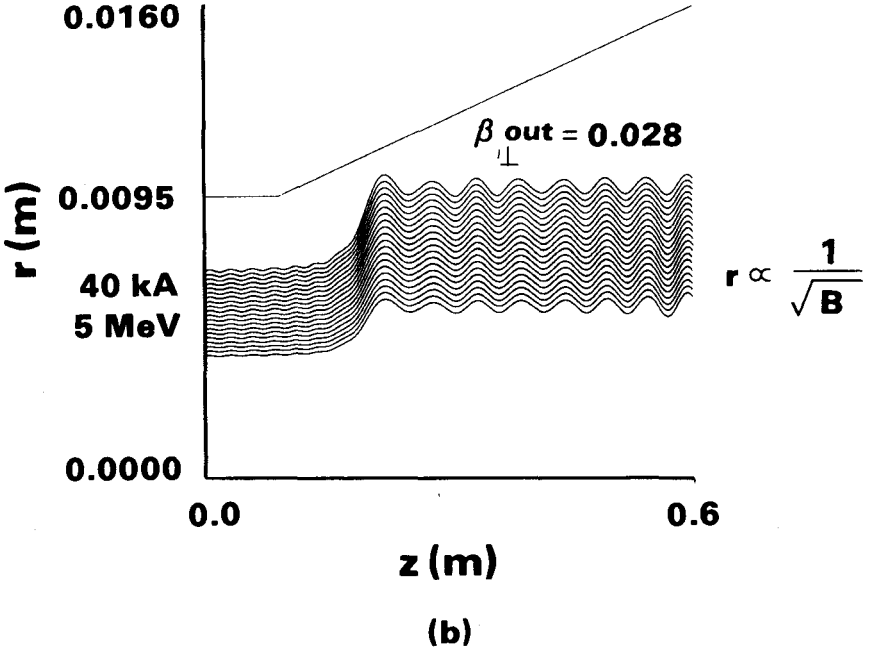

Figure 40. TRAJ run (#7 of Table VIII) of beam expansion from 40 to 20-kG field, for "fast" transition.
(a) B lines.
(b) Trajectories (every fifth shown here).
Input beam: 40 kA, 5 MeV, cold.
Output beam: $\beta_{\perp}$ = 0.028.

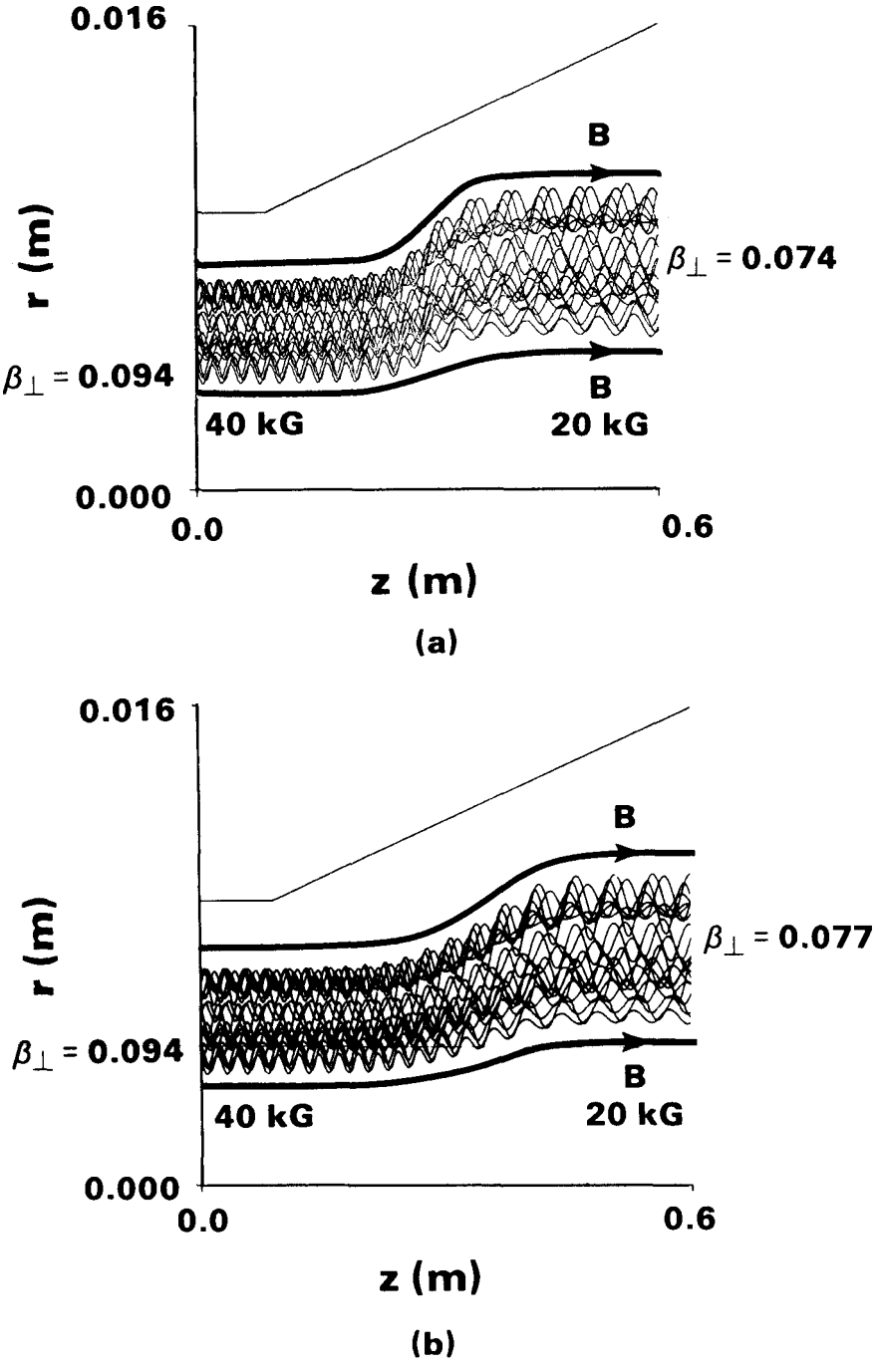

Figure 41. As in Fig. 40, except transition from 40 → 20 kG is over longer distance, and input beam is warm: $\beta_\perp$ = 0.094 (see #4 of Table VIII).
(a) "Medium" transition.
(b) "Gradual" transition.

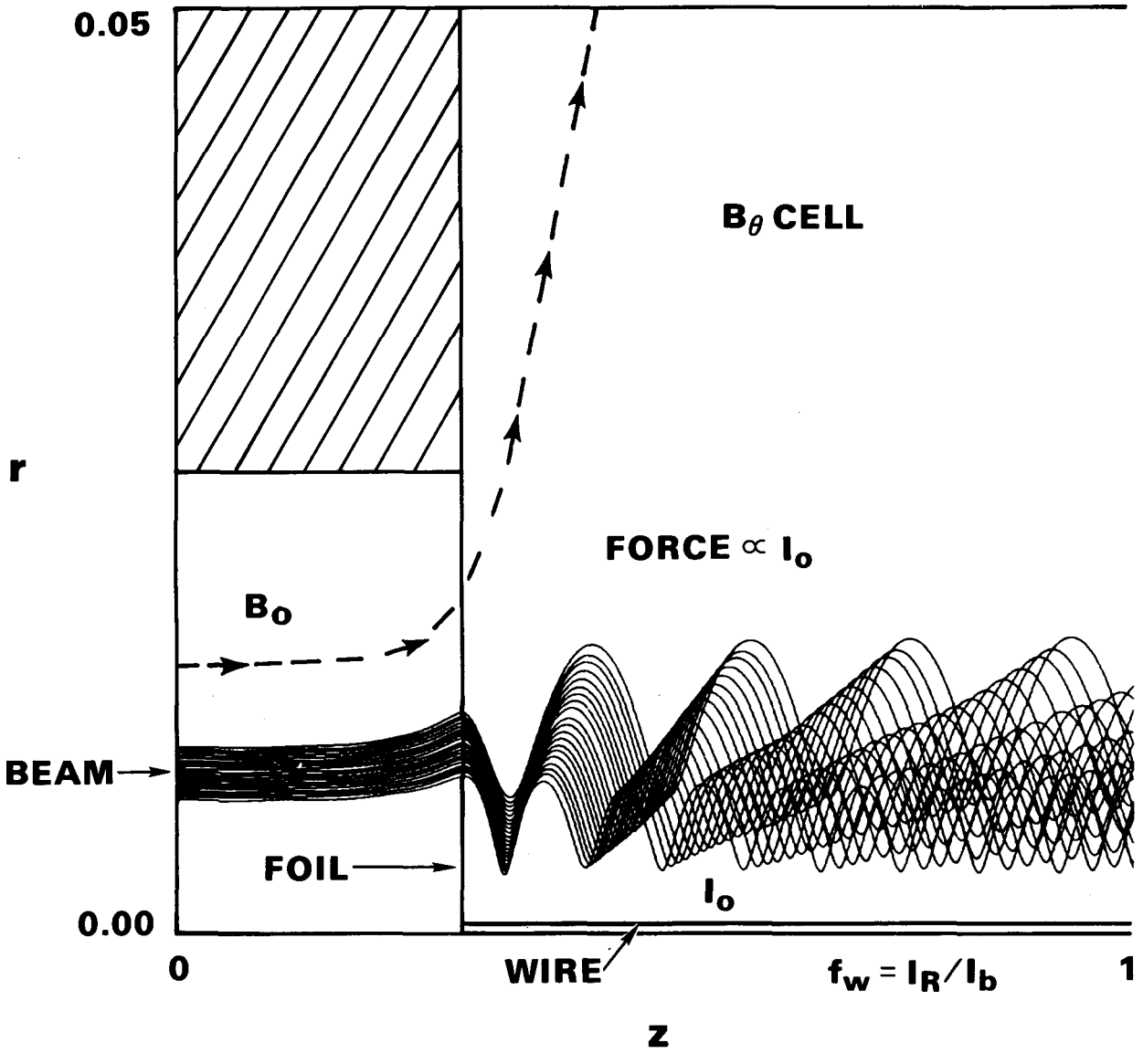

Figure 42. Set-up for B_θ cell problem. The beam is extracted from B_o in the accelerator, through a foil into the B_θ cell, a vacuum region where the beam is attracted by a wire on axis carrying current I_o. Return current = I_R, induced charge neutralization = f_w. The particular case shown is a TRAJ run for I_o = 15 kA, r_w = 0.5 mm, I_R = 7 kA, I_b = 20 kA, γ = 20, B_o = 20 kG. The output beam has $\beta_\perp$ = 0.31, r_b = 0.92 cm.

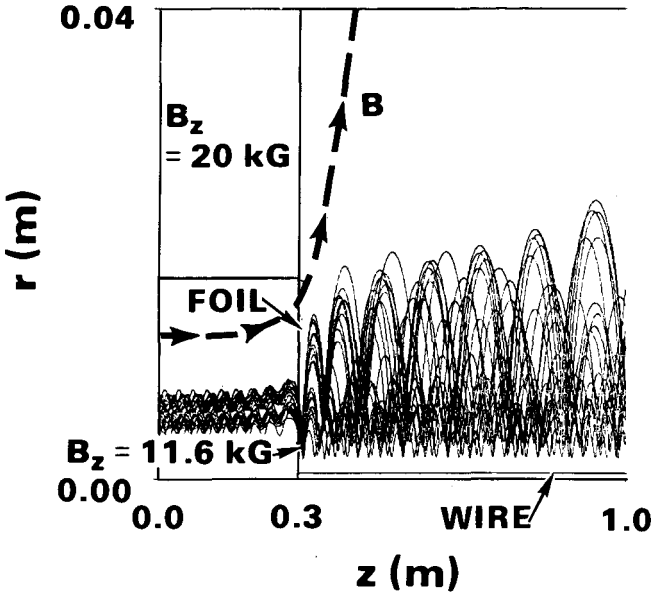

(a)

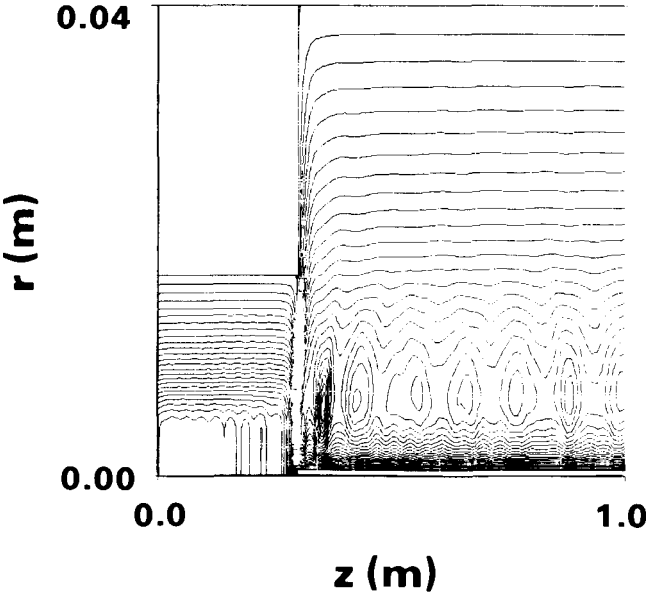

(b)

Figure 43. TRAJ B_θ wire cell base case equilibrium for IBEX. Input beam 32 kA, 4 MeV (total), rms $\beta_\perp$ = 0.1, rms r_b = 0.57 cm. B_Z (lhs) = 20 kG. Wire: I_o = 15 kA.

(a) Trajectories: Output $\beta_\perp$ = 0.5, r_b = 1.0 cm. f_w = 0.41 (electric, calculated), I_R/I_b = 0.41 (magnetic; assumed). The final equilibrium is a balance between the I_o force (inward) and emittance (outward).

(b) Equipotentials with beam.

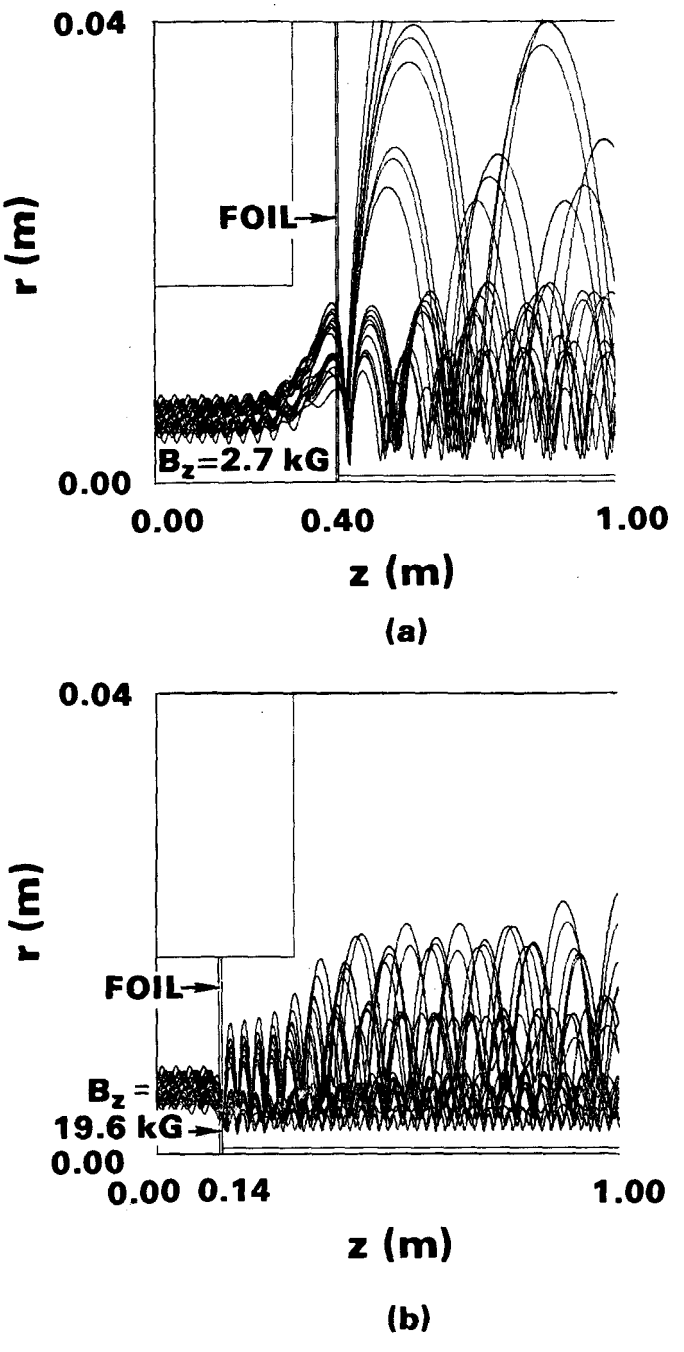

Figure 44.

(a) As in Fig. 43, but move foil out to where B_z (axis) = 2.7 kG. Note beam expansion before foil. Loss 38%.

(b) As in Fig. 43, but move foil in to where B_z (axis) = 19.6 kG. Output beam: $\beta_\perp$ = 0.4, r_b = 1.2 cm.

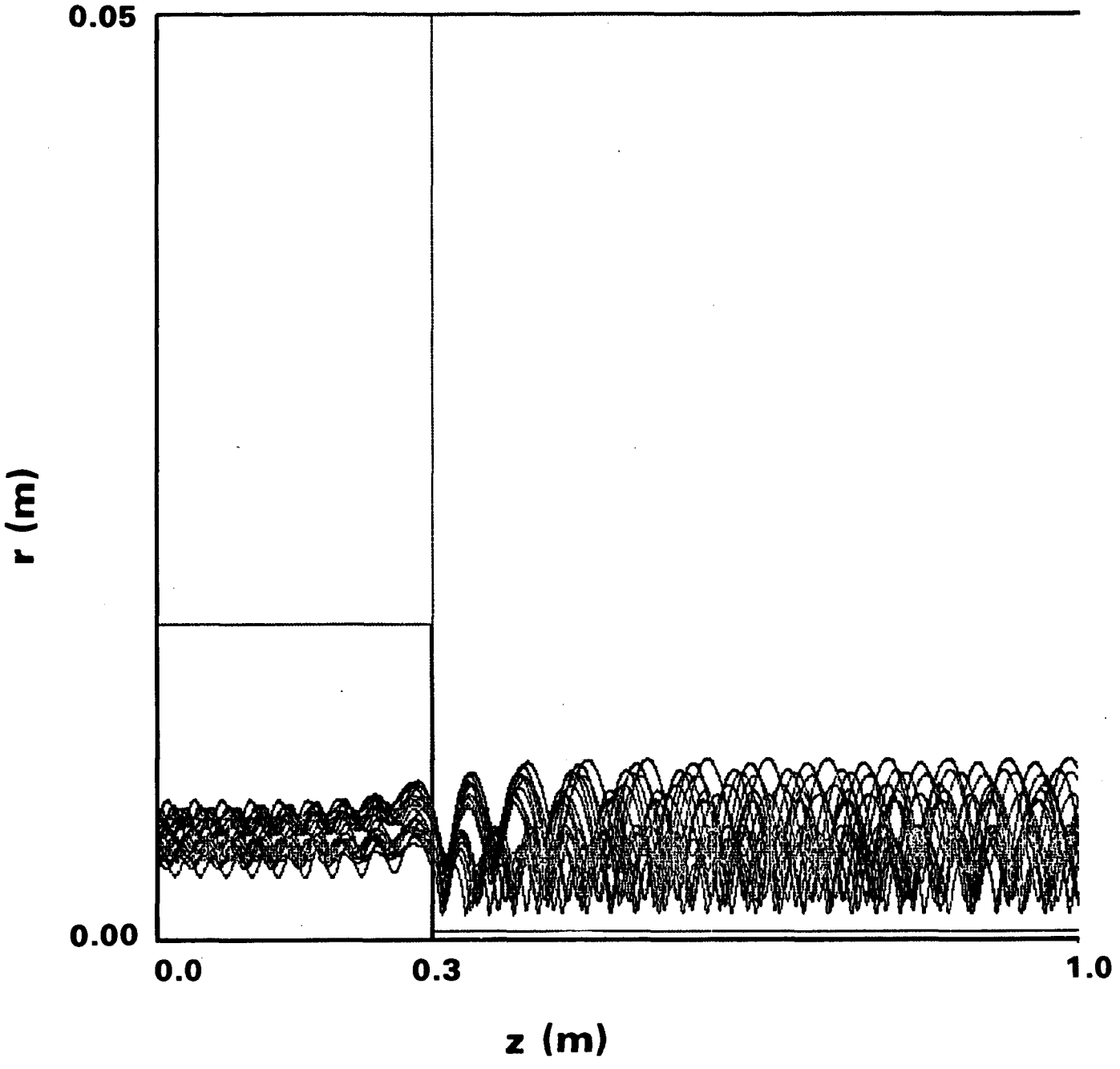

Figure 45. As in Fig. 43, but assume a background plasma ($z > 30$ cm) such that $f_e = f_m = 1$. $I_o = 30$ kA and $I_r = 14$ kA; or, if no I_R assumed, $I_o = 16$ kA. Input: 4 MeV, 32 kA, $\beta_\perp = 0.098$, r(rms) = 0.57 cm. Output: $\beta_\perp = 0.42$, r(rms) = 0.63 cm.

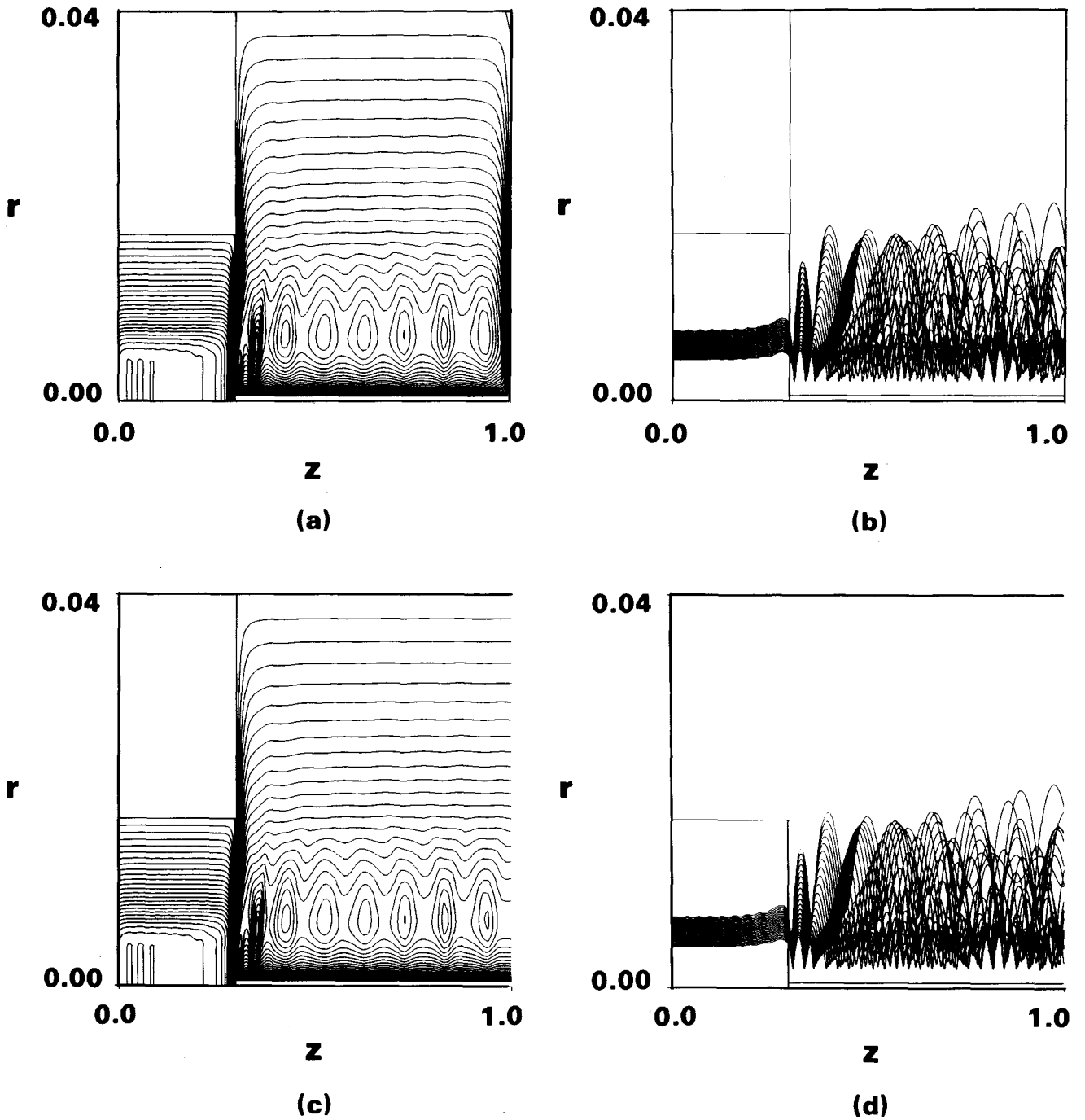

Figure 46. TRAJ study of rhs endfoil effect in IBEX B_θ cell. See Table X. I_o = 15 kA. Input beam: cold, 4 MeV, 32 kA, r_b = 5.7 mm.
(a) Equipotentials with foil.
(b) Trajectories with foil.
(c) Equipotentials without foil.
(d) Trajectories without foil.

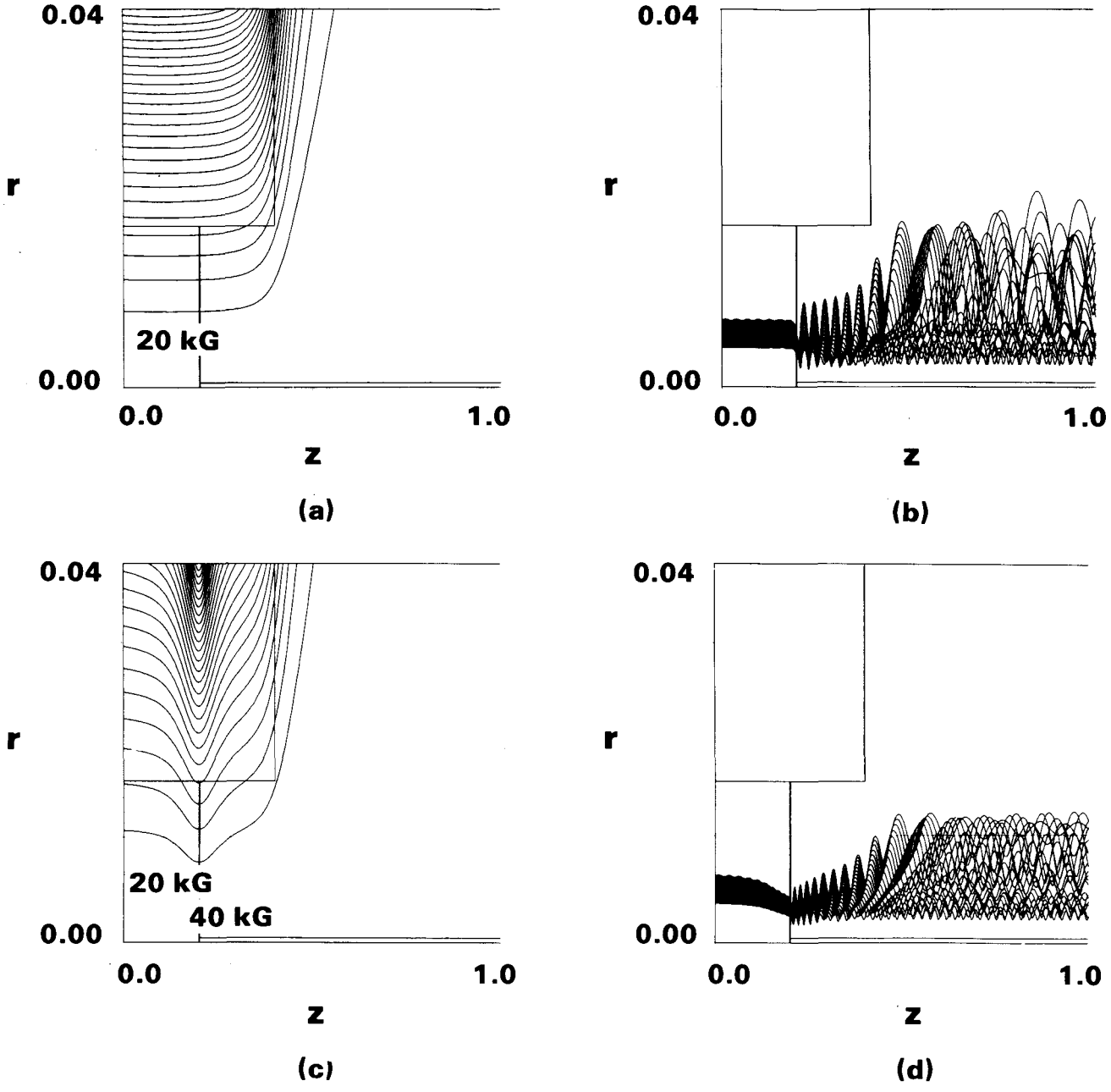

Figure 47. TRAJ runs of IBEX B_θ cell to study effect of an increase in B_z near the entrance foil. Input beam: cold, 4 MeV, 32 kA, r_b = 5.7 mm. Wire: I_o = 15 kA, r_w = 0.5 mm, I_R = 13 kA.
(a) B lines, no bump in B_z.
(b) Trajectories, no bump. Output $\beta_\perp$ = 0.52, r_b = 8.9 mm, $r\gamma\beta_\perp$ = 2.6.
(c) B lines, with bump in B_z at foil.
(d) Trajectories, with bump. Output $\beta_\perp$ = 0.49, r_b = 8.5 mm, $r\gamma\beta_\perp$ = 2.4. Most of the final $\beta_\perp$ value is due to rotation.

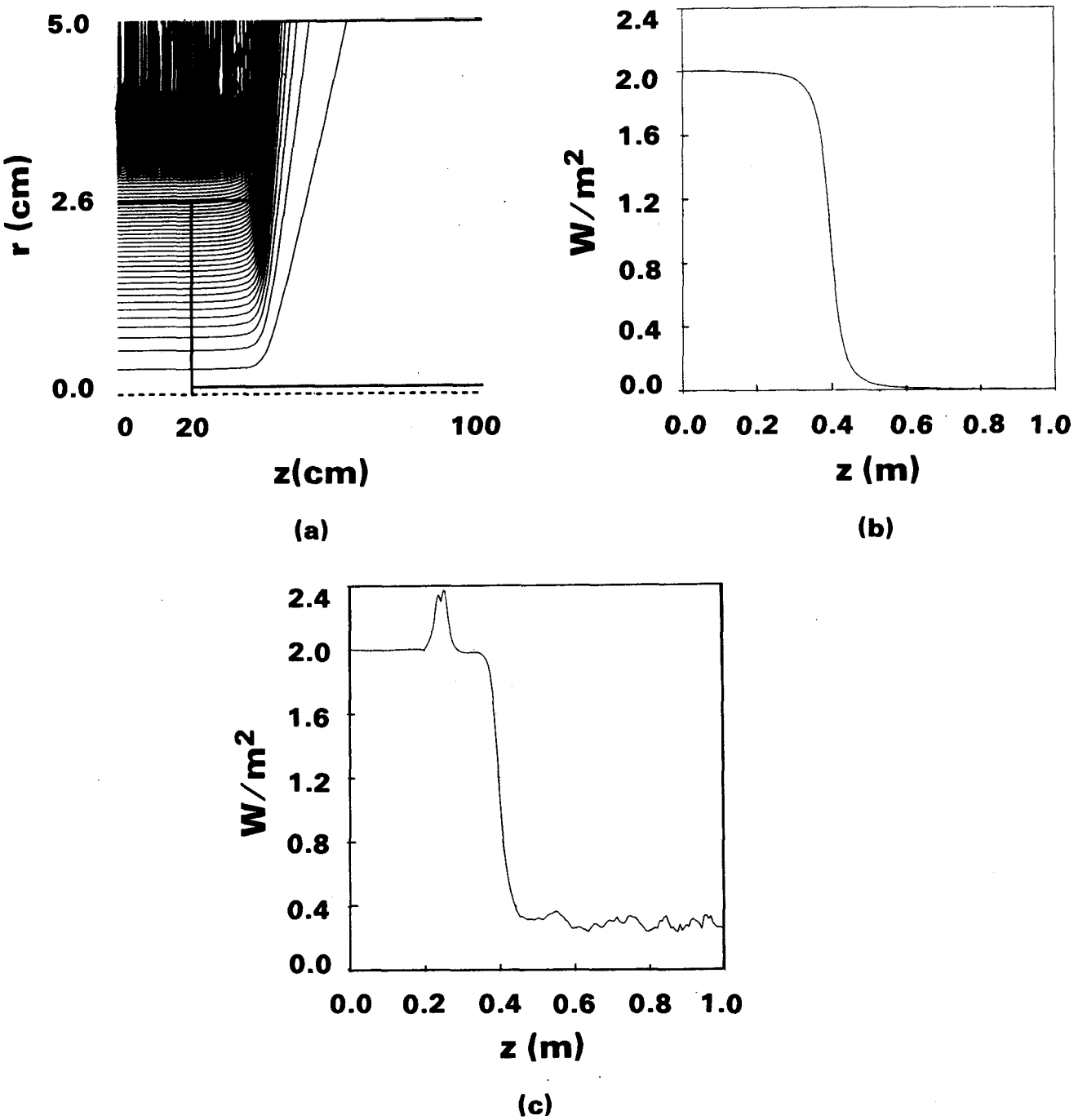

Figure 48. MAGIC calculation of RADLAC beam extraction into B_θ wire (r_w = 1 mm) cell with applied I_o = 20 kA. The input beam has parameters 40 kA, γ = 40, 7 < r < 10 mm annulus, cold, 15-ns risetime on I and γ.
(a) Applied B lines.
(b) $B_z(z)$ applied near axis.
(c) $B_z(z)$ with beam.

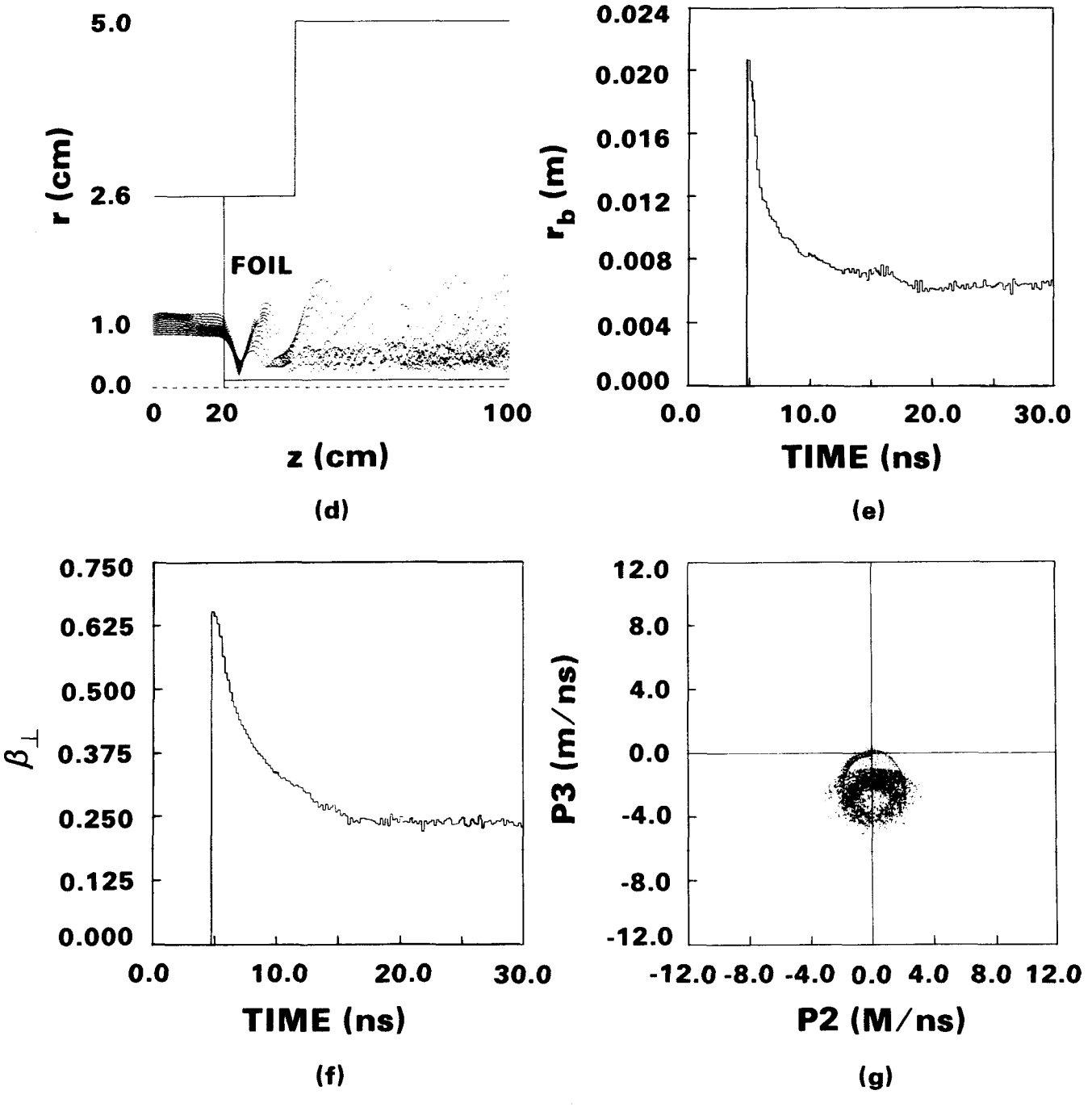

Figure 48. MAGIC calculation of RADLAC beam extraction into B_θ wire (r_w = 1 mm) cell with applied I_o = 20 kA. The input beam has parameters 40 kA, γ = 40, 7< r < 10 mm annulus, cold, 15-ns risetime on I and γ.
(d) Electron map of beam in steady state.
(e) Beam rms radius vs. t.
(f) Beam rms $\beta_\perp$ vs. t.
(g) Transverse phase space γV_θ vs. γV_r.

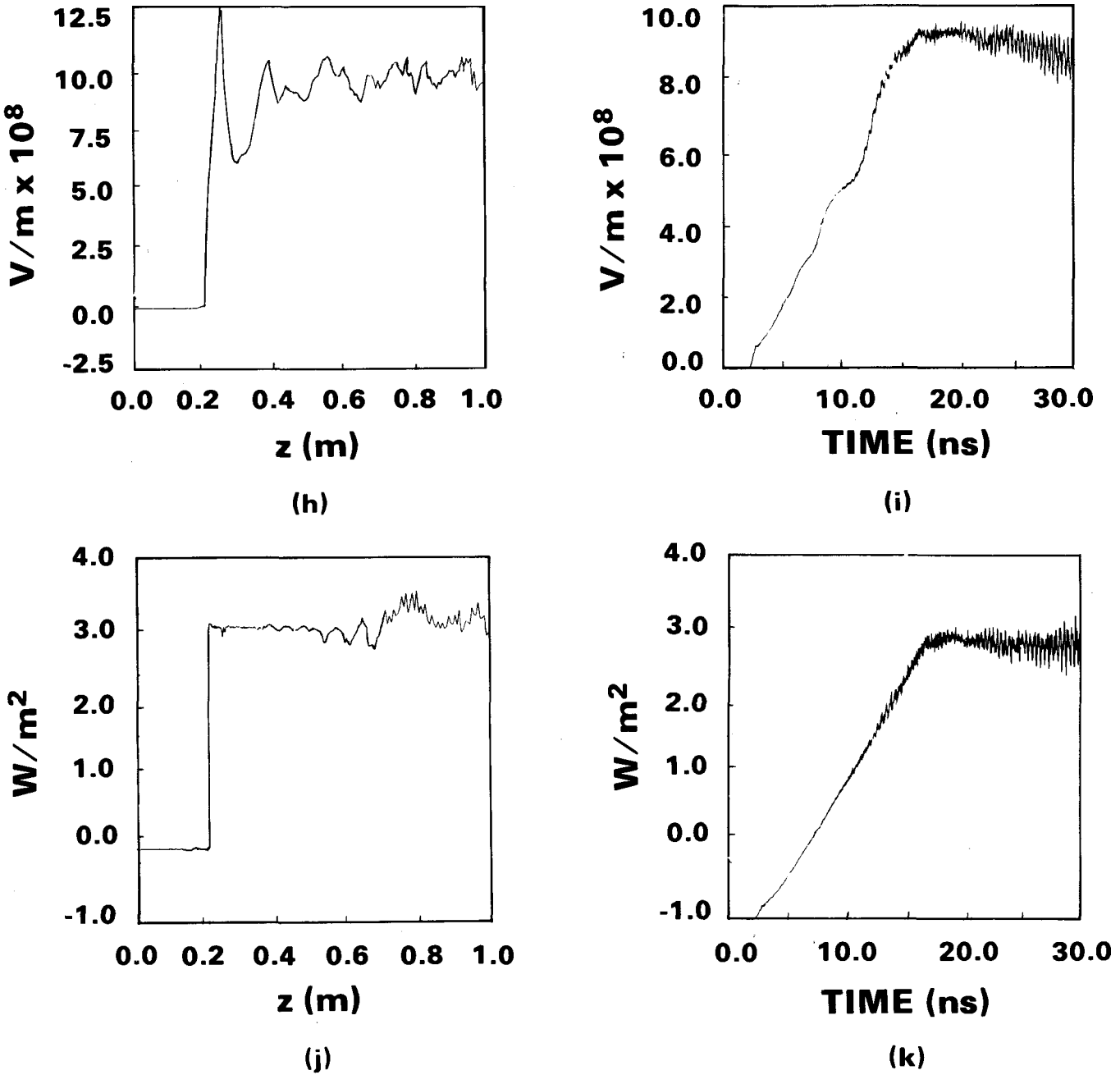

Figure 48. MAGIC calculation of RADLAC beam extraction into B_θ wire (r_w = 1 mm) cell with applied I_o = 20 kA. The input beam has parameters 40 kA, γ = 40, 7 < r < 10 mm annulus, cold, 15-ns risetime on I and γ.
(h) $E_r(z)$ near wire.
(i) $E_r(t)$ near wire.
(j) $B_\theta(z)$ near wire.
(k) $B_\theta(t)$ near wire.

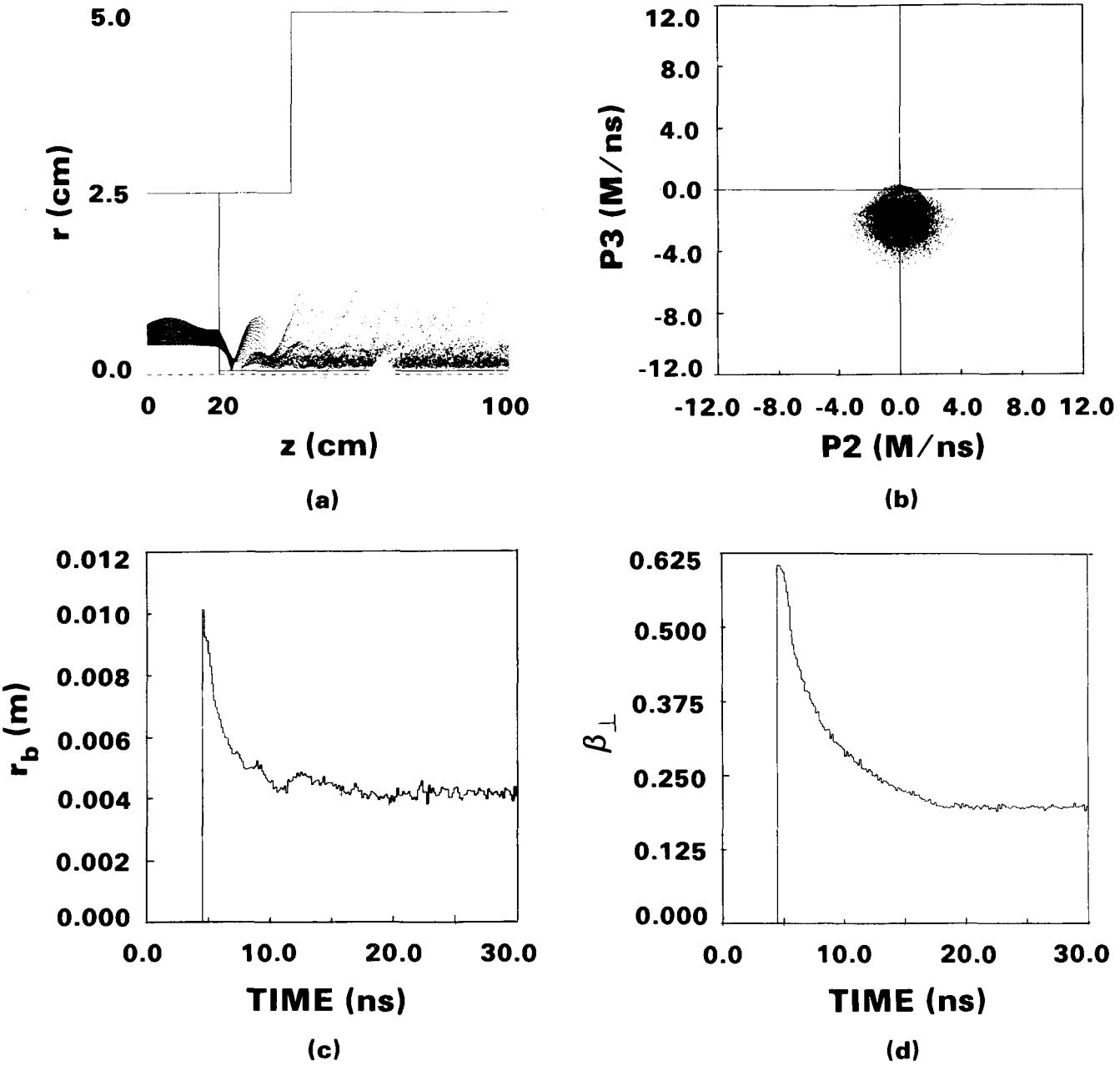

Figure 49. As in Fig. 48, but smaller beam ($4 < r < 7$ mm), smaller wire (0.5 mm) carrying 15 kA.
(a) Beam in steady state, all 40 kA propagates.
(b) γV_θ vs. γV_r (compare Fig. 48g).
(c) rms beam radius vs. t.
(d) rms $\beta_\perp$ vs. t.

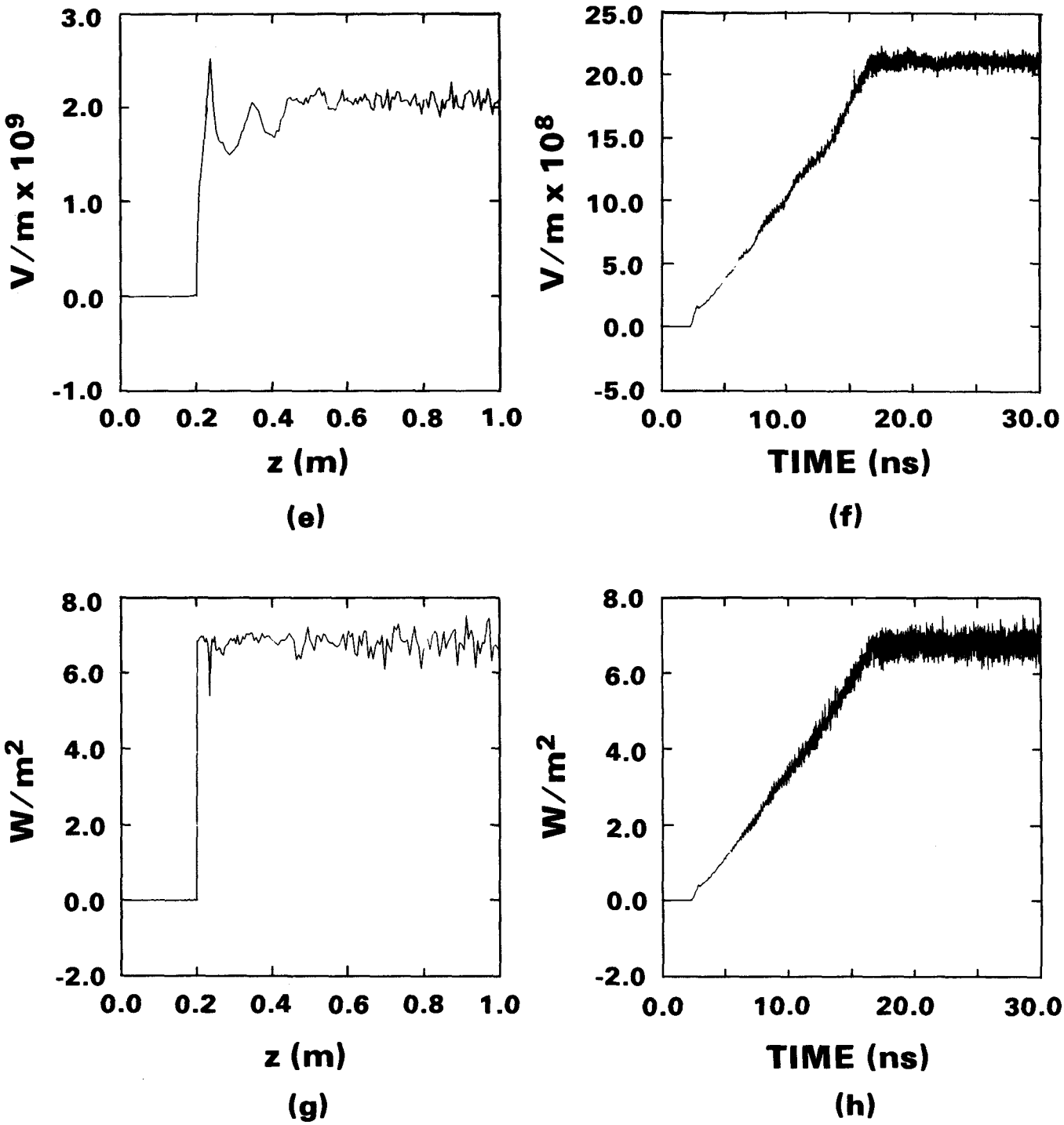

Figure 49. As in Fig. 48, but smaller beam ($4 < r < 7$ mm), smaller wire (0.5 mm) carrying 15 kA.
(e) $E_r(z)$ near wire.
(f) $E_r(t)$ near wire.
(g) $B_\theta(z)$ near wire.
(h) $B_\theta(t)$ near wire.

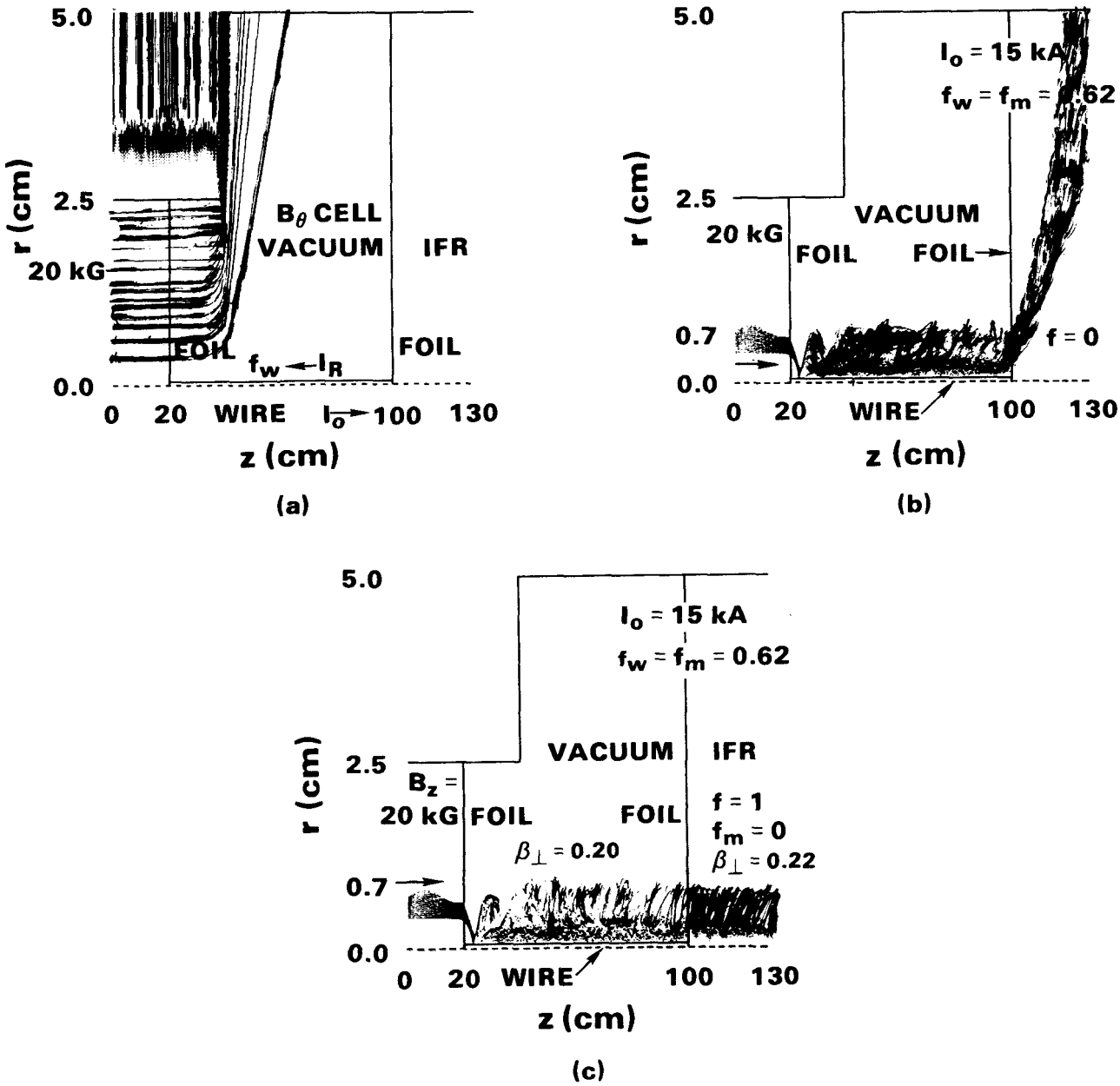

Figure 50. MAGIC run of RADLAC B_θ cell including rhs endfoil and matching to IFR region ($z > 100$ cm). Parameters as in Fig. 49 except risetime on I and γ is 10 ns.

(a) Simulation setup; note the three regions: uniform B_z($z < 20$ cm); B_θ cell ($20 < z < 100$ cm); IFR ($z > 100$ cm).

(b) Electrons in steady state with electric f = 0 in IFR region.

(c) Electrons in steady state with f = 1, f_m = 0 in IFR region; note good match of both r_b and $\beta_\perp$.

REFERENCES

1. J. W. Poukey and P. D. Coleman, SAND84-2652, March 1985.
2. J. W. Poukey, SAND85-2670, Feb. 1986.
3. J. W. Poukey, SAND87-0384, March 1987.
4. J. W. Poukey, SAND87-0494, April 1987.
5. J. W. Poukey, SAND87-3068, Jan. 1988.
6. J. W. Poukey, SAND88-0039, Feb. 1988.
7. D. E. Hasti et al., SAND88-1032, May 1988.
8. J. S. Wagner et al., SAND88-1119, Nov. 1988.
9. M. G. Mazarakis et al., J. Appl. Phys. 62, 4024 (1987).
10. R. B. Miller et al., J. Appl. Phys. 62, 3535 (1987).
11. J. W. Poukey, memo "Flat Cathode Size Effects," April 14, 1988.
12. J. W. Poukey, memo "Summary of RADLAC Feed Injector MAGIC Runs," May 23, 1988.
13. J. W. Poukey, memo "RADLAC Gap Studies via MAGIC and TRAJ," May 27, 1988.
14. J. W. Poukey, memo "Summary of Recent Studies of IBEX Diodes and Conditioning Cells," June 9, 1988.
15. J. W. Poukey, memo "RLA (Recirc) Diode Studies," June 22, 1988.
16. J. W. Poukey, memo "RADLAC Diode and Beam Expansion Studies," July 21, 1988.
17. J. W. Poukey, memo "Latest RADLAC Calculations," Oct. 13, 1988.
18. J. W. Poukey, Proc. 12th Conf. on Numerical Simulation of Plasmas, San Francisco, CA, 1987.
19. P. T. Kirstein, G. S. Kino, and W. E. Waters, Space-Charge Flow (McGraw-Hill, 1967), pp. 154, 331.
20. R. J. Adler, private communication.
21. Suggested by B. B. Godfrey (MRC).
22. M. G. Mazarakis, private communication.
23. C. A. Frost et al., to be presented at Particle Accelerator Conf., Chicago, March 20-23, 1989.
24. M. E. Jones, M. A. Mostrom, and L. E. Thode, J. Appl. Phys. 52, 4942 (1981).
25. The magnetic moment is given by $\gamma^2(V_+ - U_E)^2/B$ generally, where U_E is the E x B drift velocity. In cold beam cases we cannot use $V_+ >> U_E$.
26. J. R. Freeman, memo "BUCKSHOT Simulations for RADLAC II," June 29, 1988.
27. J. R. Freeman and J. W. Poukey, memo "Further Wire-Cell Simulations for Troll," Dec. 6, 1988.
28. They also compare well for IFR conditioning cells, as discussed in Ref. 8.
29. Problem suggested by B. B. Godfrey (MRC).

DISTRIBUTION:
Unlimited Release

Air Force Weapons Laboratory
Kirtland AFB, NM 87117
Attn: Dr. W. Baker, AWP
Dr. R. Lemke, AWP

Applied Physics Branch
Ballistic Modeling Division
Department of the Army
U.S. Army Ballistic Research Lab.
Aberdeen Proving Ground, MD 21005
Attn: D. Eccleshall

Austin Research Associates
1901 Rutland Drive
Austin, TX 78758
Attn: M. L. Sloan

Lawrence Livermore National Laboratory
Livermore, CA 94550
Attn: W. A. Barletta

Los Alamos National Laboratory
University of California
P. O. Box 1663
Los Alamos, NM 87544
Attn: H. O. Dogliani, H818
J. Mack, P940
T. P. Starke, P942

Mission Research Corporation
1720 Randolph Road, SE
Albuquerque, NM 87106
Attn: B. B. Godfrey

Mission Research Corporation
5503 Cherokee Avenue
Alexandria, VA 22312
Attn: Bruce Goplen

Naval Research Laboratory
Department of the Navy
Washington, D.C. 20375
Attn: M. Lampe
R. Hubbard
I. Vitkovitsky

Naval Surface Weapons Center
White Oak Laboratory
Silver Spring, MD 20910
Attn: B. Hui

Pulse Sciences, Inc.
600 McCormick Street
San Leandro, CA 94577-1110
Attn: S. D. Putnam

Science Applications International Corp.
5150 El Camino Real, Suite B-31
Los Altos, CA 94022
Attn: R. R. Johnston

Science Applications International Corp.
1710 Goodridge Drive
McLean, VA 22102
Attn: A. T. Drobot
W. Reinstra

Strategic Defense Initiative Org. (SDIO)
Directed Energy Weapons (DEW)
Office of the Secretary of Defense
Room 3E1034
Washington, D.C. 20301-7100
Attn: Lt. Col. R. Gullickson

Titan Technologies-Spectron Division
2017 Yale Blvd., SE
Albuquerque, NM 87106
Attn: R. B. Miller

Internal Distribution:

1000	V. Narayanamurti
1200	J. P. VanDevender
1230	J. E. Powell
1231	J. R. Lee
1232	W. Beezhold
1235	J. M. Hoffman
1240	K. R. Prestwich
1241	J. R. Freeman
1241	B. M. Marder
1241	K. J. O'Brien
1241	C. L. Olson
1241	J. W. Poukey (10)
1241	D. B. Seidel
1241	J. S. Wagner
1242	D. E. Hasti
1242	C. A. Frost
1242	G. T. Leifeste
1242	M. G. Mazarakis
1242	S. L. Shope
1245	J. J. Ramirez
1248	M. T. Buttram
1250	T. H. Martin
1260	D. L. Cook
1261	M. J. Clauser
1265	J. P. Quintenz
1270	J. K. Rice
1274	R. J. Lipinski
1274	P. D. Coleman
1275	R. A. Gerber
3141	S. A. Landenberger (5)
3151	W. I. Klein (3)
3154-1	C. L. Ward for DOE/OSTI (8)
8524	J. A. Wackerly (1)